Spring 2004

A numerical method to solve the two-step parabolic heat transport equations in a microsphere subjected to an ultrafast laser pulse

Ibrahima Khalil Fiman Kaba

A NUMERICAL METHOD TO SOLVE THE TWO-STEP PARABOLIC HEAT

TRANSPORT EQUATIONS IN A MICROSPHERE SUBJECTED TO AN

ULTRAFAST LASER PULSE

by

Ibrahima Khalil Fiman Kaba, B.S., M.S.

A Dissertation Presented in Partial Fulfillment
of the requirements for the Degree
Doctor of Philosophy

COLLEGE OF ENGINEERING AND SCIENCE
LOUISIANA TECH UNIVERSITY

MAY 2004

UMI Number: 3125115

INFORMATION TO USERS

The quality of this reproduction is dependent upon the quality of the copy submitted. Broken or indistinct print, colored or poor quality illustrations and photographs, print bleed-through, substandard margins, and improper alignment can adversely affect reproduction.

In the unlikely event that the author did not send a complete manuscript and there are missing pages, these will be noted. Also, if unauthorized copyright material had to be removed, a note will indicate the deletion.

UMI®

UMI Microform 3125115

Copyright 2004 by ProQuest Information and Learning Company.

All rights reserved. This microform edition is protected against unauthorized copying under Title 17, United States Code.

ProQuest Information and Learning Company
300 North Zeeb Road
P.O. Box 1346
Ann Arbor, MI 48106-1346

LOUISIANA TECH UNIVERSITY

THE GRADUATE SCHOOL

<u>Monday April 26th, 2004</u>

Date

We hereby recommend that the dissertation prepared under our supervision

by_____IBRAHIMA KHALIL FIMAN KABA_____

entitled____A NUMERICAL METHOD TO SOLVE THE TWO-STEP PARABOLIC HEAT____

_TRANSPORT EQUATIONS IN A MICROSPHERE SUBJECTED TO AN ULTRAFAST LASER___

_PULSE_____

be accepted in partial fulfillment of the requirements for the Degree of

_____DOCTOR OF PHILOSOPHY_____

_____
Supervisor of Dissertation Research

_____
Head of Department

_____
Department

Recommendation concurred in:

_____

_____

_____   Advisory Committee

_____

Approved:

_____
Director of Graduate Studies

_____
Dean of the College

Approved:

_____
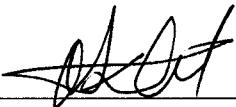Dean of the Graduate School

ABSTRACT

Heat transport at the microscale is the subject of intense investigation due to the growing need to fabricate microstructures for applications in nanotechnology. The need to control the spread of the thermal process zone has led to the development of high power short-pulse lasers. During thermal processing, impurities may form in the material. An amplification of the thermal energy around the impurities may result in severe damage occurring or in the failure of the thermal process. A thorough analysis of the way the impurities dissipates the thermal energy is therefore necessary to minimize the potential damage and optimize the thermal processing.

The classical theory of heat diffusion, which is averaged over many grains, is inadequate in describing the transport phenomenon. Single energy equations developed to describe the transport phenomenon include a third-order mixed derivative with respect to space which makes them numerically inefficient. In this study, we will consider a microsphere subjected to an ultrafast laser pulse. The transport phenomenon is modeled by the two-step parabolic heat transport equations in three dimensional spherical coordinates. We will develop an energy estimate to establish the well-posedness of the problem, a three-level finite difference scheme to solve the transport equations, and prove that the finite difference scheme is unconditionally stable. The scheme will be applied to investigate the temperature rise in a gold sphere subjected to a short-pulse laser.

iii

APPROVAL FOR SCHOLARLY DISSEMINATION

The author grants to the Prescott Memorial Library of Louisiana Tech University the right to reproduce, by appropriate methods, upon request, any or all portions of this Dissertation. It is understood that "proper request" consists of the agreement, on the part of the requesting party, that said reproduction is for his personal use and that subsequent reproduction will not occur without written approval of the author of this Dissertation. Further, any portions of the Dissertation used in books, papers, and other works must be appropriately referenced to this Dissertation.

Finally, the author of this Dissertation reserves the right to publish freely, in the literature, at any time, any or all portions of this Dissertation.

Author _____

Date   04/29/2004 _____

TABLE OF CONTENTS

LIST OF TABLES

LIST OF FIGURES

x

NOMENCLATURE

A	constant coefficient
B	constant coefficient
C	constant coefficient
	thermal wave speed, m/s
$C_{(e,l)}$	volumetric heat capacity of electron gas (e) and metal lattice (l), $J/m^3 K$
C_ρ	volumetric heat capacity, $J/m^3 K$
d_i	i=1,2,3. Distance traveled by phonons or electrons, nm
E	phonon/electron energy, J
	Fermi energy of electrons
$E^{-\frac{1}{2}}$	finite difference operator
G	phonon-electron coupling factor, $W/m^3 K$
H	constant coefficient
h	Planck's constant, Js
J	laser fluence, J/m^2
K	thermal conductivity of the electron gas, W/mK
	thermal conductivity, W/mK
k_e	thermal conductivity of the electron gas, W/mK

xii

	thermal conductivity, W/mK
L	the radius of the sphere, μm
l	effective mean free path in phonon collision, μm
M	atomic mass, kg
m	effective mass of electrons, kg
m_e	electron mass, kg
N	number of grid points
n_a	atomic number density per unit volume, $1/m^3$
n_e	number density of electrons per unit volume, $1/m^3$
P	finite difference operator
Q	volumetric heat source, W/m^2
q	heat flux, W/m^2
R	reflectivity
r	spherical coordinate
	position, μm
S	volumetric heat source, W/m^2
S_{ijk}^n	mesh function where n is the time level and i,j,k represent the grid point
T	absolute temperature, K
	transient matrix element
T_0	initial temperature, K
T_{ijk}^n	mesh function where n is the time level and i,j,k represent the grid point

t	physical time, s
t_0	physical time, s
t_i	$i=1,2,3$. Travel times of phonons or electrons in successive collisions
t_p	laser pulse duration, fs
u_{ijk}^n	mesh function where n is the time level and i,j,k represent the grid point
v_s	speed of sound, m/s

Greek Symbols

α	thermal diffusivity, m/s^2
Δ	average volume of the unit cell, m^3
Δr	grid size
ΔT	change in temperature
Δt	time increment
$\Delta \varphi$	grid size
$\Delta \theta$	grid size
δ	laser penetration depth, nm
φ	spherical coordinate
κ	Boltzmann's constant, J/K
Λ	constant
ν	vibration frequency of metal lattice, $1/s$
θ	spherical coordinate
τ	mean free time or relaxation time, s
τ_F	relaxation time calculated at the Fermi surface, s

xiv

∇_r	first order forward finite difference
$\nabla_{\bar{r}}$	first order backward finite difference
∇_φ	first order forward finite difference
$\nabla_{\bar{\varphi}}$	first order backward finite difference
∇_θ	first order forward finite difference
$\nabla_{\bar{\theta}}$	first order backward finite difference

Subscripts and Superscripts

0	initial value
a	atom
D	Debye Temperature
E	equivalent quantity
e	electron
i	index in a series
j	index in a series
k	index in a series
l	metal lattice
max	maximum value
r	spherical coordinate
φ	spherical coordinate
θ	spherical coordinate

ACKNOWLEDGEMENTS

This dissertation owes many thanks to a number of people for their assistance, support, and encouragement.

I wish to express my deepest gratitude to my advisor, Dr. Weizhong Dai, for his guidance, kindness, encouragement and the countless hours he spent with me investigating the issues presented in this dissertation. This dissertation could not have been completed without his helpful advice and suggestions.

I would also like to thank the other members of my committee, Dr. Richard Greechie, Dr. Raja Nassar and Dr. Andrei Paun for their questions, comments, advice and their precious time spent editing this manuscript. I am especially grateful to Dr. Richard Greechie for being a tireless mentor. I would not be here today without your support and guidance.

I am forever indebted to my family and friends. Their patience, support and love have always been my inspiration. To my parents, El. Hadj Karamoko Fiman Kaba and Hadja Saran Daraba Kaba, thank you for believing in me and for instilling your values in me. I hope that I have made you proud. This dissertation is dedicated to you.

xvi

CHAPTER 1

INTRODUCTION

1.1 Overview

Ultra short-pulsed lasers with pulse durations of the order of sub-picosecond to

femtosecond domain possesses exclusive capabilities in limiting the undesirable spread of

the thermal process zone in the heated sample [Tzou 2002]. They have been widely

applied in structural monitoring of thin metal films [Opsal 1991], laser micromachining

[Knapp 1990] and patterning [Elliot 1989], structural tailoring of microfilms

[Grigoropolus 1994], and laser synthesis and processing in thin-film deposition [Narayan

1991] as well as in physics, chemistry, biology, medicine and optic technology [Hopkins

2000], [Liu 2000], [Momma 1997], [Shirk 1998], [Tzou 1999, 2000a, 2000b].

For an ultra short-pulsed laser, the heating involves high-rate heat flow from electrons

to metal lattices in the picoseconds' domains. Depending on the temperature, electrons

have a heat capacity several orders of magnitude smaller than that of lattices. When

heated by photons (lasers), the laser energy is primarily absorbed by the free electrons

that are confined within skin depth during the excitation. Electrons first shoot up to

several hundreds or thousands of degrees within a few picoseconds without disturbing the

metal lattices. A major portion of the thermal electron energy is then transferred to the

1

lattices.

Meanwhile, another part of the energy diffuses to the electrons in the deeper region of the target. Since the pulse duration is so short, the laser is turned off before thermal equilibrium between the electrons and the metal lattices is reached. In this time interval, the heat flux is thus essentially limited to the region within the electron thermal diffusion length. This stage is termed non-equilibrium due to the large difference in temperatures in electrons and lattices [Chen 2001b]. The lattice temperature then increases as a result of lattice-electron coupling, resulting in a new thermal property termed the lattice-electron coupling factor. The single energy equations describing the heat transport phenomenon at the micro scale are not numerically efficient as they include a second-order derivative of temperature with respect to time and a mixed-order derivative of temperature with respect to space and time [Tzou 1997]. Thus, the process is modeled by the two-step parabolic heat transport equations as described in [Tzou 1997]; the significance of the parabolic two-step model as opposed to the classical and single energy heat conduction equations has been discussed in [Tzou 1997]. In this sense, the parabolic two-step model in spherical coordinates can be useful when investigating heat transfer around a micro void. Micro voids may form during the thermal processing of materials due to thermal expansion. When such impurities occur in the work piece, the thermal energy in their neighborhood may be amplified which could result in severe damage and, consequently, lead to a total failure of the thermal processing. A detailed understanding of the way dissipation occurs in the defects is thus crucial not only to prevent damage to the micro device but also to optimize the thermal process [Tzou 1997]. Additionally, a micro sphere is an important component in the fabrication of microelectronic devices, since the

dimensions under study relate favorably to those of elementary physical particles; the micro sphere can be used to model the heat transport phenomenon in physical particles; therefore, understanding the temperature distribution in this microelectronic device is of vital importance.

1.2 Research Objectives

The research objective is to develop a numerical method to solve the two-step parabolic heat transport equations in a micro sphere subjected to an ultra short laser pulse. Our coordinates of reference will be the spherical coordinates system.

To achieve our objective, these steps will be followed:

(1) Develop an energy estimate to establish that the problem is well posed.

(2) Develop a second order, in both space and time, finite difference scheme, three-level in time and central in the spatial directions, to simultaneously solve the electron and the lattice temperature distribution.

(3) Prove the stability of the numerical method by the discrete energy method.

(4) Apply the numerical scheme to investigate the temperature distribution in a gold micro sphere subjected to an ultra short laser pulse. Three cases will be considered under the applications: a symmetric heat source, a heat source applied to the hemisphere, and the heat source applied on a spot on the sphere.

The results of the research will provide a numerically efficient method to solve the two-step parabolic heat transport in spherical coordinates and improve our understanding of the transport phenomenon in a micro sphere. The results will also have an impact on the design and calibration of short-pulse lasers for applications in the structural

monitoring of thin metal films, laser micro-machining and patterning, structural tailoring of microfilms, and laser synthesis and processing in thin film deposition, as well as in other disciplines where high-energy short-pulse lasers are important.

1.3 Organization of the Dissertation

The dissertation is organized as follows: in Chapter 2, we will present the classical theory of heat transfer at the macro scale with a review of the heat transport equation derived from Fourier's Law and the Thermal Wave model of Cattaneo and Vernotte. Then, we will discuss heat transfer at the micro scale, essentially the phonon-electron interaction model and its associated two-step hyperbolic and parabolic transport equations. We will then introduce the two-step parabolic transport equations in spherical coordinates. The chapter will conclude with a review of previous researches.

In Chapter 3, we will proceed to a description of the problem, define the geometry and state the governing equations along with the initial and boundary conditions. Subsequently, we will develop an energy estimate to prove that the problem is well posed. Then, the numerical scheme is introduced and its stability will be proven.

In Chapter 4, we will set up the linear systems necessary to solve the finite difference scheme introduced in Chapter 3 and define the numerical algorithm used to find the solutions.

In Chapter 5, we will investigate the temperature change and distribution in a gold micro sphere subjected to an ultra-short laser pulse. The symmetric heat source case, the heat source applied to a hemisphere case, and the heat source applied to a spot case will be studied. Conclusions and future work will be discussed in Chapter 6.

CHAPTER 2

BACKGROUND AND PREVIOUS WORK

2.1 Macroscopic Heat Transfer Models

2.1.1 Classical Theory of Heat Transfer

In thermodynamics, heat is defined as energy transfer due to temperature gradients or differences. Consistent with this view point, only two modes of heat transfer are recognized: *conduction* and *radiation*. For example, heat transfer across a steel pipe is by conduction, whereas heat transfer from the sun to earth is by radiation. These modes of transfer occur on a molecular or subatomic scale.

In the atmosphere at normal pressure, conduction is by molecules that travel a very short distance before colliding with another molecule and exchanging energy. On the other hand, radiation is by photons, which travel almost unimpeded through the air from one surface to another. Thus, an important distinction between conduction and radiation is that the energy carriers for conduction have a shorter *mean free path*, whereas for radiation, the carriers have a long mean free path. Additionally, a fluid, by virtue of its mass and velocity, can transport momentum, and by virtue of its temperature, it can transport energy. Therefore, convection is defined as the transport of energy by bulk motion of a medium. We will focus our discussions on the conduction mode of heat

5

transfer.

On a microscopic level, the physical mechanisms of conduction are complex, ranging from molecular collisions in gases to lattice vibration in crystals, and flow of free electrons in metals. Heat conduction at the macro scale is a description of macroscopic conditions averaged over many grains. Thus, microscopic behaviors need to be aggregated over the domain by placing an emphasis on *phenomenological laws*, more suitable to the macroscopic level. In the classical theory of heat transfer, the main phenomenological law that governs heat conduction is *Fourier's Law*. It is a constitutive equation that depicts the way in which cause varies with effects. It is necessary along with the conservation of energy law to derive the heat transport equations. Regardless of the assumptions formulated in the constitutive equation, it must be admissible under the framework of the second law of thermodynamics.

Fourier's Law of Heat Conduction,

$$\vec{q}(\vec{r},t) = -k\nabla T(\vec{r},t),$$
$$(2.1)$$

where $\vec{r}$ denotes the position vector of the material volume, k is the *thermal conductivity* of the material, and t the physical time, dictates that the heat flux vector $(\vec{q})$ and the temperature gradient (∇T) across a material volume occur at the same *instant* of time. The energy equation derived from the first law of thermodynamics is:

$$-\nabla \vec{q} = C_p \frac{\partial T}{\partial t},$$
$$(2.2)$$

where C_p is the volumetric heat capacity. Taking the divergence of equation (2.1) and substituting it in equation (2.2), we obtain the traditional heat diffusion equation:

$$C_p \frac{\partial T}{\partial t} = k\nabla \cdot (\nabla T).$$ (2.3)

The immediate response dictated by Fourier's Law results in an infinite speed of heat propagation, implying that a disturbance applied at a certain location in a solid medium is immediately sensed anywhere else in the medium. Because the heat flux vector and the temperature gradient are simultaneous, there is no difference between the cause and the effect of heat flow.

2.1.2 Thermal Wave Model

[Cattaneo 1958] and [Vernotte 1958, 1961] proposed the Thermal Wave Model (CV Model) to resolve the paradox of infinite speed of heat propagation. The novelty was the introduction of a time delay τ, called the relaxation time. In this case, the constitutive equation can be written as [Ozisik 1994], [Tzou 1997, 1999, 2002]:

$$\vec{q}(\vec{r}, t+\tau) = -k\nabla T(\vec{r}, t).$$ (2.4)

Expanding equation (2.4) in the first order with respect to t yields:

$$\vec{q}(\vec{r}, t) + \tau \frac{\partial \vec{q}}{\partial t} \cong -k\nabla T(\vec{r}, t),$$ (2.5)

and taking the divergence of equation (2.5) in conjunction with the conservation of energy law, equation (2.3), we obtain,

$$C_p \frac{\partial T}{\partial t} + \tau \frac{\partial}{\partial t}\left(C_p \frac{\partial T}{\partial t}\right) = k\nabla \cdot (\nabla T).$$ (2.6)

The CV Model removes the paradox of infinite heat propagation assumed in Fourier's Law as it relates the time delay τ to the thermal wave speed by [Chester 1963]:

$$\tau = \frac{\alpha}{C^2},$$ (2.7)

where α is the thermal diffusivity and C is the thermal wave speed. As C approaches infinity, the relation time decreases to zero ($\alpha = 0$), and the CV Model, equations (2.4) or (2.6), reduces to Fourier's Law [Tzou 1997]. Even though the CV Model allows for a delayed response between the heat flux vector and the temperature gradient, there is still the assumption of an immediate response between the temperature gradient and the energy transport. This response occurs right after the establishment of a temperature gradient across a material volume, meaning there is still the assumption of an instantaneous heat flow. The temperature gradient always causes the heat transfer while the heat flux is always the effect [Tzou 1997]. While the CV Model takes a microscopic approach to the time domain, it still considers the spatial domain to be macroscopic, making it innapropriate to explain the heat transport phenomenon at the micro scale.

2.2 Microscopic Heat Transfer Models

2.2.1 Micro Scale Heat Transfer

At the micro scale, the process of heat transfer is determined by phonon-electron interaction in metallic films and by phonon scattering in dielectric films, conductors and semiconductors [Tien 1998]. The classical theories established at the macro scale, such as heat conduction subjected to Fourier's Law, are not expected to be informative at the micro scale as they describe macroscopic behavior aggregated over many grains. They break down further as the temporal domain becomes extremely small, say, on the order of picoseconds or femtoseconds. A typical case occurs in the ultra fast laser heating in the thermal processing of materials. In this instance, the quasi-equilibrium assumption established in Fourier's Law does not hold along with other macroscopic behaviors.

In this Chapter, we will present some existing micro scale heat transfer models, including the phonon-electron interaction model, the phonon-scattering model, the phonon radiative transfer model and the dual phase lag model. The four models emphasize micro scale effects in time. Rather than a detailed review of each model, we will place an emphasis on the phonon-electron interaction model, as it leads to the microscopic two-step parabolic heat transfer equations, which serves as the basis of our research. To develop a more comprehensive view of the other models, the readers should refer to the papers cited in each section. In this case, special attention should be paid to the review articles by Tien and Chen [Tien 1994] and Duncan and Peterson [Duncan 1994], for those interested in a broader view of micro scale heat conduction, and those by Joseph and Preziosi [Joseph 1989, 1990], and Ozisik and Tzou [Ozisik 1994] for a closer look at the wave theory of heat conduction.

2.2.2 General Properties

Heat transfer requires sufficient collisions among energy carriers regardless of the type of medium where conduction is taking place. In metals, these energy carriers include phonons and electrons. In dielectric crystals, insulators and other semiconductors, phonons are the primary energy carriers. The phonon gas can be viewed as a group of "mass particles" that define the energy state of the metal lattice. For a metal lattice vibrating at a frequency v at a certain temperature T, the energy state of the metal lattice, and therefore the energy state of the phonon, is

$$E = hv, \tag{2.8}$$

with h being the Planck constant. The frequency of the lattice is of the order of tens of terahertz $(10^{13} \, 1/s)$ at room temperature. It can be assumed that the lattice frequency is

proportional to the temperature of the metal lattice. Energy transport can therefore be viewed as the consequence of a series of phonons collisions in time history, as illustrated in Figure 2.1. Bearing energy hv at time t_1, phonon 1 collides with phonon 2 at t_2 and with phonon 3 at time t_3. In the course of each successive collision, energy is transferred from phonon 1 to phonon 2 and 3, causing a successive change of vibrating frequency of phonon 1. To illustrate the phenomenon, the mean free path (d in space) is defined as the algebraic mean of the distances traveled by phonon 1 between the two successive collisions with phonons 2 and 3:

$$d = \frac{d_1 + d_2 + d_3}{3}.$$

(2.9a)

The mean free time τ is defined similarly as the algebraic mean of the times traveled by phonon 1 between the two successful collisions with phonons 2 and 3:

$$\tau = \frac{(\tau_2 - \tau_1) + (\tau_3 - \tau_2) + (t - \tau_3)}{3} = \frac{(t - \tau_1)}{3},$$

(2.9b)
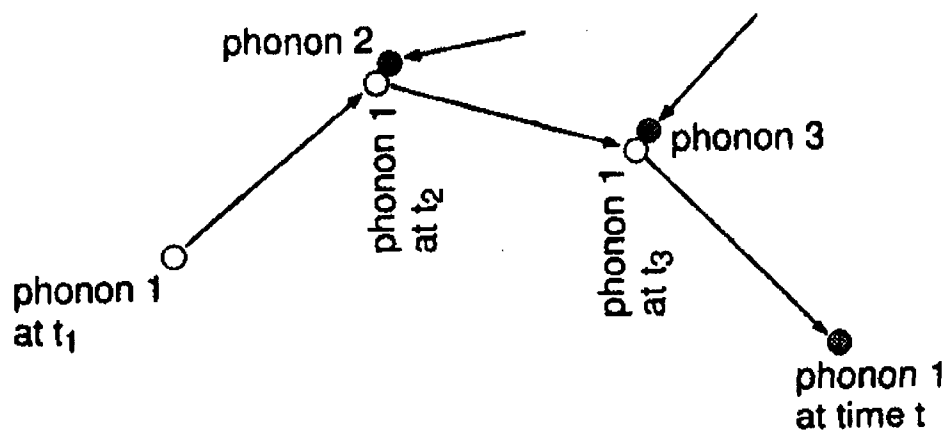
Figure 2.1 Energy Transport through phonon collision [Tzou 1997].

To simplify our analysis, two collisions were used in this example. To determine a statistically meaningful sample space, a "sufficient" number of collisions must be collected to determine the mean free path and the mean free time.

The heat transfer models at the macro scale assume that the physical domain under consideration is so large that hundreds of thousands of phonon collisions are supposed to have occurred before an observation or description of the process of heat transfer is made. Since phonon collision requires a finite amount of time to occur, hundreds of thousands of those collisions would require a sufficiently long time for the process of heat transfer to occur. It is therefore clear that the macroscopic models not only require a sufficiently large physical domain for conducting heat (much larger than the mean free path), but also a sufficiently long time for heat conduction to take place (much longer than the mean free time). It should be pointed out that the sufficiently long time for the stabilization of energy transport by phonons should not be confused with the time required for the steady state to be reached. The sufficiently long time required in phonon collisions is to provide a statistically meaningful concept in regards to the mean free path and the mean free time. The heat transport phenomenon can still be time dependent after phonon transport becomes stabilized. In a phenomenological sense, the mean free time as illustrated in Figure 2.1 is parallel to the characteristic time describing the relaxation behavior in the fast-transient process. For metals, the mean free time, or relaxation time is of the order of picoseconds. In dielectrics crystals and insulators, the relaxation time is longer, roughly of the order of nanoseconds to picoseconds. As a rough estimate, any response time being shorter than one nanosecond should be closely investigated. The fast-transient effect, such as wave behavior in heat conduction, may activate and

introduce unexpected effects in heat transport. Such a threshold value of nanoseconds however depends on the combined effects of geometric configuration (of the specimen) and thermal loading imposed upon the system. It may vary by one order of magnitude if the system involves an abrupt change of geometric curvatures (specifically around a crack or notch tips), or be the subject to discontinuous thermal loading (irradiation of a short pulse laser, for instance).

The mean free path for electrons is of the order of tens of nanometers $\left(10^{-8}\,m\right)$ at room temperature. As a function of temperature, the mean free path's value may increase to the order of millimeters in the liquid helium temperature range, roughly 4 K. The mean free path in phonon collision or phonon scattering (from the boundaries of the grains) is much longer. For example, the mean free path is of the order of tenths of a micron $\left(10^{-7}\,m\right)$ for a type IIa diamond film at room temperature [Majumdar 1993]. As an approximation, a physical device with a characteristic dimension in submicrons deserves special attention. The micro structural interaction effect, such as phonon-electron or phonon scattering, may dramatically enhance heat transfer in short times. Enhancement of heat transfer enlarges the thermal processing zone and increases temperature levels, which in turn may lead to early burnout of micro devices if not properly monitored.

Since the physical dimensions, under consideration at the micro scale, are of the same order of magnitude as the mean free path, and therefore the response time is of the same order of magnitude as the mean free time, the quantities derived from the concept of aggregation at the macro scale need to be reexamined for their meaning in a microscopic environment. The temperature gradient, which had been simply derived in macro scale heat transfer, may lose its physical meaning for a thin film of thickness, the same order of

magnitude as the mean free path. As illustrated in Figure 1.2, while we can still divide the temperature difference $T_2 - T_1$, by the film thickness l ($\cong d$, the mean free path of phonon interaction/scattering) to obtain a "gradient like" quantity, the temperature gradient obtained in this fashion loses its usual physical meaning because of the lack of sufficient energy carriers between the two surfaces of the film and, consequently, the temperature field is discontinuous across the film thickness. Therefore, the concept of temperature gradient fails. Due to this failure, the macroscopic way of ascertaining the heat flux vector assuming Fourier's Law becomes questionable. Thus, there is an immediate ambiguity, which exists in both the concept of temperature gradient and the concept of heat flux, as we introduce the microscopic effects in space in the conventional theories of macro scale heat transfer.

A similar situation appears as the response time for the temperature is analyzed. The typical response time in the thin film is of the same order of magnitude as the mean free time, as a result of phonons traveling in the threshold of the mean free path. If the response time of primary concern (for the temperature or the heat flux vector) is of the same order of magnitude as the mean free time (relaxation time), the individual effects of phonon interaction and phonon scattering must be taken into account in the short time transient of heat transport. Thus we have another situation that requires a closer look at the macroscopic assumptions of heat transfer. From Figure 2.2, it is evident that the macro scale effects in space interfere with the macro scale effects in time. They cannot be separated and must be accounted for *simultaneously* in any framework seeking to develop a theory of heat transfer at the micro scale. This becomes obvious as the finite speed of phonon transport in short time is considered. Phonons propagate at the speed of sound, on

average, which is of the order of 10^4 to 10^5 m/s at room temperature, depending on the

type of solid medium. A response time of the order of picoseconds $\left(10^{-12}\,s\right)$ thus implies

a traveling distance (the penetration depth of heat by phonon transport) of the order of

submicrons $\left(10^{-8}\text{ to }10^{-7}\text{ m}\right)$. Since the penetration depth is microscopic, a simultaneous

consideration of the micro scale effect in space is necessary.
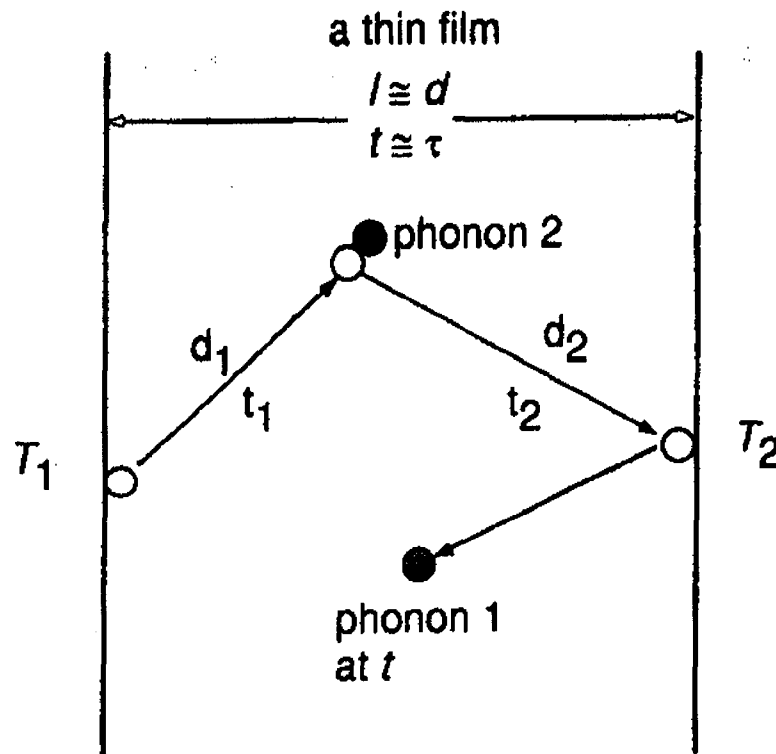
Figure 2.2 Phonon interactions in a film of the same order of magnitude as the mean free path [Tzou 1997].

2.2.3 Phonon-Electron Interaction Model

Phenomenologically, the phonons illustrated in Figures 1.1 and 1.2 can be replaced by

phonons/electrons to depict the phonon-electron interaction for heat transport in metals.

Since the heat capacity of the electrons is one to two orders of magnitude smaller than the

heat capacity of metal lattices, the heating mechanism requires excitation of the electron gas and then the heating of the metal lattice through phonon-electron interaction in short times. The phonon-electron interaction model was proposed to describe this two-step mechanism of heat transfer at the micro scale. The early version of the two-step model (phonon-electron interaction model) was proposed by Kaganov, et al. [Kaganov 1957] and Anisimov, et al. [Anisimov 1974] without a rigorous proof. It remained as a phenomenological model until the efforts of Qiu and Tien [Qiu 1993] placed the two-step model on a quantum and statistical basis. In the next two sections, we derive the two principal phonon-interaction models: the hyperbolic two-step model and the parabolic two-step model.

2.2.4 Hyperbolic Two-Step Model

In the absence of an electrical current during short time heating, the generalized *hyperbolic* constitutive equation for heat transport through the electron gas was derived from the Boltzmann transport equation. Three coupled equations are used to describe the energy exchange between phonons and electrons, the multidimensional case being obtained without much difficulty, we will limit the derivations to the one dimensional case:

$$C_e \frac{\partial T_e}{\partial t} = -\frac{\partial q}{\partial x} - G(T_e - T_l) + S, \qquad (2.10a)$$

$$C_l \frac{\partial T_l}{\partial t} = G(T_e - T_l), \qquad (2.10b)$$

$$\tau_F \frac{\partial q}{\partial t} + K \frac{\partial T_e}{\partial x} + q = 0, \qquad (2.10c)$$

with C denoting the volumetric heat capacity, K the thermal conductivity of the electron gas, subscripts e and l standing for electron and metal lattice, G is the phonon-electron

coupling factor, S represents the heating source, τ_F is the relaxation time evaluated at the Fermi surface, q is the flux, and T is the temperature.

In the first step, the externally supplied photons (the source S) increase the temperature of the electron gas as represented by equation (2.10a). Clearly, diffusion is assumed at this stage. Through phonon-electron interactions, the second step, the hot electron gas then heats up the metal lattice as represented by equation (2.10b). The constitutive equation, equation (2.10c), describes the way in which heat propagates through the electron gas. Distinct from the Cattaneo-Vernotte equation for *macroscopic* thermal waves, equations (2.10a) and (2.10c) describe *micro scale* heat transport through the electron gas. Consequently, the thermal conductivity (K) in the phonon-electron system may vary with the microscopic quantities such as the electron temperature. The quantity τ_F is the relaxation time calculated at the Fermi surface:

$$\tau_F = (2)^{4/3} \Lambda^{-1} \left(\frac{T_D}{T_l} \right) E_0 E^{3/2} , \tag{2.11}$$

where E_0 is the Fermi energy of electrons at 0 K, T_D is the Debye temperature, and Λ is a constant defined as

$$\Lambda = \frac{3\pi^2 P^2 (m/2)^{1/2}}{M \kappa T_D} \left(\frac{3}{4\pi\Delta} \right)^{1/3} , \tag{2.12}$$

with P standing for the transient matrix element, m the effective mass of electrons, M the atomic mass, κ the Boltzmann constant, and Δ the average volume of the unit cell [Qiu 1993]. The energy exchange between phonons and electrons is characterized by the coupling factor G, as shown by [Qiu 1992],

$$G = \frac{\pi^4 \left(n_e v_s \kappa \right)^2}{K} .$$ (2.13)

The coupling factor depends on the number density of free electrons in per unit volume (n_e), the Boltzmann constant κ, and the speed of sound v_s:

$$v_s = \frac{\kappa}{2\pi h} \left(6\pi^2 n_a \right)^{-\frac{1}{3}} T_D .$$ (2.14)

The phonon-electron coupling factor, through the speed of sound, is further dependent on the Planck constant (h), the atomic number density per volume (n_a), and the Debye temperature T_D. [Qiu 1992] showed that the s-band approximation provides an accurate estimate for the number density of free electrons in pure metals. The volumetric heat capacities of the electron gas and the metal lattice, C_e and C_l in equations (2.10a) and (2.10b), respectively, are functions of the electron gas temperature (T_e) and the lattice temperature (T_l). Qiu and Tien, [Qiu 1992, 1993], numerically solved equation (2.10a) by specifying the heat source term, $S(x, t)$, as the energy absorption rate in a gold film with the laser wavelength in the visible light range. The film thickness was $0.1\ \mu m$, and the laser pulse duration was 100 femtoseconds. The predicted temperature change in the electron gas established in picoseconds agreed well with the experimental data. The classical diffusion model and the thermal wave models, owing to the absence of modeling the micro structural effect in the short-time transient, predicted a *reversed* trend for the surface reflectivity at the rear of the thin film. The analysis supported the hyperbolic two-step model when used to describe the heat transfer phenomenon during short pulse laser heating of metals.

To explore the *wave* structure of temperatures behind equations (2.10a) to (2.10c), we will focus on the metal-lattice temperature (T_l) by eliminating the electron gas temperature from equations (2.10a) to (2.10c). Since the temperature-dependent properties, such as the volumetric heat capacity of the electron gas, only affect the quantitative behavior of the temperature waves while the fundamental behavior remains unchanged, all the thermal properties are assumed constant in the treatment to follow. Differentiating equation (2.10a) with respect to t,

$$C_e \frac{\partial^2 T_e}{\partial t^2} = -\frac{\partial^2 q}{\partial x \partial t} - G \frac{\partial}{\partial t}(T_e - T_l) + \frac{\partial S}{\partial t}, \qquad (2.15a)$$

and equation (2.10c) with respect to x,

$$\tau_F \frac{\partial^2 q}{\partial x \partial t} + K \frac{\partial^2 T_e}{\partial x^2} + \frac{\partial q}{\partial x} = 0, \qquad (2.15b)$$

and combining the results with equation (2.10a) to eliminate the terms $\partial^2 q / \partial x \partial t$ and $\partial q / \partial x$, the following equation is obtained:

$$K \frac{\partial^2 T_e}{\partial x^2} + \left(S + \tau_F \frac{\partial S}{\partial t} \right) = C_e \frac{\partial T_e}{\partial t} + C_e \tau_F \frac{\partial^2 T_e}{\partial t^2} + G(T_e - T_l) + \tau_F G \frac{\partial}{\partial t}(T_e - T_l). \qquad (2.16)$$

The quantities T_e and $(T_e - T_l)$ can be related to the lattice temperature by equation (2.10b):

$$T_e = T_l + \frac{C_l}{G} \frac{\partial T_l}{\partial t}, \quad \text{consequently}, \quad T_e - T_l = \frac{C_l}{G} \frac{\partial T_l}{\partial t}. \qquad (2.17)$$

Substituting equation (2.17) into equation (2.16) results in

$$\frac{\partial^2 T}{\partial x^2} + \left(\frac{C_l}{G} \right) \frac{\partial^3 T}{\partial x^2 \partial t} + \frac{1}{K} \left(S + \tau_F \frac{\partial S}{\partial t} \right)$$

$$= \tau_F \left(\frac{C_e C_l}{KG} \right) \frac{\partial^3 T}{\partial t^3} + \left[\frac{\tau_F (C_e + C_l)}{K} + \frac{C_e C_l}{KG} \right] \frac{\partial^2 T}{\partial t^2} + \left[\frac{C_e + C_l}{K} \right] \frac{\partial T}{\partial t}, \tag{2.18}$$

where $T \equiv T_l$, with the subscript "l" omitted for simplicity. The mixed-derivative term involving the second-order derivative in space and the first-order derivative in time, $\partial^3 T / \partial x^2 \partial t$, is a common feature of both parabolic and hyperbolic two-step models. In the presence of τ_F, (1) the time derivative in the energy equation is raised to the *third order* and (2) an *apparent* heat source term containing the time derivative of the real heat source applied to the body, ($\partial S / \partial t$), exists. While the third-order time derivative alters the fundamental structure of the temperature solution, the apparent heating in equation (2.18) resembles that in the classic thermal wave model [Frankel 1985].

Along with the relaxation time of the electron gas (τ_F), the phonon-electron coupling factor G is the most important factor characterizing equation (2.18). In the case that τ_F approaches zero and G approaches infinity, implying that either the number density of free electrons (n_e) approaches infinity (according to equation (2.13)), or the speed of sound approaches infinity (the atomic number density per unit volume n_a approaches zero according to equation (2.14)); equation (2.18) reduces to the classical diffusion equation. Fourier's Law embedded in diffusion thus inherits all these assumptions.

2.2.5 Parabolic Two-Step Model

As the relaxation time of the electron gas calculated at the Fermi surfaces, τ_F, vanishes, the hyperbolic two-step model perfectly reduces to the *parabolic* two-step model originally proposed by Kaganov, et al. [Kaganov 1957] and Anisimov, et al. [Anisimov 1974].

Equations (2.10a) to (2.10c) become

$$C_e \frac{\partial T_e}{\partial t} = -\frac{\partial q}{\partial x} - G(T_e - T_l) + S, \qquad (2.19a)$$

$$C_l \frac{\partial T_l}{\partial t} = G(T_e - T_l), \qquad (2.19b)$$

$$K \frac{\partial T_e}{\partial x} + q = 0. \qquad (2.19c)$$

Differentiating equation (2.19c) with respect to x yields

$$K \frac{\partial^2 T_e}{\partial x^2} + \frac{\partial q}{\partial x} = 0. \qquad (2.20)$$

Solving for the term $(\partial q / \partial x)$ in equation (2.20) and substituting in equation (2.19a),

$$C_e \frac{\partial T_e}{\partial t} = K \frac{\partial^2 T_e}{\partial x^2} - G(T_e - T_l) + S, \qquad (2.21a)$$

$$C_l \frac{\partial T_l}{\partial t} = G(T_e - T_l). \qquad (2.21b)$$

Mathematically, we can generalize equations (2.21a) and (2.21b) to three dimensions, thus obtaining the generalized parabolic two-step model,

$$C_e \frac{\partial T_e}{\partial t} = \nabla \bullet (K \nabla T_e) - G(T_e - T_l) + S, \qquad (2.22a)$$

$$C_l \frac{\partial T_l}{\partial t} = G(T_e - T_l). \qquad (2.22b)$$

The energy exchange is still characterized by the phonon-electron coupling factor G [Kaganov 1957]:

$$G = \frac{\pi^2}{6} \frac{m_e n_e v_s^2}{\tau_e T_e} \quad \text{for} \quad T_e \gg T_l, \qquad (2.23)$$

where m_e represents the electron mass, n_e the number density (concentration) of

electrons per unit volume, τ_e the electronic relaxation time and v_s the speed of sound.

The electron gas temperature (T_e) is much higher than the metal lattice temperature (T_l) in the early-time response. The condition of $T_e \gg T_l$ in equation (2.23) for the applicability of the G expression is thus valid in the fast-transient process of electron-phonon dynamics. Within the limits of Wiedemann-Frenz's Law, which states that for metals of moderate temperatures (roughly for $T_l > 0.48T_D$) the ratio of thermal conductivity to the electrical conductivity is proportional to the temperature [Tzou 1997], and the constant of proportionality is independent of the particular metal (a metal-type-independent constant), the electronic thermal conductivity can be expressed as

$$K = \frac{\pi^2 n_e \kappa^2 \tau_e T_e}{3m_e},$$ (2.24)

resulting in

$$m_e = \frac{\pi^2 n_e \kappa^2 \tau_e T_e}{3K}.$$ (2.25)

Substituting equation (2.25) into equation (2.23) for the electron mass gives

$$G = \frac{\pi^4 \left(n_e v_s \kappa\right)^2}{18K}.$$ (2.26)

The phonon-electron coupling factor, therefore, depends on the thermal conductivity (K) and the number density (n_e) of the electron gas. Through the speed of sound, it further depends on the number density of the atoms (n_a) and the Debye temperature (T_D). The coupling factor does not show a strong dependence on the electron gas temperature (T_e), and it does not seem to be affected by the electronic relaxation time τ_e.

To estimate the value of the phonon-electron coupling factor G according to equation (2.26), the number density of the electron gas (n_e) is a crucial quantity. Qiu and Tien

[Qiu 1992] assumed one free electron per atom for noble metals (silver (Ag) and gold (Au), for example) and employed the s-band approximation for the valence electrons in transition metals. Due to the relatively heavy mass of the d-band electrons in the valence electrons, only a fraction of the s-band electrons can be viewed as free electrons. The value of (n_e), therefore, is chosen as a fraction of the valence electrons. The phonon-electron coupling factor thus calculated, and the experimentally measured values are listed in Table 2.1 for comparison [Qiu 1992]. Except for copper (Cu) and lead (Pb), which may exhibit certain ambiguous transition characteristics, the s-band approximation seems to agree well with the experimental results.

Table 2.1 Phonon-electron coupling factor G for some noble and transition metals [Qiu 1992]

Metal	Calculated, $\times 10^{16}$ W/m^3 K	Measured, $\times 10^{16}$ W/m^3 K
Cu	14	4.8 ± 0.7 [Brorson 1990] 10 [Elsayed-Ali 1987]
Ag	3.1	2.8 [Groeneveld 1990]
Au	2.6	2.8 ± 0.5 [Brorson 1990]
Cr	45 ($n_e / n_a = 0.5$)	42 ± 5 [Brorson1990]
W	27 ($n_e / n_a = 1.0$)	26 ± 3 [Brorson 1990]
V	648 ($n_e / n_a = 2.0$)	523 ± 37 [Brorson 1990]
Nb	138 ($n_e / n_a = 2.0$)	387 ± 36 [Brorson 1990]
Ti	202 ($n_e / n_a = 1.0$)	185 ± 16 [Brorson 1990]
Pb	62	12.4 ± 1.4 [Brorson 1990]

As a general trend, a higher free electron number density (n_e) and a higher Debye temperature (T_D) would result in higher values of G and smaller values of the electronic relaxation time τ_e.

From a mathematical point of view, equations (2.22a) and (2.22b) provide two equations for two unknowns, the electron gas temperature (T_e) and the metal lattice temperature (T_l). They can be solved in a coupled manner, or they can be combined to obtain a *single* energy equation, describing heat transport through phonon-electron interaction in micro scale, similar to equation (2.18). The complexity of the solutions for equations (2.22a) and (2.22b) lies in the temperature dependent heat capacity of the electron gas, i.e., $C_e \equiv C_e(T_e)$. For an electron gas temperature lower than the Fermi temperature, which is of the order of $10^4 K$, the electron heat capacity is proportional to the electron gas temperature. Such temperature dependence makes equations (2.22a) and (2.22b) nonlinear. For a gold film subjected to femtoseconds laser heating, Qiu and Tien [Qiu 1992] employed the Crank-Nicholson finite difference scheme to obtain numerical solutions. Comparing to experimental results, the normalized temperature change in the electron gas is identical to the normalized reflectivity change on the film surfaces:

$$\frac{\Delta R}{(\Delta R)_{max}} = \frac{\Delta T_e}{(\Delta T_e)_{max}}, \tag{2.27}$$

where R denotes the reflectivity and the subscript "max" refers to the maximum value occurring in the transient process. Both ratios in equation (2.27) are less than one. The left hand side of equation (2.27) can be measured by the front-surface-pump and back-surface-probe technique [Brorson 1987], [Elsayed-Ali 1991], [Qiu 1994a, 1994b]. The right hand side of equation (2.27), is obtained by solving equations (2.22a) and (2.22b)

for the electron gas temperature and normalizing with respect to the maximum value in the transient response time at various times [Qiu 1992]. For a gold film subjected to irradiation of a 96 femtoseconds (fs, 10^{-15} s) laser with an energy flux of 1 mJ/cm^2, the results of the reflectivity change at the front surface of the film are reproduced in Figure 2.3 [Qiu 1992].

Figure 2.3 Transient reflectivity change at the front surface of gold films (thickness of 0.05 and 0.1 μm) subjected to laser irradiation (pulse width 96 fs, energy flux 1 mJ/cm^2) [Qiu 1992], [Brorson 1987].

The time delay indicated on the horizontal axis is the time difference between the pump (heating) and the probe (detecting) lasers, which is equivalent to the physical time in the transient response. For both thicknesses of the films, 0.05 and 0.1 μm, the microscopic two-step model describing the phonon-electron interaction effect captures the heating $\left(0 \leq t \leq 0.096 \text{ picoseconds (ps)}\right)$ and thermalization $\left(0.096 \leq t \leq 3 \text{ps}\right)$ processes of the

electron gas temperature. The temperature level, as expected, increases as the thickness

of the film decreases. The classical theory of diffusion, which assumes an immediate

equilibrium between phonons (lattice) and electrons and is called the one-step heating

model by [Qiu 1992], fails to describe the fast energy transport process. Particularly in

the thermalization stage, it clearly overestimates the transient temperature. The transient

temperature at the front surface does not seem to depend on the film thickness according

to the diffusion model. The transient temperature remains almost at the same level as the

film thickness increases from 0.05 to 0.1 μm.
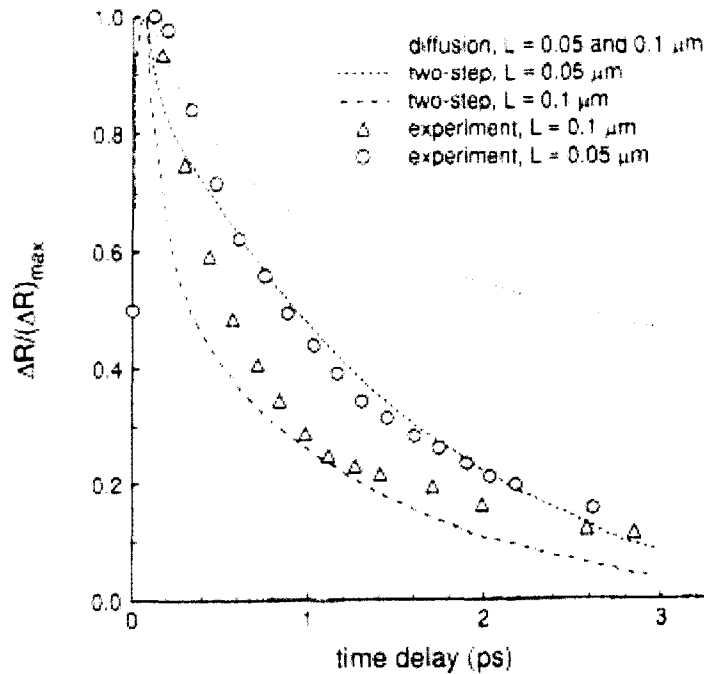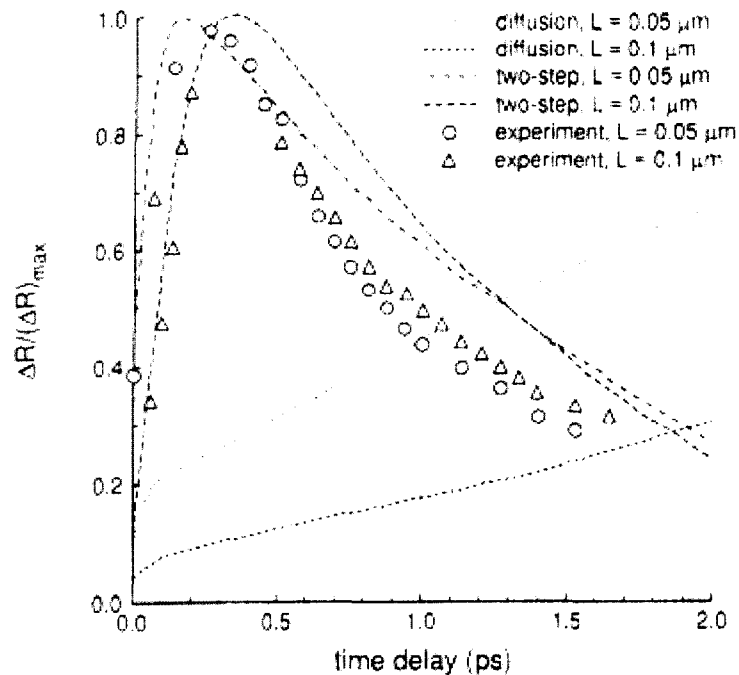

Figure 2.4 Transient reflectivity change at the rear surface of gold films (thickness of
0.05 and 0.1 μm) subjected to laser irradiation (pulse width 96 fs, energy flux 1 mJ/cm^2)
[Qiu 1992], [Brorson 1987].

Figure 2.4 shows the transient reflectivity change at the rear surface of the film. The

difference in time (between the heating and thermalization stages) increases with film

thickness. Thus, the plot displays a "wave like" behavior even as we assume diffusion of heat transport through the electron gas. The one-step heating model (diffusion) fails to describe the thermalization process at the rear surface of the film. Unlike Figure 1.3, where the qualitative trend was preserved in the same domain of response times, the heating stage predicted by the diffusion model shown in Figure 2.4 (the rear surface) lasts beyond the threshold of 2 ps, resulting in a transient response of reflectivity change that significantly differs from the experimental result, both quantitatively and qualitatively. From Figures 2.3 and 2.4, it is clear that, for metals, the microscopic phonon-electron interaction is an important effect to be incorporated for an accurate description of micro scale heat transport. In addition to the familiar thermal properties such as heat capacity and thermal conductivity, the phonon-electron coupling factor describing the short-time energy exchange between phonons and electrons is a dominating property in the fast-transient process of laser heating.

Similar to the hyperbolic two-step model, we can derive a single energy equation for the parabolic two-step model by combining equations (2.22a) and (2.22b). Given their forms, equations (2.22a) and (2.22b) can be solved simultaneously for (Te) and (T_l). This coupled approach is a more efficient numerical method, and we will use that approach in this study. The derivation of the single energy will illustrate the fact, as seen in equation (2.18) for the hyperbolic model, that the appearance of mixed order derivative makes the single energy equation less numerically efficient. In the following derivation, the characteristics of the electron gas and lattice temperatures, all thermal properties, including heat capacities for the electron gas (C_e) and metal lattice (C_l) as well as the thermal conductivity (K), are assumed to be temperature independent (i.e. constant).

A single energy equation governing the lattice temperature can be obtained by eliminating the electron gas temperature, T_e, from equations (2.22a) and (2.22b).

From equation (2.22b), the electron gas temperature can be expressed in terms of the metal lattice temperature and its time derivative:

$$T_e = T_l + \frac{C_l}{G}\frac{\partial T_l}{\partial t}. \tag{2.28}$$

Substituting equation (2.28) into equation (2.22a), and using the result of $G(T_e - T_l)$ from equation (2.22b) results in

$$\nabla^2 T_l + \left(\frac{C_l}{G}\right)\frac{\partial}{\partial t}\nabla^2 T_l = \left(\frac{C_l + C_e}{K}\right)\frac{\partial T_l}{\partial t} + \left(\frac{C_l C_e}{KG}\right)\frac{\partial^2 T_l}{\partial t^2}. \tag{2.29}$$

Equation (2.29), governing the lattice temperature alone, introduces a new type of energy equation in conductive heat transfer. It has a usual diffusion term $\left(\partial T_l / \partial t\right)$, a thermal wave term $\left(\partial^2 T_l / \partial t^2\right)$, and a mixed-derivative term $\left(\partial\left[\nabla^2 T_l\right]/\partial t\right)$ that reflects the combined effects of microscopic phonon-electron interaction and macroscopic diffusion. In the case that the phonon-electron coupling factor G approaches infinity $(G \to \infty)$, implying that the energy transfer from electrons to phonons is occurring at an infinite rate, equation (2.29) reduces to the conventional diffusion equation employing Fourier's Law, with the coefficient $(C_e + C_l)/K$ appearing as the equivalent thermal diffusivity.

A single energy equation describing the electron gas temperature can be obtained similarly. From equation (2.22a),

$$T_l = T_e - \frac{K}{G}\nabla^2 T_e + \frac{C_e}{G}\frac{\partial T_e}{\partial t}. \tag{2.30}$$

Substituting equation (2.30) into equation (2.22b), and using the result of $G(T_e - T_l)$

from equation (2.22a) results in

$$\nabla^2 T_e + \left(\frac{C_l}{G}\right)\frac{\partial}{\partial t}\nabla^2 T_e = \left(\frac{C_l + C_e}{K}\right)\frac{\partial T_e}{\partial t} + \left(\frac{C_l C_e}{KG}\right)\frac{\partial^2 T_e}{\partial t^2}. \tag{2.31}$$

It comes as no surprise that equation (2.31) has the same exact form as equation (2.29).

2.3 Previous Work

High-power lasers play an important role in the fabrication of micro scale devices. Due to the microscopic size of the devices, the thermal process needs to be carefully monitored to prevent thermal damages [Al-Nimr 1997a, 1997b, 1999]. The use of continuous-pulse or long-pulse lasers in micro manufacturing creates a risk of melting the micro device under fabrication. The immediate consequence is an uncontrollable spreading of the thermal process zone. As an alternative, ultrashort-pulsed lasers with pulse durations of the order of sub-picosecond to femtosecond domain possess exclusive capabilities in limiting the spread of the thermal process zone [Qiu 1992], [Antaki 2002]. For an ultrashort-pulsed laser, the heating of the material involves a high-rate flow from electrons to lattices in the picosecond time domain. Depending on the temperature, electrons have a heat capacity two to three orders of magnitude smaller than that of metal lattices [Tzou 1997]. When the external photons are supplied by the lasers, the laser energy is primarily absorbed by the free electrons that are confined within skin depth during the excitation. Electrons first shoot up to several hundreds or thousands of degrees within a few picoseconds without disturbing the metal lattices. A major portion of the thermal electron energy is then transferred to the lattices. Meanwhile, another part of the energy diffuses to the electrons in the deeper regions of the target [Kaganov 1957]

[Anisimov 1974] [Qiu 1993] [Tien 1994]. Because the laser pulse is so short, the laser is turned off before thermal equilibrium between the electron gas and the lattices is reached [Al-Nimr 1999, 2000a, 2001, 2003], [Fujimoto 1984]. In this time interval, the heat flux is essentially limited to the region within the electron thermal diffusion length. This stage is termed non-equilibrium heating due to the large difference in temperature between the electron gas and the metal lattice. The lattice temperature then increases as a result of phonon-electron coupling, resulting in a new thermal property called the phonon-electron interaction factor. The energy equations describing the continuous energy flow from the hot electron gas to the metal lattice during non-equilibrium can be written as [Kaganov 1957], [Anisimov 1974], [Qiu 1993]:

$$C_e \frac{\partial T_e}{\partial t} = \nabla \cdot (K \nabla T_e) - G(T_e - T_l) + S, \tag{2.22a}$$

$$C_l \frac{\partial T_l}{\partial t} = G(T_e - T_l), \tag{2.22b}$$

with C denoting the volumetric heat capacity, K the thermal conductivity of the electron gas, subscripts e and l standing for electron and metal lattice, G is the phonon-electron coupling factor, S represents the ultrashort-pulsed laser heating source, and T is the temperature. In the classical theory of diffusion, $T_e = T_l$ because of the equilibrium condition in Fourier's Law; thus, equations (2.22a) and (2.22b) reduce to the classical heat conduction equation at equilibrium. However, for sub-picosecond and sub-micro scale conditions, $T_e \geq T_l$ during the non-equilibrium heating stage. The significance of the heat transport equations (2.22a) and (2.22b) as opposed to the classical conduction equation has been discussed in the previous sections.

The above coupled equations, often referred to as the parabolic two-step micro heat transport equations, have been widely applied for thermal analysis of thin metal films exposed to picosecond thermal pulses. Among these studies, Qiu and Tien, [Qiu 1992, 1993, 1994a, 1994b] studied the heat transfer mechanism during short-pulse laser heating of metals using both experimental and numerical methods. Joshi and Majumdar, [Joshi 1993], obtained a numerical solution using the explicit upstream difference method. Tzou and others, [Tzou 1997], [Al-Nimr 2000b], [Antaki 1998a, 1998b], [Chen 1999, 2000, 2001a], [Ho 2003], [Wang 2000, 2001a, 2001b, 2002], modified equations (2.22a) and (2.22b) by introducing the concept of a dual-phase-lag. They developed both analytical and numerical methods to study the lagging behavior in micro scale heat transfer. [Tzou 1997] contains most of the early formulations and results obtained by the dual-phase-lag model. In [Tzou 1997] and [Ozisik 1994], the dual-phase-lag model was considered in one dimension, and the heat flux was eliminated to derive a dimensionless heat transport equation. The lagging behavior was investigated with the new equation in a semi-infinite interval. The solutions were obtained by using the Laplace transform method and the Riemann-sum approximation for the inversion.

Additionally, [Ozisik 1994] investigated three major issues: the engineering applications of the thermal wave theory, the special features that existed in the thermal wave propagation, and the relationship between the thermal wave model and the microscopic two-step model. The study showed that special features in thermal wave propagation included the sharp wavefront and rate effects, the thermal shock phenomenon, the thermal resonance phenomenon, and reflections of thermal waves across a material interface. Using the dual-phase-lag concept, the study established that

the governing energy equation could be reduced to the heat transport equation through the metal lattice in the microscopic two step model.

Chen and Beraun employed the corrective smoothed particle method to obtain a numerical solution of ultrashort laser pulse interactions with metal films [Chen 1999, 2000, 2001a, 2001b]. The study introduces a dual hyperbolic two-step radiation heating to investigate the ultrashort laser pulse interactions with the films, thus providing an extension of Qiu and Tien's theory by the introduction of the effect of heat conduction in the metal lattice. Furthermore, to account for the ballistic behavior in particle transport, the study introduces a modified laser intensity depth distribution by adding the ballistic range to the optical penetration depth. The study then proceeded to compare their results to the existing models, the parabolic two-step method, Qiu and Tien's proposed models and Fourier's Law of heat conduction, which were solved by using a mesh-free particle method. The numerical analysis was performed with gold films and the results were compared to the experimental data of Qiu, Jubhasz, Suarez, Bron, Tien, Wellershoff, Hohfeld, Gudde, and Matthais. The study showed that Chen's method is a better predictor of the thermal response. It also showed that the inclusion of the ballistic effect to the depth distribution of the laser intensity significantly improves the melting threshold fluence prediction.

Tang and Araki introduced a generalized macroscopic model in the treatment of transient heat conduction problems in finite rigid slabs under short-pulse laser irradiation. The analytical solution is derived by using Green's function method and a finite integral transform technique [Tang 1999].

In [Lin 1997], the authors attempt to investigate the possibility of a unified heat conduction equation, and an analytic solution was obtained by using Fourier's series. A discussion of the exact solution shows a discrepancy between some of Lin's results and previous results obtained by [Tzou 1997].

Al-Nimr and Arpaci proposed a new method, based on a physical decoupling of the two-step hyperbolic model, to study the effects of radiative and convective thermal losses during short-pulse lasers heating of thin film metals [Al-Nimr 1997a, 1997b, 1999, 2001, 2003]. The decoupling keeps the basic two-step model assumption that the metal film thermal behaviors occurs in two phases. An initial phase during which the electron gas energy is transferred to the metal lattice through phonon-electron coupling, other mechanisms of heat transport are considered to be negligible at this stage, and a secondary phase, where thermal equilibrium is reached between the electron gas and the metal lattice. At this stage, the phonon-electron coupling is considered negligible and thermal diffusion is the transport method that dominates. This method succeeds in eliminating the coupling between the hyperbolic equations, thus making the resulting differential equations easier to manipulate. An applicability criterion is developed for metal films whenever the dimensionless parameter $\dfrac{GL^2}{K_e}$ is much larger than 1.

Dai and Nassar developed several unconditionally stable finite difference schemes to solve a dual-phase-lag heat transport equations [Dai 1999, 2000b, 2001a]. Additionally, they developed several domain decomposition methods to solve Tzou's dimensionless heat transport equation in double layered films, [Dai 2000a, 2001b], and devised an approximate analytic method to solve the dual-phase-lag equations [Dai 2002]. In

collaboration with Shen, they developed a convergent finite difference scheme to solve the dual-phase-lag heat transport equations in spherical coordinates [Dai 2004].

Wang, Zhou and Xu developed techniques to measure the phase-lags of the heat flux and the temperature gradients. They derived analytical solutions for one to three dimensional heat conduction domains under arbitrary initial and boundary conditions. Furthermore, structural theorems were developed for mixed and Cauchy problems of dual-phase-lag heat transport. The studies included a proof of the well-posedness of the dual-phase-lag model under Dirichlet, Neumann and Robin's boundary conditions [Wang 2000, 2001a, 2001b, 2002].

CHAPTER 3

MATHEMATICAL MODEL AND FINITE

DIFFERENCE SCHEME

3.1 Mathematical Model

3.1.1 Problem Description

This chapter investigates the heat transport phenomenon in a microsphere subjected to an ultrashort laser pulse. As described in Chapter Two, there is a risk of cracking during the microfabrication process. These cracks may lead to an accumulation of energy in the neighborhood of the cracks. Additionally, microvoids may form during the thermal processing of materials due to thermal expansion. When such impurities occur in the work piece, the thermal energy in their neighborhood may be amplified which could result in severe damage and, consequently, lead to a total failure of the thermal processing. A detailed understanding of the way dissipation occurs in the defects is thus crucial not only to prevent damage to the micro device but also to optimize the thermal process [Tzou 1997]. From a microfabrication standpoint, a micro sphere is an important component in the fabrication of microelectronic devices, and understanding the temperature distribution at the sub-atomic level as well as in the metal lattice is the

34

subject of important investigations. Geometrically, since the dimensions of a microsphere relate favorably to those of elementary physical particles, the micro sphere can be used to model the heat transport phenomenon in physical particles. Thus, a clear understanding of the temperature distribution in this microelectronic device is of vital importance. To this end, the well-posedness of the problem is investigated; a numerical scheme is proposed to solve the governing equations. A stability analysis of the scheme is done and the scheme will be applied to numerical examples.

3.1.2 Geometry Description

Figure 3.1 shows a sphere in a three-dimensional coordinates system. Considering the spherical coordinates system, the point P is defined by the following spherical coordinates: r, θ, φ, where r is the length OP, ranging from 0 to ∞; θ is the angle between the projection of OP on the xy-plane with the positive x-axis ranging from 0 to 2π; φ is the angle between OP and the positive z-axis ranging from 0 to π.
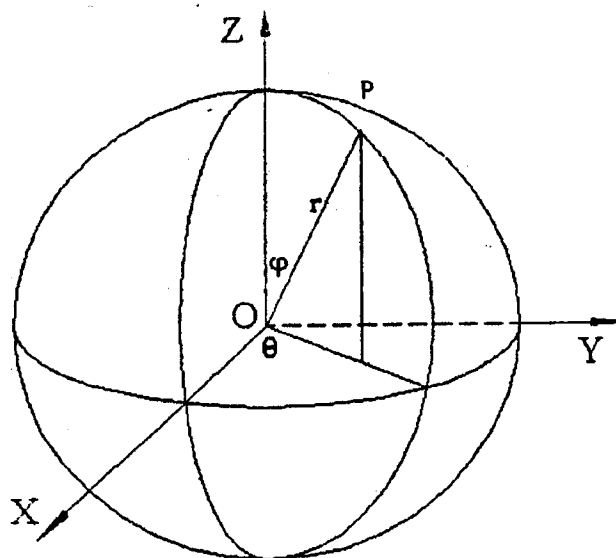
Figure 3.1 Spherical coordinates system.

3.1.3 Governing Equations

Using the two-step parabolic heat transport equations at the microscale to model the microsphere, we take advantage of the geometry of the sphere by rewriting equations (2.22a) and (2.22b) in spherical coordinates. The spherical coordinates of a point P (r, θ, φ) are related to x, y, and z as follows:

$$x = r \sin \varphi \cos \theta, \qquad y = r \sin \varphi \sin \theta, \qquad z = r \cos \varphi.$$
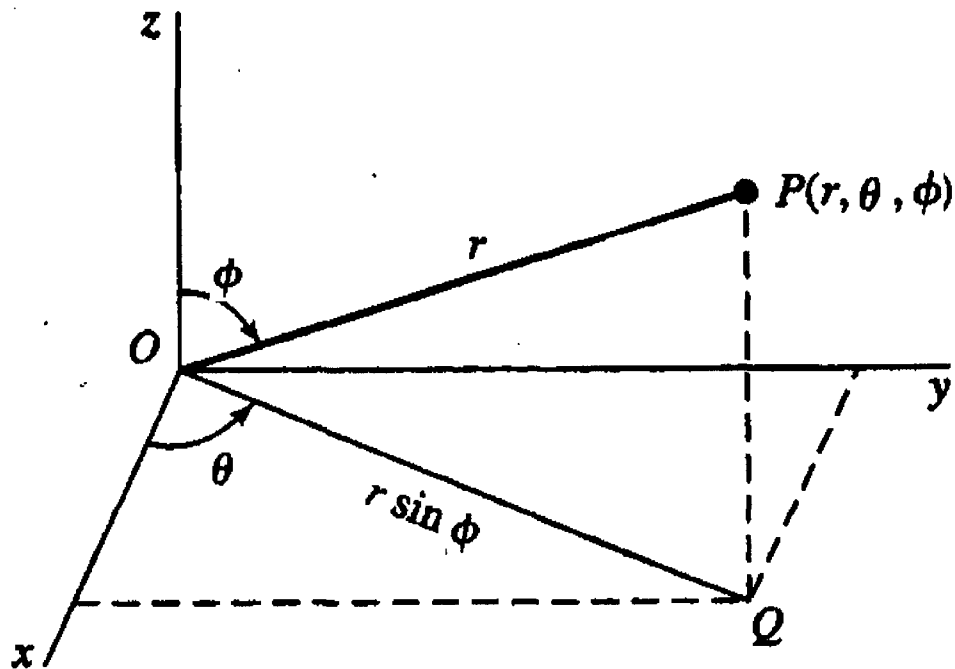
Figure 3.2 Change of Coordinates

Performing the derivations as in [Brown 2001], we obtain

$$C_e \frac{\partial T_e}{\partial t} = \frac{k_e}{r^2} \frac{\partial}{\partial r} \left(r^2 \frac{\partial T_e}{\partial r} \right) + \frac{k_e}{r^2 \sin^2 \varphi} \frac{\partial^2 T_e}{\partial \theta^2}$$

$$+ \frac{k_e}{r^2 \sin^2 \varphi} \frac{\partial}{\partial \varphi} \left(\sin \varphi \frac{\partial T_e}{\partial \varphi} \right) - G(T_e - T_l) + S, \tag{3.1}$$

$$C_l \frac{\partial T_l}{\partial t} = G(T_e - T_l), \tag{3.2}$$

where r, θ, φ are the spherical coordinates with $0 < r < L, 0 \leq \theta \leq 2\pi, 0 < \varphi < \pi$.

3.1.4 Initial and Boundary Conditions

The initial conditions are assumed to be

$$T_e(r, \theta, \varphi, 0) = T_l(r, \theta, \varphi, 0) = T_0, \tag{3.3}$$

$$\frac{\partial T_e(r, \theta, \varphi, 0)}{\partial t} = \frac{\partial T_l(r, \theta, \varphi, 0)}{\partial t} = 0 \tag{3.4}$$

and the boundary conditions are

$$\frac{\partial T_e(r, \theta, 0, t)}{\partial \varphi} = \frac{\partial T_e(r, \theta, \pi, t)}{\partial \varphi} = 0, \quad \frac{\partial T_l(r, \theta, 0, t)}{\partial \varphi} = \frac{\partial T_l(r, \theta, \pi, t)}{\partial \varphi} = 0; \tag{3.5}$$

$$\frac{\partial T_e(L, \theta, \varphi, t)}{\partial r} = \frac{\partial T_l(L, \theta, \varphi, t)}{\partial r} = 0; \tag{3.6}$$

$$T_e(r, \theta, \varphi, t) = T_e(r, \theta + 2\pi, \varphi, t), \quad T_l(r, \theta, \varphi, t) = T_l(r, \theta + 2\pi, \varphi, t). \tag{3.7}$$

These boundary conditions arise when the micro sphere is subjected to an ultrashort pulse

laser irradiation. Due to the extremely short time domain, it can be assumed that no heat

losses occur at the boundary (equation 3.6), and due to the symmetric nature of the sphere

equations (3.5) and (3.8) are obtained [Tzou 1997]. For simplicity of the theoretical

analysis, we will further assume that

$$\frac{\partial T_e(0, \theta, \varphi, t)}{\partial r} = \frac{\partial T_l(0, \theta, \varphi, t)}{\partial r} = 0. \tag{3.8}$$

3.2 Energy Estimate and Well-Posedness

THEOREM 1. Assume that the coefficients C_e, C_l, k_e and G are positive constants, and that the solutions T_e and T_l of the above initial and boundary value problem are smooth. A stronger estimate holds as follows:

$$F(t) \le e^t [F(0) + \int_0^t \Phi(s) ds], \tag{3.9}$$

where

$$F(t) = C_e \int_0^L \int_0^{2\pi} \int_0^\pi r^2 T_e^2 \sin\varphi \, dr d\theta d\varphi + C_l \int_0^L \int_0^{2\pi} \int_0^\pi r^2 T_l^2 \sin\varphi \, dr d\theta d\varphi, \tag{3.10}$$

and

$$\Phi(t) = \frac{1}{C_e} \int_0^L \int_0^{2\pi} \int_0^\pi r^2 S^2 \sin\varphi \, dr d\theta d\varphi, \tag{3.11}$$

which implies that the problem is well-posed in the sense of the definition described in [Strikwerda 1989].

Proof. Multiplying equation (3.1) by $r^2 T_e \sin\varphi$ and equation (3.2) by $r^2 T_l \sin\varphi$, and integrating over the domain $\{0 \le r \le L, 0 \le \theta \le 2\pi, 0 \le \varphi \le \pi\}$, and summing the results together, we obtain

$$\int_0^L \int_0^{2\pi} \int_0^\pi C_e r^2 \sin\varphi \frac{\partial T_e}{\partial t} T_e \, dr d\theta d\varphi + \int_0^L \int_0^{2\pi} \int_0^\pi C_l r^2 \sin\varphi \frac{\partial T_l}{\partial t} T_l \, dr d\theta d\varphi$$

$$= \int_0^L \int_0^{2\pi} \int_0^\pi k_e \sin\varphi T_e \frac{\partial}{\partial r}\left(r^2 \frac{\partial T_e}{\partial r}\right) dr d\theta d\varphi + \int_0^L \int_0^{2\pi} \int_0^\pi \frac{k_e}{\sin\varphi} T_e \frac{\partial^2 T_e}{\partial \theta^2} dr d\theta d\varphi$$

$$+ \int_0^L \int_0^{2\pi} \int_0^\pi k_e \sin\varphi T_e \frac{\partial}{\partial \varphi}\left(\sin\varphi \frac{\partial T_e}{\partial \varphi}\right) dr d\theta d\varphi - \int_0^L \int_0^{2\pi} \int_0^\pi r^2 \sin\varphi \, G(T_e - T_l) dr d\theta d\varphi$$

$$+ \int_0^L \int_0^{2\pi} \int_0^{\pi} r^2 \sin\varphi \, T_e \, S \, dr \, d\theta \, d\varphi. \tag{3.12}$$

Rearranging the left-hand side of equation (3.12) we obtain:

$$\frac{C_e}{2} \int_0^L \int_0^{2\pi} \int_0^{\pi} r^2 \sin\varphi \, \frac{\partial (T_e)^2}{\partial t} \, dr \, d\theta \, d\varphi + \frac{C_l}{2} \int_0^L \int_0^{2\pi} \int_0^{\pi} r^2 \sin\varphi \, \frac{\partial (T_l)^2}{\partial t} \, dr \, d\theta \, d\varphi$$

$$= \int_0^L \int_0^{2\pi} \int_0^{\pi} k_e \sin\varphi \, T_e \, \frac{\partial}{\partial r} \left(r^2 \frac{\partial T_e}{\partial r} \right) dr \, d\theta \, d\varphi + \int_0^L \int_0^{2\pi} \int_0^{\pi} \frac{k_e}{\sin\varphi} \, T_e \, \frac{\partial^2 T_e}{\partial \theta^2} \, dr \, d\theta \, d\varphi$$

$$+ \int_0^L \int_0^{2\pi} \int_0^{\pi} k_e \sin\varphi \, T_e \, \frac{\partial}{\partial \varphi} \left(\sin\varphi \, \frac{\partial T_e}{\partial \varphi} \right) dr \, d\theta \, d\varphi - \int_0^L \int_0^{2\pi} \int_0^{\pi} r^2 \sin\varphi \, G \left(T_e - T_l \right)^2 dr \, d\theta \, d\varphi$$

$$+ \int_0^L \int_0^{2\pi} \int_0^{\pi} r^2 \sin\varphi \, T_e \, S \, dr \, d\theta \, d\varphi. \tag{3.13}$$

Now, we may use Green's Theorem and equations (3.6) and (3.8) to simplify the first term on the right hand side of equation (3.13) as follows:

$$\int_0^L \int_0^{2\pi} \int_0^{\pi} k_e \sin\varphi \, T_e \, \frac{\partial}{\partial r} \left(r^2 \frac{\partial T_e}{\partial r} \right) dr \, d\theta \, d\varphi$$

$$= \int_0^{2\pi} \int_0^{\pi} \left[k_e \sin\varphi \, T_e r^2 \frac{\partial T_e}{\partial r} \right]_0^L d\theta \, d\varphi - \int_0^L \int_0^{2\pi} \int_0^{\pi} k_e \sin\varphi \, \frac{\partial T_e}{\partial r} r^2 \frac{\partial T_e}{\partial r} \, dr \, d\theta \, d\varphi$$

$$= -k_e \int_0^L \int_0^{2\pi} \int_0^{\pi} \sin\varphi \, r^2 \left(\frac{\partial T_e}{\partial r} \right)^2 dr \, d\theta \, d\varphi. \tag{3.14}$$

Similarly, we simplify the second term on the right hand side of equation (3.13) using equation (3.7) as follows:

$$\int_0^L \int_0^{2\pi} \int_0^{\pi} \frac{k_e}{\sin\varphi} T_e \frac{\partial^2 T_e}{\partial\theta^2} \, dr\,d\theta\,d\varphi$$

$$= \int_0^L \int_0^{\pi} \left[\frac{k_e}{\sin\varphi} T_e \frac{\partial T_e}{\partial\theta} \right]_0^{2\pi} dr\,d\varphi - \int_0^L \int_0^{2\pi} \int_0^{\pi} \frac{k_e}{\sin\varphi} \frac{\partial T_e}{\partial\theta} \frac{\partial T_e}{\partial\theta} \, dr\,d\theta\,d\varphi$$

$$= -k_e \int_0^L \int_0^{2\pi} \int_0^{\pi} \frac{1}{\sin\varphi} \left(\frac{\partial T_e}{\partial\theta} \right)^2 dr\,d\theta\,d\varphi. \tag{3.15}$$

The third term can be simplified in the same fashion using equation (3.5) as:

$$\int_0^L \int_0^{2\pi} \int_0^{\pi} k_e T_e \frac{\partial}{\partial\varphi} \left(\sin\varphi \frac{\partial T_e}{\partial\varphi} \right) dr\,d\theta\,d\varphi$$

$$= \int_0^L \int_0^{2\pi} \left[k_e T_e \sin\varphi \frac{\partial T_e}{\partial\varphi} \right]_0^{\pi} dr\,d\theta - \int_0^L \int_0^{2\pi} \int_0^{\pi} k_e \frac{\partial T_e}{\partial\varphi} \sin\varphi \frac{\partial T_e}{\partial\varphi} \, dr\,d\theta\,d\varphi$$

$$= -k_e \int_0^L \int_0^{2\pi} \int_0^{\pi} \sin\varphi \left(\frac{\partial T_e}{\partial\varphi} \right)^2 dr\,d\theta\,d\varphi. \tag{3.16}$$

Furthermore, we can rewrite the left-hand side of equation (3.13) as:

$$LHS = \frac{d}{dt} \left(\frac{C_e}{2} \int_0^L \int_0^{2\pi} \int_0^{\pi} r^2 \sin\varphi \, T_e^2 \, dr\,d\theta\,d\varphi + \frac{C_l}{2} \int_0^L \int_0^{2\pi} \int_0^{\pi} r^2 \sin\varphi \, T_l^2 \, dr\,d\theta\,d\varphi \right) \tag{3.17}$$

Substituting equations (3.14)-(3.17) into equation (3.13), we obtain:

$$\frac{d}{dt} \left(\frac{C_e}{2} \int_0^L \int_0^{2\pi} \int_0^{\pi} r^2 \sin\varphi \, T_e^2 \, dr\,d\theta\,d\varphi + \frac{C_l}{2} \int_0^L \int_0^{2\pi} \int_0^{\pi} r^2 \sin\varphi \, T_l^2 \, dr\,d\theta\,d\varphi \right)$$

$$+ \int_0^L \int_0^{2\pi} \int_0^{\pi} r^2 \sin\varphi \, G \left(T_e - T_l \right)^2 dr\,d\theta\,d\varphi + k_e \int_0^L \int_0^{2\pi} \int_0^{\pi} \sin\varphi \, r^2 \left(\frac{\partial T_e}{\partial r} \right)^2 dr\,d\theta\,d\varphi$$

$$+k_e \int_0^L \int_0^{2\pi} \int_0^{\pi} \frac{1}{\sin\varphi} \left(\frac{\partial T_e}{\partial \theta}\right)^2 dr d\theta d\varphi + k_e \int_0^L \int_0^{2\pi} \int_0^{\pi} \sin\varphi \left(\frac{\partial T_e}{\partial \varphi}\right)^2 dr d\theta d\varphi$$

$$= \int_0^L \int_0^{2\pi} \int_0^{\pi} r^2 \sin\varphi \, T_e \, S \, dr d\theta d\varphi. \tag{3.18}$$

Dropping the positive integrals in the second, third, fourth and fifth terms on the left-hand side of equation (3.18), we have

$$\frac{d}{dt}\left(C_e \int_0^L \int_0^{2\pi} \int_0^{\pi} r^2 \sin\varphi \, T_e^2 \, dr d\theta d\varphi + C_l \int_0^L \int_0^{2\pi} \int_0^{\pi} r^2 \sin\varphi \, T_l^2 \, dr d\theta d\varphi\right)$$

$$\leq \int_0^L \int_0^{2\pi} \int_0^{\pi} 2r^2 \sin\varphi \, T_e \, S \, dr d\theta d\varphi. \tag{3.19}$$

By Cauchy-Schwartz's inequality, we have

$$2T_e S \leq \varepsilon (T_e)^2 + \frac{1}{\varepsilon} S^2, \tag{3.20}$$

for $\varepsilon > 0$. Letting $\varepsilon = C_e$ and substituting equation (3.20) into equation (3.19) gives

$$\frac{d}{dt}\left(C_e \int_0^L \int_0^{2\pi} \int_0^{\pi} r^2 \sin\varphi \, T_e^2 \, dr d\theta d\varphi + C_l \int_0^L \int_0^{2\pi} \int_0^{\pi} r^2 \sin\varphi \, T_l^2 \, dr d\theta d\varphi\right)$$

$$\leq \int_0^L \int_0^{2\pi} \int_0^{\pi} r^2 [C_e(T_e)^2 + \frac{1}{C_e} S^2] \sin\varphi \, dr d\theta d\varphi$$

$$= C_e \int_0^L \int_0^{2\pi} \int_0^{\pi} r^2 (T_e)^2 \sin\varphi \, dr d\theta d\varphi + \frac{1}{C_e} \int_0^L \int_0^{2\pi} \int_0^{\pi} r^2 S^2 \sin\varphi \, dr d\theta d\varphi. \tag{3.21}$$

Using the notations of $F(t)$ and $\Phi(t)$, equation (3.21) can be simplified as:

$$F'(t) \leq F(t) + \Phi(t). \tag{3.22}$$

By Gronwall's inequality [Evans 1998], we obtain

$$F(t) \leq e^t [F(0) + \int_0^t \Phi(s) ds],$$

(3.23)

which completes the proof.

3.3 Finite Difference Scheme

3.3.1 Difference Operators

We denote T_{ijk}^n as the numerical approximation of $T(i\Delta r, j\Delta\theta, k\Delta\varphi, n\Delta t)$, where

$\Delta r, \Delta\theta, \Delta\varphi$ and Δt are the r, θ, φ directional spatial and temporal mesh sizes,

respectively, and $0 \leq i \leq N_r, 0 \leq j \leq N_\theta, 0 \leq k \leq N_\varphi$ so that $N_r \Delta r = L$, $N_\theta \Delta\theta = 2\pi$,

$N_\varphi \Delta\varphi = \pi$. We introduce the following difference operators:

$$\nabla_r T_{ijk}^n = \frac{T_{i+1jk}^n - T_{ijk}^n}{\Delta r};$$

(3.24)

$$\nabla_{\bar{r}} T_{ijk}^n = \frac{T_{ijk}^n - T_{i-1jk}^n}{\Delta r};$$

(3.25)

$$\nabla_\theta T_{ijk}^n = \frac{T_{ij+1k}^n - T_{ijk}^n}{\Delta\theta};$$

(3.26)

$$\nabla_{\bar{\theta}} T_{ijk}^n = \frac{T_{ijk}^n - T_{ij-1k}^n}{\Delta\theta};$$

(3.27)

$$\nabla_\varphi T_{ijk}^n = \frac{T_{ijk+1}^n - T_{ijk}^n}{\Delta\varphi};$$

(3.28)

$$\nabla_{\bar{\varphi}} T_{ijk}^n = \frac{T_{ijk}^n - T_{ijk-1}^n}{\Delta\varphi};$$

(3.29)

Furthermore, we introduce the following operators,

$$P_r(T_{ijk}^n) = r_{i+\frac{1}{2}}^2 \frac{T_{i+1\,jk}^n - T_{ijk}^n}{(\Delta r)^2} - r_{i-\frac{1}{2}}^2 \frac{T_{ijk}^n - T_{i-1\,jk}^n}{(\Delta r)^2};$$ (3.30)

$$P_\theta(T_{ijk}^n) = \frac{T_{ij-1k}^n - 2T_{ijk}^n + T_{ij-1k}^n}{(\Delta\theta)^2};$$ (3.31)

$$P_\varphi(T_{ijk}^n) = \sin\varphi_{k+\frac{1}{2}} \frac{T_{ijk+1}^n - T_{ijk}^n}{(\Delta\varphi)^2} - \sin\varphi_{k-\frac{1}{2}} \frac{T_{ijk}^n - T_{ijk-1}^n}{(\Delta\varphi)^2};$$ (3.32)

and a temporal weighted average for stability purposes,

$$W_t(T_{ijk}^n) = \frac{T_{ijk}^{n+1} + 2T_{ijk}^n + T_{ijk}^{n-1}}{4}.$$ (3.33)

3.3.2 Finite Difference Scheme

We develop a three-level finite difference scheme to solve equations (3.1) and (3.2) as follows:

$$C_e \frac{(T_e)_{ijk}^{n+1} - (T_e)_{ijk}^{n-1}}{2\Delta t} = \frac{k_e}{r_i^2} P_r\{W_t[(T_e)_{ijk}^n]\} + \frac{k_e}{r_i^2(\sin\varphi_k)^2} P_\theta\{W_t[(T_e)_{ijk}^n]\}$$

$$+ \frac{k_e}{r_i^2 \sin\varphi_k} P_\varphi\{W_t[(T_e)_{ijk}^n]\} - G \cdot W_t[(T_e)_{ijk}^n - (T_l)_{ijk}^n]$$

$$+ S_{ijk}^n,$$ (3.34)

$$C_l \frac{(T_l)_{ijk}^{n+1} - (T_l)_{ijk}^{n-1}}{2\Delta t} = G \cdot W_t[(T_e)_{ijk}^n - (T_l)_{ijk}^n].$$ (3.35)

Here, $r_i = i\Delta r$ and $\varphi_k = k\Delta\varphi$. The boundary conditions are discretized as follows:

$$\nabla_{\bar{r}}(T_e)_{N_r jk}^n = \nabla_{\bar{r}}(T_e)_{1jk}^n = 0, \quad \nabla_{\bar{r}}(T_l)_{N_r jk}^n = \nabla_{\bar{r}}(T_l)_{1jk}^n = 0;$$ (3.36)

$$(T_e)_{ijk}^n = (T_e)_{ij+N_\theta k}^n, \quad (T_l)_{ijk}^n = (T_l)_{ij+N_\theta k}^n;$$ (3.37)

$$\nabla_{\bar{\varphi}}(T_e)^n_{ijN_\varphi} = \nabla_{\bar{\varphi}}(T_e)^n_{ij1} = 0, \quad \nabla_{\bar{\varphi}}(T_l)^n_{ijN_\varphi} = \nabla_{\bar{\varphi}}(T_l)^n_{ij1} = 0. \tag{3.38}$$

Since the scheme is three-level in time, the discretized initial conditions are assumed to be

$$(T_e)^0_{ijk} = (T_l)^0_{ijk} = (T_e)^1_{ijk} = (T_l)^1_{ijk} = T_0. \tag{3.39}$$

It can be seen that the truncation errors for Equations (3.34) and (3.35) are

$$O(\Delta t^2 + \Delta r^2 + \Delta \theta^2 + \Delta \varphi^2).$$

3.4 Stability Analysis

Using the discrete energy method [Lees 1961, 1966] to prove the stability of our numerical scheme, Equations (3.34)-(3.39), we need to introduce the definitions of the inner products and norms between the mesh functions u^n_{ijk} and v^n_{ijk}. Let S_h be the set

$\left\{ u = \{u_{ijk}\} \middle| 0 \le i \le N_r, 0 \le j \le N_\theta, 0 \le k \le N_\varphi \right\}$. For any $u, v \in S_h$, the inner products and norms are defined as follows:

$$(u,v) = \Delta r \, \Delta \theta \, \Delta \varphi \sum_{i=1}^{N_r-1} \sum_{j=1}^{N_\theta} \sum_{k=1}^{N_\varphi-1} u_{ijk} \cdot v_{ijk}, \tag{3.40}$$

$$(u,u) = \|u\|^2, \tag{3.41}$$

$$\|\nabla_{\bar{r}} u\|^2_1 = (\nabla_{\bar{r}} u, \nabla_{\bar{r}} u)_1 = \Delta r \, \Delta \theta \, \Delta \varphi \sum_{i=1}^{N_r} \sum_{j=1}^{N_\theta} \sum_{k=1}^{N_\varphi-1} (\nabla_{\bar{r}} u), \tag{3.42}$$

$$\|\nabla_{\bar{\theta}} u\|^2_1 = (\nabla_{\bar{\theta}} u, \nabla_{\bar{\theta}} u)_1 = \Delta r \, \Delta \theta \, \Delta \varphi \sum_{i=1}^{N_r-1} \sum_{j=1}^{N_\theta} \sum_{k=1}^{N_\varphi-1} (\nabla_{\bar{\theta}} u), \tag{3.43}$$

$$\|\nabla_{\bar{\varphi}} u\|^2_1 = (\nabla_{\bar{\varphi}} u, \nabla_{\bar{\varphi}} u)_1 = \Delta r \, \Delta \theta \, \Delta \varphi \sum_{i=1}^{N_r-1} \sum_{j=1}^{N_\theta} \sum_{k=1}^{N_\varphi} (\nabla_{\bar{\varphi}} u), \tag{3.44}$$

The following lemmas are easily derived:

LEMMA 1. Let $T \in S_h$. For any n,

$$\Delta r \, \Delta \theta \, \Delta \varphi \sum_{i=1}^{N_r-1} \sum_{j=1}^{N_\theta} \sum_{k=1}^{N_\varphi-1} r_i^2 \sin \varphi_k (T_{ijk}^{n+1} + 2T_{ijk}^n + T_{ijk}^{n-1}) \cdot (T_{ijk}^{n+1} - T_{ijk}^{n-1})$$

$$= \Delta r \, \Delta \theta \, \Delta \varphi \sum_{i=1}^{N_r-1} \sum_{j=1}^{N_\theta} \sum_{k=1}^{N_\varphi-1} r_i^2 \sin \varphi_k \left[(T_{ijk}^{n+1} + T_{ijk}^n)^2 - (T_{ijk}^n + T_{ijk}^{n-1})^2 \right]$$

$$= \left\| r\sqrt{\sin \varphi}(T^{n+1} + T^n) \right\|^2 - \left\| r\sqrt{\sin \varphi}(T^n + T^{n-1}) \right\|^2. \tag{3.45}$$

LEMMA 2. For any mesh function T_{ijk} and S_{ijk},

$$\Delta r \sum_{i=1}^{N_r-1} P_r(T_{ijk}) \cdot S_{ijk} = -\Delta r \sum_{i=1}^{N_r} r_{i-\frac{1}{2}}^2 \nabla_{\bar{r}} T_{ijk} \cdot \nabla_{\bar{r}} S_{ijk} - r_{\frac{1}{2}}^2 \nabla_{\bar{r}} T_{1jk} \cdot S_{0jk}$$

$$+ r_{N_r-\frac{1}{2}}^2 \nabla_{\bar{r}} T_{N_r jk} \cdot S_{N_r jk}. \tag{3.46}$$

Proof. From equation (3.30), we get

$$\Delta r \sum_{i=1}^{N_r-1} P_r(T_{ijk}) \cdot S_{ijk}$$

$$= \Delta r \sum_{i=1}^{N_r-1} r_{i+\frac{1}{2}}^2 \frac{T_{i+1jk} - T_{ijk}}{(\Delta r)^2} \cdot S_{ijk} - \Delta r \sum_{i=1}^{N_r-1} r_{i-\frac{1}{2}}^2 \frac{T_{ijk} - T_{i-1jk}}{(\Delta r)^2} \cdot S_{ijk}$$

$$= \Delta r \sum_{i=2}^{N_r} r_{i-\frac{1}{2}}^2 \frac{T_{ijk} - T_{i-1jk}}{(\Delta r)^2} \cdot S_{i-1jk} - \Delta r \sum_{i=1}^{N_r-1} r_{i-\frac{1}{2}}^2 \frac{T_{ijk} - T_{i-1jk}}{(\Delta r)^2} \cdot S_{ijk}$$

$$= \Delta r \sum_{i=1}^{N_r} r_{i-\frac{1}{2}}^2 \frac{T_{ijk} - T_{i-1jk}}{(\Delta r)^2} \cdot S_{i-1jk} - \Delta r \sum_{i=1}^{N_r} r_{i-\frac{1}{2}}^2 \frac{T_{ijk} - T_{i-1jk}}{(\Delta r)^2} \cdot S_{ijk}$$

$$- r_{\frac{1}{2}}^2 \frac{T_{1jk} - T_{0jk}}{\Delta r} \cdot S_{0jk} + r_{N_r-\frac{1}{2}}^2 \frac{T_{N_rjk} - T_{N_r-1jk}}{\Delta r} \cdot S_{N_rjk}$$

$$= -\Delta r \sum_{i=1}^{N_r} r_{i-\frac{1}{2}}^2 \nabla_{\bar{r}} T_{ijk} \cdot \nabla_{\bar{r}} S_{ijk} - r_{\frac{1}{2}}^2 \frac{T_{1jk} - T_{0jk}}{\Delta r} \cdot S_{0jk} + r_{N_r-\frac{1}{2}}^2 \frac{T_{N_rjk} - T_{N_r-1jk}}{\Delta r} \cdot S_{N_rjk}$$

$$= -\Delta r \sum_{i=1}^{N_r} r_{i-\frac{1}{2}}^2 \nabla_{\bar{r}} T_{ijk} \cdot \nabla_{\bar{r}} S_{ijk} - r_{\frac{1}{2}}^2 \nabla_{\bar{r}} T_{1jk} \cdot S_{0jk} + r_{N_r-\frac{1}{2}}^2 \nabla_{\bar{r}} T_{N_rjk} \cdot S_{N_rjk}.$$

LEMMA 3. For any mesh function T_{ijk} and S_{ijk},

$$\Delta\theta \sum_{j=1}^{N_\theta} P_\theta(T_{ijk}) \cdot S_{ijk} = -\Delta\theta \sum_{j=1}^{N_\theta} \nabla_{\bar{\theta}} T_{ijk} \cdot \nabla_{\bar{\theta}} S_{ijk} - \nabla_{\bar{\theta}} T_{i1k} \cdot S_{i0k}$$

$$+ \nabla_{\bar{\theta}} T_{iN_\theta+1k} \cdot S_{iN_\theta k}. \tag{3.47}$$

Proof. From equation (3.31), we get

$$\Delta\theta \sum_{j=1}^{N_\theta} P_\theta(T_{ijk}) \cdot S_{ijk}$$

$$= \Delta\theta \sum_{j=1}^{N_\theta} \frac{T_{ij+1k} - 2T_{ijk} + T_{ij-1k}}{(\Delta\theta)^2} \cdot S_{ijk}$$

$$= \Delta\theta \sum_{j=1}^{N_\theta} \frac{T_{ij+1k} - T_{ijk}}{(\Delta\theta)^2} \cdot S_{ijk} - \Delta\theta \sum_{j=1}^{N_\theta} \frac{T_{ijk} - T_{ij-1k}}{(\Delta\theta)^2} \cdot S_{ijk}$$

$$= \Delta\theta \sum_{j=2}^{N_\theta+1} \frac{T_{ijk} - T_{ij-1k}}{(\Delta\theta)^2} \cdot S_{ij-1k} - \Delta\theta \sum_{j=1}^{N_\theta} \frac{T_{ijk} - T_{ij-1k}}{(\Delta\theta)^2} \cdot S_{ijk}$$

$$= \Delta\theta \sum_{i=1}^{N_\theta+1} \frac{T_{ijk} - T_{ij-1k}}{(\Delta\theta)^2} \cdot S_{ij-1k} - \Delta\theta \sum_{j=1}^{N_\theta} \frac{T_{ijk} - T_{ij-1k}}{(\Delta\theta)^2} \cdot S_{ijk} - \frac{T_{i1k} - T_{i0k}}{\Delta\theta} \cdot S_{i0k}$$

$$= \Delta\theta \sum_{j=1}^{N_\theta} \frac{T_{ijk} - T_{ij-1k}}{(\Delta\theta)^2} \cdot S_{ij-1k} - \Delta\theta \sum_{j=1}^{N_\theta} \frac{T_{ijk} - T_{ij-1k}}{(\Delta\theta)^2} \cdot S_{ijk}$$

$$-\frac{T_{i1k}-T_{i0k}}{\Delta\theta}\cdot S_{i0k}+\frac{T_{iN_\theta+1k}-T_{iN_\theta k}}{\Delta\theta}\cdot S_{iN_\theta k}$$

$$=-\Delta\theta\sum_{j=1}^{N_\theta}\nabla_{\bar\theta}T_{ijk}\cdot\nabla_{\bar\theta}S_{ijk}-\frac{T_{i1k}-T_{i0k}}{\Delta\theta}\cdot S_{i0k}+\frac{T_{iN_\theta+1k}-T_{iN_\theta k}}{\Delta\theta}\cdot S_{iN_\theta k}$$

$$=-\Delta\theta\sum_{j=1}^{N_\theta}\nabla_{\bar\theta}T_{ijk}\cdot\nabla_{\bar\theta}S_{ijk}-\nabla_{\bar\theta}T_{i1k}\cdot S_{i0k}+\nabla_{\bar\theta}T_{iN_\theta+1k}\cdot S_{iN_\theta k}.$$

LEMMA 4. For any mesh function T_{ijk} and S_{ijk},

$$\Delta\varphi\sum_{k=1}^{N_\varphi-1}P_\varphi(T_{ijk})\cdot S_{ijk}=-\Delta\varphi\sum_{k=1}^{N_\varphi}\sin\varphi_{k-\frac{1}{2}}\nabla_{\bar\varphi}T_{ijk}\cdot\nabla_{\bar\varphi}S_{ijk}-\sin\varphi_{\frac{1}{2}}\nabla_{\bar\varphi}T_{ij1}\cdot S_{ij0}$$

$$+\sin\varphi_{N_\varphi-\frac{1}{2}}\nabla_{\bar\varphi}T_{ijN_\varphi}\cdot S_{ijN_\varphi}. \tag{3.48}$$

Proof. From equation (3.32), we get

$$\Delta\varphi\sum_{k=1}^{N_\varphi-1}P_\varphi(T_{ijk})\cdot S_{ijk}$$

$$=\Delta\varphi\sum_{k=1}^{N_\varphi-1}\sin\varphi_{k+\frac{1}{2}}\frac{T_{ijk+1}-T_{ijk}}{(\Delta\varphi)^2}\cdot S_{ijk}-\Delta\varphi\sum_{k=1}^{N_\varphi-1}\sin\varphi_{k-\frac{1}{2}}\frac{T_{ijk}-T_{ijk-1}}{(\Delta\varphi)^2}\cdot S_{ijk}$$

$$=\Delta\varphi\sum_{k=2}^{N_\varphi}\sin\varphi_{k-\frac{1}{2}}\frac{T_{ijk}-T_{ijk-1}}{(\Delta\varphi)^2}\cdot S_{ijk-1}-\Delta\varphi\sum_{k=1}^{N_\varphi-1}\sin\varphi_{k-\frac{1}{2}}\frac{T_{ijk}-T_{ijk-1}}{(\Delta\varphi)^2}\cdot S_{ijk}$$

$$=\Delta\varphi\sum_{k=1}^{N_\varphi}\sin\varphi_{k-\frac{1}{2}}\frac{T_{ijk}-T_{ijk-1}}{(\Delta\varphi)^2}\cdot S_{ijk-1}-\Delta\varphi\sum_{k=1}^{N_\varphi}\sin\varphi_{k-\frac{1}{2}}\frac{T_{ijk}-T_{ijk-1}}{(\Delta\varphi)^2}\cdot S_{ijk}$$

$$-\sin\varphi_{\frac{1}{2}}\frac{T_{ij1}-T_{ij0}}{\Delta\varphi}\cdot S_{ij0}+\sin\varphi_{N_\varphi-\frac{1}{2}}\frac{T_{ijN_\varphi}-T_{ijN_\varphi-1}}{\Delta\varphi}\cdot S_{ijN_\varphi}$$

$$= -\Delta\varphi \sum_{k=1}^{N_\varphi} \sin\varphi_{k-\frac{1}{2}} \nabla_{\overline{\varphi}} T_{ijk} \cdot \nabla_{\overline{\varphi}} S_{ijk} - \sin\varphi_{\frac{1}{2}} \frac{T_{ij1} - T_{ij0}}{\Delta\varphi} \cdot S_{ij0} + \sin\varphi_{N_\varphi - \frac{1}{2}} \frac{T_{ijN_\varphi} - T_{ijN_\varphi - 1}}{\Delta\varphi} \cdot S_{ijN_\varphi}$$

$$= -\Delta\varphi \sum_{k=1}^{N_\varphi} \sin\varphi_{k-\frac{1}{2}} \nabla_{\overline{\varphi}} T_{ijk} \cdot \nabla_{\overline{\varphi}} S_{ijk} - \sin\varphi_{\frac{1}{2}} \nabla_{\overline{\varphi}} T_{ij1} \cdot S_{ij0} + \sin\varphi_{N_\varphi - \frac{1}{2}} \nabla_{\overline{\varphi}} T_{ijN_\varphi} \cdot S_{ijN_\varphi}.$$

It should be noted that if both T_{ijk} and S_{ijk} satisfy the boundary conditions, i.e. Equations (3.36)-(3.38), then Equations (3.46)-(3.48) reduce to:

$$\Delta r \sum_{i=1}^{N_r - 1} P_r(T_{ijk}) \cdot S_{ijk} = -\Delta r \sum_{i=1}^{N_r} r_{i-\frac{1}{2}}^2 \nabla_{\overline{r}} T_{ijk} \cdot \nabla_{\overline{r}} S_{ijk} \tag{3.49}$$

$$\Delta\theta \sum_{j=1}^{N_\theta} P_\theta(T_{ijk}) \cdot S_{ijk} = -\Delta\theta \sum_{j=1}^{N_\theta} \nabla_{\overline{\theta}} T_{ijk} \cdot \nabla_{\overline{\theta}} S_{ijk} \tag{3.50}$$

$$\Delta\varphi \sum_{k=1}^{N_\varphi - 1} P_\varphi(T_{ijk}) \cdot S_{ijk} = -\Delta\varphi \sum_{k=1}^{N_\varphi} \sin\varphi_{k-\frac{1}{2}} \nabla_{\overline{\varphi}} T_{ijk} \cdot \nabla_{\overline{\varphi}} S_{ijk} \tag{3.51}$$

THEOREM 2. Assume that $(T_e)_{ijk}^n, (T_l)_{ijk}^n$ and $(S_e)_{ijk}^n, (S_l)_{ijk}^n$ satisfy the numerical scheme, Equations (3.34) and (3.35) with the same initial and boundary conditions, Equations (3.36)-(3.39), but different source terms Q_1 and Q_2, respectively. Let

$(u_e)_{ijk}^n = (T_e)_{ijk}^n - (S_e)_{ijk}^n$, $(u_l)_{ijk}^n = (T_l)_{ijk}^n - (S_l)_{ijk}^n$, and $g^n = Q_1^n - Q_2^n$. Then $(u_e)_{ijk}^n$ and

$(u_l)_{ijk}^n$ will satisfy for any $0 \le n\Delta t \le t_0$,

$$2C_e \left\| r\sqrt{\sin\varphi} [(u_e)^{n+1} + (u_e)^n] \right\|^2 + 2C_l \left\| r\sqrt{\sin\varphi} [(u_l)^{n+1} + (u_l)^n] \right\|^2$$

$$\le \frac{8e^{3t_0}}{C_e} \max_{0 \le m \le n} \left\| r\sqrt{\sin\varphi} g^m \right\|^2. \tag{3.52}$$

Hence, the scheme is unconditionally stable with respect to the source term.

Proof. It can be seen that $(u_e)_{ijk}^n$ and $(u_l)_{ijk}^n$ satisfy

$$C_e \frac{(u_e)_{ijk}^{n+1} - (u_e)_{ijk}^{n-1}}{2\Delta t} = \frac{k_e}{r_i^2} P_r \{W_t[(u_e)_{ijk}^n]\} + \frac{k_e}{r_i^2 (\sin \varphi_k)^2} P_\theta \{W_t[(u_e)_{ijk}^n]\}$$

$$+ \frac{k_e}{r_i^2 \sin \varphi_k} P_\varphi \{W_t[(u_e)_{ijk}^n]\} - G \cdot W_t[(u_e)_{ijk}^n - (u_l)_{ijk}^n]$$

$$+ g_{ijk}^n, \tag{3.53}$$

$$C_l \frac{(u_l)_{ijk}^{n+1} - (u_l)_{ijk}^{n-1}}{2\Delta t} = G \cdot W_t[(u_e)_{ijk}^n - (u_l)_{ijk}^n], \tag{3.54}$$

and initial and boundary conditions

$$\nabla_{\bar{r}}(u_e)_{N_r jk}^n = \nabla_{\bar{r}}(u_e)_{1jk}^n = 0, \quad \nabla_{\bar{r}}(u_l)_{N_r jk}^n = \nabla_{\bar{r}}(u_l)_{1jk}^n = 0, \tag{3.55}$$

$$(u_e)_{ijk}^n = (u_e)_{ij+N_\theta k}^n, \quad (u_l)_{ijk}^n = (u_l)_{ij+N_\theta k}^n, \tag{3.56}$$

$$\nabla_{\bar{\varphi}}(u_e)_{ijN_\varphi}^n = \nabla_{\bar{\varphi}}(u_e)_{ij1}^n = 0, \quad \nabla_{\bar{\varphi}}(u_l)_{ijN_\varphi}^n = \nabla_{\bar{\varphi}}(u_l)_{ij1}^n = 0, \tag{3.57}$$

$$(u_e)_{ijk}^0 = (u_l)_{ijk}^0 = (u_e)_{ijk}^1 = (u_l)_{ijk}^1 = 0. \tag{3.58}$$

Multiplying equation (3.53) by $4\Delta r \Delta\theta \Delta\varphi \, r_i^2 \sin\varphi_k [(u_e)_{ijk}^{n+1} + 2(u_e)_{ijk}^n + (u_e)_{ijk}^{n-1}]$, and

equation (3.54) by $4\Delta r \Delta\theta \Delta\varphi \, [(u_l)_{ijk}^{n+1} + 2(u_l)_{ijk}^n + (u_l)_{ijk}^{n-1}]$, and adding the two equations

together and summing over the i, j, k, $1 \le i \le N_r - 1, 1 \le j \le N_\theta, 1 \le k \le N_\varphi - 1$, , we obtain

by Lemmas 1-4 and Equations (3.55)-(3.58):

$$2C_e \left\{ \left\| r\sqrt{\sin\varphi}[(u_e)^{n+1} + (u_e)^n] \right\|^2 - \left\| r\sqrt{\sin\varphi}[(u_e)^n + (u_e)^{n-1}] \right\|^2 \right\}$$

$$+ 2C_l \left\{ \left\| r\sqrt{\sin\varphi}[(u_l)^{n+1} + (u_l)^n] \right\|^2 - \left\| r\sqrt{\sin\varphi}[(u_l)^n + (u_l)^{n-1}] \right\|^2 \right\}$$

$$= -k_e\Delta t \left\| \left(E^{-\frac{1}{2}}r \right) \sqrt{\sin\varphi} \nabla_{\bar{r}}[(u_e)^{n+1} + 2(u_e)^n + (u_e)^{n-1}] \right\|_1^2$$

$$-k_e \Delta t \left\| \frac{1}{\sqrt{\sin \varphi}} \nabla_{\bar{\theta}} [(u_e)^{n+1} + 2(u_e)^n + (u_e)^{n-1}] \right\|_1^2$$

$$-k_e \Delta t \left\| \sqrt{(E^{-\frac{1}{2}} \sin \varphi)} \nabla_{\bar{\varphi}} [(u_e)^{n+1} + 2(u_e)^n + (u_e)^{n-1}] \right\|_1^2$$

$$-G \Delta t \left\| r \sqrt{\sin \varphi} \left\{ [(u_e)^{n+1} + 2(u_e)^n + (u_e)^{n-1}] - [(u_l)^{n+1} + 2(u_l)^n + (u_l)^{n-1}] \right\} \right\|_1^2$$

$$+(g^n, 4\Delta t \, r^2 \sin \varphi[(u_e)^{n+1} + 2(u_e)^n + (u_e)^{n-1}]), \tag{3.59}$$

where $E^{-\frac{1}{2}}$ is a shift operator such that $E^{-\frac{1}{2}} r_i = r_{i-\frac{1}{2}}$ and $E^{-\frac{1}{2}} \sin \varphi_k = \sin \varphi_{k-\frac{1}{2}}$.

Rearranging equations (3.59), we obtain:

$$2C_e \left\| r\sqrt{\sin \varphi} [(u_e)^{n+1} + (u_e)^n] \right\|^2 + 2C_l \left\| r\sqrt{\sin \varphi}[(u_l)^{n+1} + (u_l)^n] \right\|^2$$

$$+k_e \Delta t \left\| \left(E^{-\frac{1}{2}} r \right) \sqrt{\sin \varphi} \nabla_{\bar{r}} [(u_e)^{n+1} + 2(u_e)^n + (u_e)^{n-1}] \right\|_1^2$$

$$+k_e \Delta t \left\| \frac{1}{\sqrt{\sin \varphi}} \nabla_{\bar{\theta}} [(u_e)^{n+1} + 2(u_e)^n + (u_e)^{n-1}] \right\|_1^2$$

$$+k_e \Delta t \left\| \sqrt{(E^{-\frac{1}{2}} \sin \varphi)} \nabla_{\bar{\varphi}} [(u_e)^{n+1} + 2(u_e)^n + (u_e)^{n-1}] \right\|_1^2$$

$$+G \Delta t \left\| r\sqrt{\sin \varphi} \left\{ [(u_e)^{n+1} + 2(u_e)^n + (u_e)^{n-1}] - [(u_l)^{n+1} + 2(u_l)^n + (u_l)^{n-1}] \right\} \right\|_1^2$$

$$= 2C_e \left\| r\sqrt{\sin \varphi}[(u_e)^n + (u_e)^{n-1}] \right\|^2 + 2C_l \left\| r\sqrt{\sin \varphi}[(u_l)^n + (u_l)^{n-1}] \right\|^2$$

$$+(g^n, 4\Delta t \, r^2 \sin\varphi[(u_e)^{n+1} + 2(u_e)^n + (u_e)^{n-1}]). \tag{3.60}$$

Dropping the positive values in the third, fourth, fifth, and sixth terms on the right-hand side of Equation (3.60) yields

$$2C_e \left\| r\sqrt{\sin\varphi}[(u_e)^{n+1} + (u_e)^n] \right\|^2 + 2C_l \left\| r\sqrt{\sin\varphi}[(u_l)^{n+1} + (u_l)^n] \right\|^2$$

$$\leq 2C_e \left\| r\sqrt{\sin\varphi}[(u_e)^n + (u_e)^{n-1}] \right\|^2 + 2C_l \left\| r\sqrt{\sin\varphi}[(u_l)^n + (u_l)^{n-1}] \right\|^2$$

$$+(g^n, 4\Delta t \, r^2 \sin\varphi[(u_e)^{n+1} + 2(u_e)^n + (u_e)^{n-1}]). \tag{3.61}$$

Evaluating the term $(g^n, r^2 \sin\varphi[(u_e)^{n+1} + 2(u_e)^n + (u_e)^{n-1}])$, we get

$$(g^n, r^2 \sin\varphi[(u_e)^{n+1} + 2(u_e)^n + (u_e)^{n-1}]),$$

$$= \Delta r \, \Delta\theta \, \Delta\varphi \sum_{i=1}^{N_r-1} \sum_{j=1}^{N_\theta} \sum_{k=1}^{N_\varphi-1} g_{ijk}^n \cdot r_i^2 \sin\varphi_k [(u_e)_{ijk}^{n+1} + 2(u_e)_{ijk}^n + (u_e)_{ijk}^{n-1}]$$

$$= \Delta r \, \Delta\theta \, \Delta\varphi \sum_{i=1}^{N_r-1} \sum_{j=1}^{N_\theta} \sum_{k=1}^{N_\varphi-1} g_{ijk}^n \cdot r_i^2 \sin\varphi_k [(u_e)_{ijk}^{n+1} + (u_e)_{ijk}^n]$$

$$+\Delta r \, \Delta\theta \, \Delta\varphi \sum_{i=1}^{N_r-1} \sum_{j=1}^{N_\theta} \sum_{k=1}^{N_\varphi-1} g_{ijk}^n \cdot r_i^2 \sin\varphi_k [(u_e)_{ijk}^n + (u_e)_{ijk}^{n-1}]$$

$$= \Delta r \, \Delta\theta \, \Delta\varphi \sum_{i=1}^{N_r-1} \sum_{j=1}^{N_\theta} \sum_{k=1}^{N_\varphi-1} \left(r_i \sqrt{\sin\varphi_k} g_{ijk}^n \right) \cdot r_i \sqrt{\sin\varphi_k} [(u_e)_{ijk}^{n+1} + (u_e)_{ijk}^n]$$

$$+\Delta r \, \Delta\theta \, \Delta\varphi \sum_{i=1}^{N_r-1} \sum_{j=1}^{N_\theta} \sum_{k=1}^{N_\varphi-1} \left(r_i \sqrt{\sin\varphi_k} g_{ijk}^n \right) \cdot r_i \sqrt{\sin\varphi_k} [(u_e)_{ijk}^n + (u_e)_{ijk}^{n-1}].$$

By Cauchy-Schwartz's inequality, we have

$$2(g^n, r^2 \sin\varphi[(u_e)^{n+1} + 2(u_e)^n + (u_e)^{n-1}]),$$

$$= \Delta r \, \Delta\theta \, \Delta\varphi \sum_{i=1}^{N_r-1} \sum_{j=1}^{N_\theta} \sum_{k=1}^{N_\varphi-1} \left(r_i \, \sqrt{\sin\varphi_k} \, g_{ijk}^n \right) \cdot r_i \, \sqrt{\sin\varphi_k} \, [(u_e)_{ijk}^{n+1} + (u_e)_{ijk}^n]$$

$$+ \Delta r \, \Delta\theta \, \Delta\varphi \sum_{i=1}^{N_r-1} \sum_{j=1}^{N_\theta} \sum_{k=1}^{N_\varphi-1} \left(r_i \, \sqrt{\sin\varphi_k} \, g_{ijk}^n \right) \cdot r_i \, \sqrt{\sin\varphi_k} \, [(u_e)_{ijk}^n + (u_e)_{ijk}^{n-1}]$$

$$\leq \frac{1}{\varepsilon} \left\| r\sqrt{\sin\varphi} \, g^n \right\|^2 + \varepsilon \left\| r\sqrt{\sin\varphi} \, [(u_e)^{n+1} + (u_e)^n] \right\|$$

$$+ \frac{1}{\varepsilon} \left\| r\sqrt{\sin\varphi} \, g^n \right\|^2 + \varepsilon \left\| r\sqrt{\sin\varphi} \, [(u_e)^n + (u_e)^{n-1}] \right\|, \tag{3.62}$$

where $\varepsilon > 0$. Choosing $\varepsilon = \dfrac{C_e}{2}$ and then substituting Equation (3.62) into Equation (3.61), we obtain

$$2C_e \left\| r\sqrt{\sin\varphi} \, [(u_e)^{n+1} + (u_e)^n] \right\|^2 + 2C_l \left\| r\sqrt{\sin\varphi} \, [(u_l)^{n+1} + (u_l)^n] \right\|^2$$

$$\leq 2C_e \left\| r\sqrt{\sin\varphi} \, [(u_e)^n + (u_e)^{n-1}] \right\|^2 + 2C_l \left\| r\sqrt{\sin\varphi} \, [(u_l)^n + (u_l)^{n-1}] \right\|^2$$

$$+ C_e\Delta t \left\| r\sqrt{\sin\varphi} \, [(u_e)^{n+1} + (u_e)^n] \right\|^2 + C_e\Delta t \left\| r\sqrt{\sin\varphi} \, [(u_e)^n + (u_e)^{n-1}] \right\|^2$$

$$+ \frac{8\Delta t}{C_e} \left\| r\sqrt{\sin\varphi} \, g^n \right\|^2. \tag{3.63}$$

Finally, we have

$$(2C_e - C_e\Delta t) \left\| r\sqrt{\sin\varphi} \, [(u_e)^{n+1} + (u_e)^n] \right\|^2 + 2C_l \left\| r\sqrt{\sin\varphi} \, [(u_l)^{n+1} + (u_l)^n] \right\|^2$$

$$\leq (2C_e + C_e\Delta t) \left\| r\sqrt{\sin\varphi} \, [(u_e)^n + (u_e)^{n-1}] \right\|^2 + 2C_l \left\| r\sqrt{\sin\varphi} \, [(u_l)^n + (u_l)^{n-1}] \right\|^2$$

$$+ \frac{8\Delta t}{C_e} \left\| r\sqrt{\sin\varphi} \, g^n \right\|^2. \tag{3.64}$$

Denoting

$$F(n) = 2C_e \left\| r\sqrt{\sin\varphi}[(u_e)^{n+1} + (u_e)^n] \right\|^2 + 2C_l \left\| r\sqrt{\sin\varphi}[(u_l)^{n+1} + (u_l)^n] \right\|^2 \quad (3.65)$$

and

$$\Phi(n) = \frac{8}{C_e} \left\| r\sqrt{\sin\varphi}\, g^n \right\|^2 , \quad (3.66)$$

Equation (3.64) can be written as follows:

$$(1 - \Delta t)F(n) \le (1 + \Delta t)F(n-1) + \Delta t\, \Phi(n). \quad (3.67)$$

Thus, we have

$$F(n)$$

$$\le \frac{(1 + \Delta t)}{(1 - \Delta t)} F(n-1) + \frac{\Delta t}{(1 - \Delta t)} \Phi(n)$$

$$\le \frac{(1 + \Delta t)}{(1 - \Delta t)} \left[\frac{(1 + \Delta t)}{(1 - \Delta t)} F(n-2) + \frac{\Delta t}{(1 - \Delta t)} \Phi(n-1) \right] + \frac{\Delta t}{(1 - \Delta t)} \Phi(n)$$

$$\le \ldots\ldots\ldots$$

$$\le \left(\frac{1 + \Delta t}{1 - \Delta t} \right)^n F(0) + \left(\frac{\Delta t}{1 - \Delta t} \right) \left[1 + \left(\frac{1 + \Delta t}{1 - \Delta t} \right) + \left(\frac{1 + \Delta t}{1 - \Delta t} \right)^2 + \ldots + \left(\frac{1 + \Delta t}{1 - \Delta t} \right)^{n-1} \right] \max_{0 \le k \le n} \Phi(k)$$

$$\le \left(\frac{1 + \Delta t}{1 - \Delta t} \right)^n F(0) + \left(\frac{\Delta t}{1 - \Delta t} \right) \left[\frac{1 - \left(\frac{1 + \Delta t}{1 - \Delta t} \right)^n}{1 - \left(\frac{1 + \Delta t}{1 - \Delta t} \right)} \right] \max_{0 \le k \le n} \Phi(k)$$

$$\le \left(\frac{1 + \Delta t}{1 - \Delta t} \right)^n F(0) - \frac{1}{2} \left[1 - \left(\frac{1 + \Delta t}{1 - \Delta t} \right)^n \right] \max_{0 \le k \le n} \Phi(k)$$

$$\le \left(\frac{1 + \Delta t}{1 - \Delta t} \right)^n F(0) + \left(\frac{1 + \Delta t}{1 - \Delta t} \right)^n \max_{0 \le k \le n} \Phi(k) - \frac{1}{2} \max_{0 \le k \le n} \Phi(k)$$

$$\leq \left(\frac{1+\Delta t}{1-\Delta t}\right)^n F(0) + \left(\frac{1+\Delta t}{1-\Delta t}\right)^n \max_{0 \leq k \leq n} \Phi(k)$$

$$\leq \left(\frac{1+\Delta t}{1-\Delta t}\right)^n \left(F(0) + \max_{0 \leq k \leq n} \Phi(k)\right). \tag{3.68}$$

Now using the following results: $(1+\varepsilon)^n \leq e^{n\varepsilon}$, $\varepsilon > 0$ and $(1-\varepsilon)^{-1} \leq e^{2\varepsilon}$, $0 < \varepsilon < \frac{1}{2}$, we

obtain

$$F(n) \leq e^{n\Delta t} \cdot e^{2n\Delta t} \left[F(0) + \max_{0 \leq k \leq n} \Phi(k) \right]$$

$$\leq e^{3n\Delta t} \left[F(0) + \max_{0 \leq k \leq n} \Phi(k) \right]$$

$$\leq e^{3t_0} \left[F(0) + \max_{0 \leq k \leq n} \Phi(k) \right], \tag{3.69}$$

when $\Delta t \leq \frac{1}{2}$. From Equation (3.58), we obtain that $F(0) = 0$, hence,

$$F(n) \leq e^{3t_0} \max_{0 \leq k \leq n} \Phi(k), \tag{3.70}$$

which completes the proof.

CHAPTER 4

NUMERICAL ALGORITHM

4.1 Linear Systems

The finite difference scheme defined in Chapter 3 is given by

$$C_e \frac{(T_e)_{ijk}^{n+1} - (T_e)_{ijk}^{n-1}}{2\Delta t} = \frac{k_e}{r_i^2} P_r \{W_t[(T_e)_{ijk}^n]\} + \frac{k_e}{r_i^2 (\sin \varphi_k)^2} P_\theta \{W_t[(T_e)_{ijk}^n]\}$$

$$+ \frac{k_e}{r_i^2 \sin \varphi_k} P_\varphi \{W_t[(T_e)_{ijk}^n]\} - G \cdot W_t[(T_e)_{ijk}^n - (T_l)_{ijk}^n]$$

$$+ S_{ijk}^n, \tag{4.1}$$

$$C_l \frac{(T_l)_{ijk}^{n+1} - (T_l)_{ijk}^{n-1}}{2\Delta t} = G \cdot W_t[(T_e)_{ijk}^n - (T_l)_{ijk}^n]. \tag{4.2}$$

Here, $r_i = i\Delta r$ and $\varphi_k = k\Delta\varphi$. The initial and boundary conditions are:

$$\nabla_{\bar{r}} (T_e)_{N_r jk}^n = \nabla_{\bar{r}} (T_e)_{1jk}^n = 0, \quad \nabla_{\bar{r}} (T_l)_{N_r jk}^n = \nabla_{\bar{r}} (T_l)_{1jk}^n = 0; \tag{4.3}$$

$$(T_e)_{ijk}^n = (T_e)_{ij+N_\theta k}^n, \quad (T_l)_{ijk}^n = (T_l)_{ij+N_\theta k}^n; \tag{4.4}$$

$$\nabla_{\bar{\varphi}} (T_e)_{ijN_\varphi}^n = \nabla_{\bar{\varphi}} (T_e)_{ij1}^n = 0, \quad \nabla_{\bar{\varphi}} (T_l)_{ijN_\varphi}^n = \nabla_{\bar{\varphi}} (T_l)_{ij1}^n = 0; \tag{4.5}$$

$$(T_e)_{ijk}^0 = (T_l)_{ijk}^0 = (T_e)_{ijk}^1 = (T_l)_{ijk}^1 = T_0. \tag{4.6}$$

We expand Equations (4.1) and (4.2) to set up our linear systems:

55

$$C_e \frac{(T_e)_{ijk}^{n+1} - (T_e)_{ijk}^{n-1}}{2\Delta t} = \frac{k_e}{4r_i^2} P_r \left[(T_e)_{ijk}^{n+1} + 2(T_e)_{ijk}^n + (T_e)_{ijk}^{n-1} \right]$$

$$+ \frac{k_e}{4r_i^2 (\sin \varphi_k)^2} P_\theta \left[(T_e)_{ijk}^{n+1} + 2(T_e)_{ijk}^n + (T_e)_{ijk}^{n-1} \right]$$

$$+ \frac{k_e}{4r_i^2 \sin \varphi_k} P_\varphi \left[(T_e)_{ijk}^{n+1} + 2(T_e)_{ijk}^n + (T_e)_{ijk}^{n-1} \right]$$

$$- \frac{G}{4} \left[(T_e)_{ijk}^{n+1} + 2(T_e)_{ijk}^n + (T_e)_{ijk}^{n-1} - \left[(T_l)_{ijk}^{n+1} + 2(T_l)_{ijk}^n + (T_l)_{ijk}^{n-1} \right] \right]$$

$$+ S_{ijk}^n, \tag{4.7}$$

$$C_l \frac{(T_l)_{ijk}^{n+1} - (T_l)_{ijk}^{n-1}}{2\Delta t} = \frac{G}{4} \left[(T_e)_{ijk}^{n+1} + 2(T_e)_{ijk}^n + (T_e)_{ijk}^{n-1} - \left[(T_l)_{ijk}^{n+1} + 2(T_l)_{ijk}^n + (T_l)_{ijk}^{n-1} \right] \right]. \tag{4.8}$$

We now solve for $(T_l)_{ijk}^{n+1}$ in Equation (4.8):

$$(T_l)_{ijk}^{n+1} = \frac{G\Delta t}{2C_l - G\Delta t} \left[[(T_e)_{ijk}^{n+1} + 2(T_e)_{ijk}^n + (T_e)_{ijk}^{n-1} - 2(T_l)_{ijk}^n] \right] + \frac{2C_l - G\Delta t}{2C_l + G\Delta t} (T_l)_{ijk}^{n-1}. \tag{4.9}$$

We substitute Equation (4.9) into Equation (4.8), which yields

$$C_e \frac{(T_e)_{ijk}^{n+1} - (T_e)_{ijk}^{n-1}}{2\Delta t} = \frac{k_e}{4r_i^2} P_r \left[(T_e)_{ijk}^{n+1} + 2(T_e)_{ijk}^n + (T_e)_{ijk}^{n-1} \right]$$

$$+ \frac{k_e}{4r_i^2 (\sin \varphi_k)^2} P_\theta \left[(T_e)_{ijk}^{n+1} + 2(T_e)_{ijk}^n + (T_e)_{ijk}^{n-1} \right]$$

$$+ \frac{k_e}{4r_i^2 \sin \varphi_k} P_\varphi \left[(T_e)_{ijk}^{n+1} + 2(T_e)_{ijk}^n + (T_e)_{ijk}^{n-1} \right]$$

$$- \frac{G}{4} \left[(T_e)_{ijk}^{n+1} + 2(T_e)_{ijk}^n + (T_e)_{ijk}^{n-1} - 2(T_l)_{ijk}^n - (T_l)_{ijk}^{n-1} \right]$$

$$+\frac{G}{4}\left[\frac{G\Delta t}{2C_l+G\Delta t}\left[[(T_e)_{ijk}^{n+1}+2(T_e)_{ijk}^{n}+(T_e)_{ijk}^{n-1}-2(T_l)_{ijk}^{n}]\right]+\frac{2C_l-G\Delta t}{2C_l+G\Delta t}(T_l)_{ijk}^{n-1}\right]$$

$$+S_{ijk}^{n}.\tag{4.10}$$

Simplifying we obtain

$$C_e\frac{(T_e)_{ijk}^{n+1}-(T_e)_{ijk}^{n-1}}{2\Delta t}=\frac{k_e}{4r_i^2}P_r\left[(T_e)_{ijk}^{n+1}+2(T_e)_{ijk}^{n}+(T_e)_{ijk}^{n-1}\right]$$

$$+\frac{k_e}{4r_i^2(\sin\varphi_k)^2}P_\theta\left[(T_e)_{ijk}^{n+1}+2(T_e)_{ijk}^{n}+(T_e)_{ijk}^{n-1}\right]$$

$$+\frac{k_e}{4r_i^2\sin\varphi_k}P_\varphi\left[(T_e)_{ijk}^{n+1}+2(T_e)_{ijk}^{n}+(T_e)_{ijk}^{n-1}\right]$$

$$-\frac{GC_l}{4C_l+2G\Delta t}\left[(T_e)_{ijk}^{n+1}+2(T_e)_{ijk}^{n}+(T_e)_{ijk}^{n-1}-2(T_l)_{ijk}^{n}-2(T_l)_{ijk}^{n-1}\right]$$

$$+S_{ijk}^{n}.\tag{4.11}$$

When we move all $(n+1)$ time labels to the left-hand side and all lower time labels to the right hand side, we obtain

$$\frac{C_e}{2\Delta t}(T_e)_{ijk}^{n+1}-\frac{k_e}{4r_i^2}P_r(T_e)_{ijk}^{n+1}-\frac{k_e}{4r_i^2(\sin\varphi_k)^2}P_\theta(T_e)_{ijk}^{n+1}-\frac{k_e}{4r_i^2\sin\varphi_k}P_\varphi(T_e)_{ijk}^{n+1}$$

$$+\frac{GC_l}{4C_l+2G\Delta t}(T_e)_{ijk}^{n+1}$$

$$=\frac{k_e}{4r_i^2}P_r\left[2(T_e)_{ijk}^{n}+(T_e)_{ijk}^{n-1}\right]+\frac{k_e}{4r_i^2(\sin\varphi_k)^2}P_\theta\left[2(T_e)_{ijk}^{n}+(T_e)_{ijk}^{n-1}\right]$$

$$+\frac{k_e}{4r_i^2\sin\varphi_k}P_\varphi\left[2(T_e)_{ijk}^{n}+(T_e)_{ijk}^{n-1}\right]-\frac{GC_l}{4C_l+2G\Delta t}\left[2(T_e)_{ijk}^{n}+(T_e)_{ijk}^{n-1}-2(T_l)_{ijk}^{n}-2(T_l)_{ijk}^{n-1}\right]$$

$$\frac{C_e}{2\Delta t}(T_e)_{ijk}^{n-1} + S_{ijk}^n. \tag{4.12}$$

From Equations (4.9) and (4.12), we set up our two linear systems with three time levels

$$A\,\vec{T}_e^{n+1} = B\,\vec{T}_e^n + C\,\vec{T}_e^{n-1} + D\,\vec{T}_l^n + E\,\vec{T}_l^{n-1} + S^n, \tag{4.13}$$

which is the equivalent of Equation (4.12) and

$$A'\,\vec{T}_l^{n+1} = B'\,\vec{T}_e^{n+1} + C'\,\vec{T}_e^n + D'\,\vec{T}_e^{n-1} + E'\,\vec{T}_l^n + F'\,\vec{T}_l^{n-1}, \tag{4.14}$$

which is the equivalent of Equation (4.9). $\{A, B, C, D, E, A', B', C', D', E', F'\}$ are

coefficient matrices for the temperature vectors $\vec{T}_e$ and $\vec{T}_l$. In Equation (4.13), the lower

time labels (n and n-1) on the left-hand side are all known as we perform the calculations

to determine the $\{i,j,k\}$ –th term at time label (n+1) on the right-hand side. Also, all the

lower spatial labels (i-1, j-1, k-1) at time label (n+1) are known. Thus, we can set up a

Gauss-Siedel iterative solve to determine $(T_e)_{ijk}^{n+1}$ in Equation (4.13). At this point, all

terms on the right-hand side of Equation (4.14) will be known, and we can directly

substitute to determine $(T_e)_{ijk}^{n+1}$. To this end, we expand the right-hand side (RHS) of

Equation (4.12) as

$$RHS = \frac{C_e}{2\Delta t}(T_e)_{ijk}^{n+1} + \frac{GC_l}{4C_l + 2G\Delta t}(T_e)_{ijk}^{n+1}$$

$$-\frac{k_e}{4r_i^2(\Delta r)^2}\left[r_{i+\frac{1}{2}}^2\left[(T_e)_{i+1jk}^{n+1} - (T_e)_{ijk}^{n+1}\right] - r_{i-\frac{1}{2}}^2\left[(T_e)_{ijk}^{n+1} - (T_e)_{i-1jk}^{n+1}\right]\right]$$

$$-\frac{k_e}{4r_i^2(\sin\varphi_k)^2(\Delta\theta)^2}\left[(T_e)_{ij+1k}^{n+1} - 2(T_e)_{ijk}^{n+1} + (T_e)_{ij-1k}^{n+1}\right]$$

$$-\frac{k_e}{4r_i^2\sin\varphi_k(\Delta\varphi)^2}\left[\sin\varphi_{k+\frac{1}{2}}\left[(T_e)_{ijk+1}^{n+1} - (T_e)_{ijk}^{n+1}\right] - \sin\varphi_{k-\frac{1}{2}}\left[(T_e)_{ijk}^{n+1} - (T_e)_{ijk-1}^{n+1}\right]\right].$$

We introduce the following coefficients for simplicity:

$$a_1 = \frac{C_e}{2\Delta t} \tag{4.15}$$

$$a_2 = \frac{GC_l}{4C_l + 2G\Delta t} \tag{4.16}$$

$$a_3 = \frac{k_e}{4r_i^2(\Delta r)^2} \cdot r_{i+\frac{1}{2}}^2 \tag{4.17}$$

$$a_4 = \frac{k_e}{4r_i^2(\Delta r)^2} \cdot r_{i-\frac{1}{2}}^2 \tag{4.18}$$

$$a_5 = \frac{k_e}{4r_i^2(\sin\varphi_k)^2(\Delta\theta)^2} \tag{4.19}$$

$$a_6 = \frac{k_e}{4r_i^2\sin\varphi_k(\Delta\varphi)^2} \cdot \sin\varphi_{k+\frac{1}{2}} \tag{4.20}$$

$$a_7 = \frac{k_e}{4r_i^2\sin\varphi_k(\Delta\varphi)^2} \cdot \sin\varphi_{k-\frac{1}{2}} . \tag{4.21}$$

Thus, we can rewrite the right-hand side of Equation (4.12) as

$$RHS = [a_1 + a_2 + a_3 + a_4 + 2a_5 + a_6 + a_7](T_e)_{ijk}^{n+1}$$

$$- a_3(T_e)_{i+1jk}^{n+1} - a_4(T_e)_{i-1jk}^{n+1} - a_5(T_e)_{ij+1k}^{n+1}$$

$$- a_5(T_e)_{ij-1k}^{n+1} - a_6(T_e)_{ijk+1}^{n+1} - a_7(T_e)_{ijk-1}^{n+1} . \tag{4.22}$$

We rewrite the left-hand side (LHS) of Equation (4.12) in a similar fashion:

$$LHS = -2[a_2 + a_3 + a_4 + 2a_5 + a_6 + a_7](T_e)_{ijk}^{n}$$

$$+ 2a_3(T_e)_{i+1jk}^{n} + 2a_4(T_e)_{i-1jk}^{n} + 2a_5(T_e)_{ij+1k}^{n}$$

$$+ 2a_5(T_e)_{ij-1k}^{n} + 2a_6(T_e)_{ijk+1}^{n} + 2a_7(T_e)_{ijk-1}^{n}$$

$$+\left[a_1 - a_2 - a_3 - a_4 - 2a_5 - a_6 - a_7\right](T_e)_{ijk}^{n-1}$$

$$+a_3(T_e)_{i+1jk}^{n-1} + a_4(T_e)_{i-1jk}^{n-1} + a_5(T_e)_{ij+1k}^{n-1}$$

$$+a_5(T_e)_{ij-1k}^{n-1} + a_6(T_e)_{ijk+1}^{n-1} + a_7(T_e)_{ijk-1}^{n-1}$$

$$+2a_2(T_l)_{ijk}^{n} + 2a_2(T_l)_{ijk}^{n-1} + S_{ijk}^{n} . \tag{4.23}$$

From Equations (4.22) and (4.23), we have

$$\left[a_1 + a_2 + a_3 + a_4 + 2a_5 + a_6 + a_7\right](T_e)_{ijk}^{n+1} = a_3(T_e)_{i+1jk}^{n+1} + a_4(T_e)_{i-1jk}^{n+1} + a_5(T_e)_{ij+1k}^{n+1}$$

$$+a_5(T_e)_{ij-1k}^{n+1} + a_6(T_e)_{ijk+1}^{n+1} + a_7(T_e)_{ijk-1}^{n+1}$$

$$-2\left[a_2 + a_3 + a_4 + 2a_5 + a_6 + a_7\right](T_e)_{ijk}^{n}$$

$$+2a_3(T_e)_{i+1jk}^{n} + 2a_4(T_e)_{i-1jk}^{n} + 2a_5(T_e)_{ij+1k}^{n}$$

$$+2a_5(T_e)_{ij-1k}^{n} + 2a_6(T_e)_{ijk+1}^{n} + 2a_7(T_e)_{ijk-1}^{n}$$

$$+\left[a_1 - a_2 - a_3 - a_4 - 2a_5 - a_6 - a_7\right](T_e)_{ijk}^{n-1}$$

$$+a_3(T_e)_{i+1jk}^{n-1} + a_4(T_e)_{i-1jk}^{n-1} + a_5(T_e)_{ij+1k}^{n-1}$$

$$+a_5(T_e)_{ij-1k}^{n-1} + a_6(T_e)_{ijk+1}^{n-1} + a_7(T_e)_{ijk-1}^{n-1}$$

$$+2a_2(T_l)_{ijk}^{n} + 2a_2(T_l)_{ijk}^{n-1} + S_{ijk}^{n} . \tag{4.24}$$

Rewriting Equations (4.24) and (4.8) in matrix form, we obtain

$$A_1 \vec{T}_e^{n+1} = \vec{H}^n , \tag{4.25}$$

$$\vec{T}_l^{n+1} = \vec{K}^n , \tag{4.26}$$

where $\bar{H}^n$ is the right-hand side of Equation (4.24) and $\bar{K}^n$ is the right-hand side of Equation (4.8). Equation (4.25) is solved with a Gauss-Seidel iterative solver and Equation (4.24) is solved by substitution.

4.2 Numerical Algorithm

A Fortran-77 program implementing the numerical method is attached in the appendix. The algorithm is as follows:

Step 1 Define constants, variables and data structures.

Step 2 Set tolerance (TOL) and maximum number of iterations (N_{max}).

Step 2 Set up the initial conditions, Equations (4.3)-(4.6).

Step 3 Calculate coefficients for the linear system, Equations (4.15)-(4.21).

Step 4 Calculate the value for the Heat source:

(a) Symmetric heat source $(0 \le r \le L, 0 \le \theta \le 2\pi, 0 \le \varphi \le \pi)$

(b) Heat source on a hemisphere $(0 \le r \le L, 0 \le \theta \le 2\pi, 0 \le \varphi \le \frac{\pi}{2})$

(c) Heat source on a spot $(0 \le r \le L, 0 \le \theta \le 2\pi, 0 \le \varphi \le \frac{\pi}{4})$.

Step 5 Calculate the left-hand side of linear system, Equation (4.25).

Step 6 Set $count = 1$.

Step 7 While ($count \le N_{MAX}$) do steps 8-11.

Step 8 Solve for all $(T_e)_{ijk}^{n+1}$.

Step 9 if $\max |(T_e)_{ijk}^{n+1} - (T_e)_{ijk}^n| < TOL$, then step 13.

Step 10 Set $count = count + 1$.

Step 11 For all i, j, k set $(T_e)_{ijk}^{n} = (T_e)_{ijk}^{n+1}$.

Step 12 Maximum number of iterations reached, stop.

Step 13 Solve for all $(T_l)_{ijk}^{n+1}$.

Step 14 Print results to file:

      (a) Upper surface Temperature

      (b) Cross-section

      (c) Temperature along r-axis.

CHAPTER 5

NUMERICAL EXAMPLES

5.1 Description

We will apply our numerical method to investigate the temperature distribution in a gold sphere subjected to an ultra-short laser pulse heating. The radius (L) of the sphere is $0.1\mu m$. The thermal properties of gold are shown in Table 5.1.

Table 5.1 Thermal properties of gold [Tzou 1997]

Parameters	Values
C_e	2.1×10^4 J/m^3 K
C_l	2.5×10^6 J/m^3 K
k_e	315 W/m K
G	2.6×10^{16} W/m^3 K

The initial conditions are

$$T_e(r,\theta,\varphi,0) = T_l(r,\theta,\varphi,0) = T_0, \tag{5.1}$$

where $T_0 = 300$ K,

$$\frac{\partial T_e}{\partial t}(r,\theta,\varphi,0) = \frac{\partial T_l}{\partial t}(r,\theta,\varphi,0) = 0. \tag{5.2}$$

63

The boundary conditions are

$$\frac{\partial T_e}{\partial r}(L,\theta,\varphi,t) = \frac{\partial T_l}{\partial r}(L,\theta,\varphi,t) = 0, \tag{5.3}$$

$$T_e(r,\theta,\varphi,t) = T_e(r,\theta+2\pi,\varphi,t), \quad T_l(r,\theta,\varphi,t) = T_l(r,\theta+2\pi,\varphi,t), \tag{5.4}$$

$$\frac{\partial T_e}{\partial \varphi}(r,\theta,0,t) = \frac{\partial T_l}{\partial \varphi}(r,\theta,\pi,t). \tag{5.5}$$

The scheme is applied for each case with three different mesh sizes, 50x20x20, 100x20x20, and 200x20x20 grid points in a (r,θ,φ) spherical coordinates system. The time increment (Δt) is $0.005\,ps$.

5.2 Symmetric Heat Source
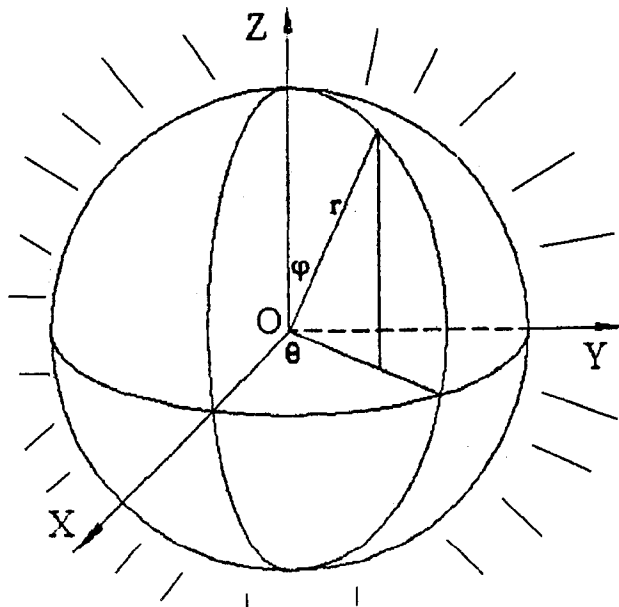
5.2.1 Heat Source

Figure 5.1 Gold sphere subjected to a symmetric ultra-short pulse laser irradiation

The heat source is chosen to be

$$Q(r,t) = 0.94J \left[\frac{1-R}{t_p \delta} \right] e^{-\frac{L-r}{\delta} - 2.77\left(\frac{t-2t_p}{t_p} \right)^2}, \qquad (5.6)$$

where J is the laser fluence, L is the radius of the sphere, δ is the penetration depth of laser irradiation, R is the radiative reflectivity of the sample to the laser beam, and t_p the full-width-at-half-maximum pulse duration.

Table 5.2 Heat source parameters [Tzou 1997]

Parameters	Values
J	13.4 J/m^2
t_p	$100\,fs$ ($1\,fs = 10^{-15}s$)
δ	$15.3\,nm$ ($1\,nm = 10^{-9}m$)
R	0.93

5.2.2 Results

Electron gas temperature. Figure 5.2 shows the normalized electron gas temperature change $\left[\frac{\Delta T_e}{(\Delta T_e)_{max}} \right]$ on the surface of the gold sphere. This temperature distribution is divided in three time intervals. In the first time interval, 0-0.25 ps, we have a very fast rise of the electron gas temperature on the surface, up to several hundred degrees $(\Delta T_e)_{max} = 910\text{K}$, due to the initial excitation of the laser pulse. Most of the supplied energy is being transferred to the inner regions of the sphere thus raising the temperature in those areas. In the second time interval, which lasts from about 0.26 ps to

1.8 *ps*, thermal equilibrium is quickly reached *within* the electron gas and then the electron gas temperature starts to drop quickly. This is due to the fact that during this time period, the energy supplied is heating the metal lattice through lattice-electron coupling. In the final time domain, 1.8 *ps* and up, the electron gas temperature is uniform as thermal equilibrium with the metal lattice is approaching. We see that the plot is very similar to the one obtained by [Tzou 1997] as seen in Figure 2.3. Additionally, the mesh size's impact on the temperature profile is insignificant which implies numerical stability.

Figures 5.3-5.7 show the contour plots of the electron gas temperatures along the $r\varphi$ cross-section ($0 \leq r \leq L$, $0 \leq \varphi \leq \pi$) at times t=0.2 *ps*, 0.25 *ps*, 0.5 *ps*, 1.0 *ps*, and 2.0 *ps*, respectively. In Figure 5.3, t=0.2 *ps*, we are in the first phase of the electronic excitation. The temperature difference is very large between the outer layer and the inner part of the sphere, $(\Delta T_e) \approx 400K$, and the outer temperature has still not reached its maximum of about 1200K. At t=0.25 *ps*, as shown in Figure 5.4. The temperature difference is still the same between the outer layer and the inner parts, $(\Delta T_e) \approx 400K$, but at this point the maximum temperature of 1200K is almost reached, signifying the end of the first phase. Figure 5.5 shows that at t=0.5 *ps*, thermal equilibrium has occurred within the electron gas around 966K, thus signaling the beginning of the second phase. Heat transfer to the metal lattice is occurring through lattice-electron coupling. In Figure 5.6, which describes t=1.0 *ps*, we see the effect of the lattice-electron coupling as the electron gas temperature has dropped by 300K in 0.5 *ps* to around 660K. Finally, in Figure 5.7, we are in the third phase, t=2.0 *ps*. The effect of the coupling is slowing down. The electron gas temperature has dropped by only 260K in 1 *ps* stabilizing around 410K as the process is headed toward thermal equilibrium *between* the electron gas temperature and the metal lattice

temperature. Figure 5.8 describes the electron gas temperature along the radial axis, r. We see that at t=0.2 ps and t=0.25 ps the electron gas temperature is rising to its maximum value near the surface while the central regions are lagging a few hundred degrees behind. It should also be noted that the exponential decay along the radial axis assumed in Equation (5.6) holds very well at this stage. At t=0.5 ps, the thermal equilibrium is reached within the electron gas and the temperature has started its downward shift which is continued at t=1.0 ps and t=2.0 ps.
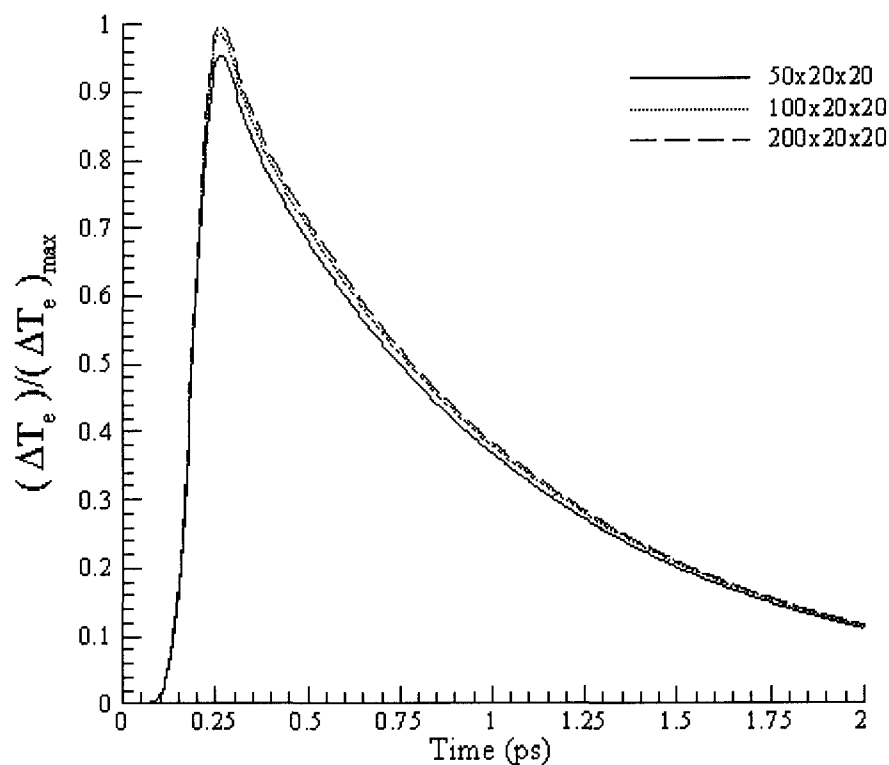
Figure 5.2 Normalized electron gas temperature change plotted against time.
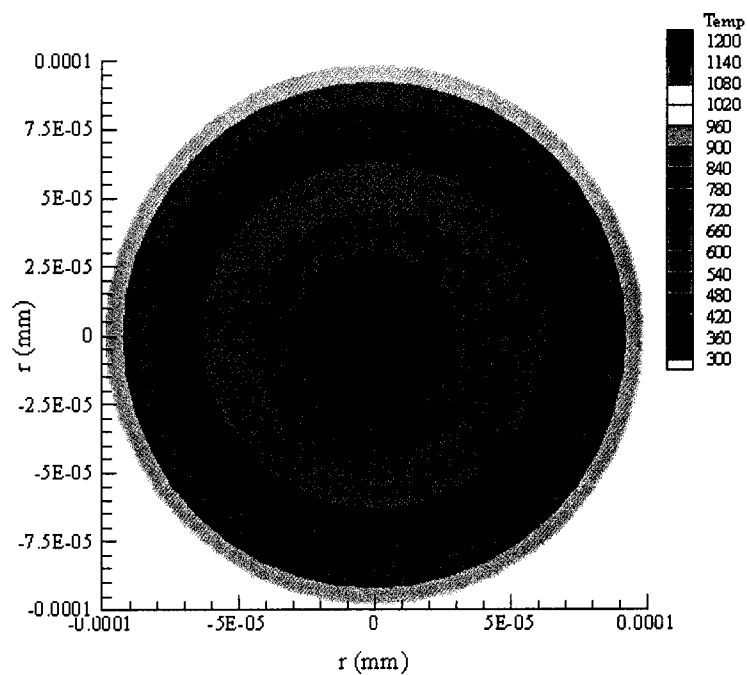(Symmetric heat source)

Figure 5.3 Contour plot of electron gas temperature along the $r\varphi$ cross-section at $t=0.2\,ps$. (Symmetric heat source)
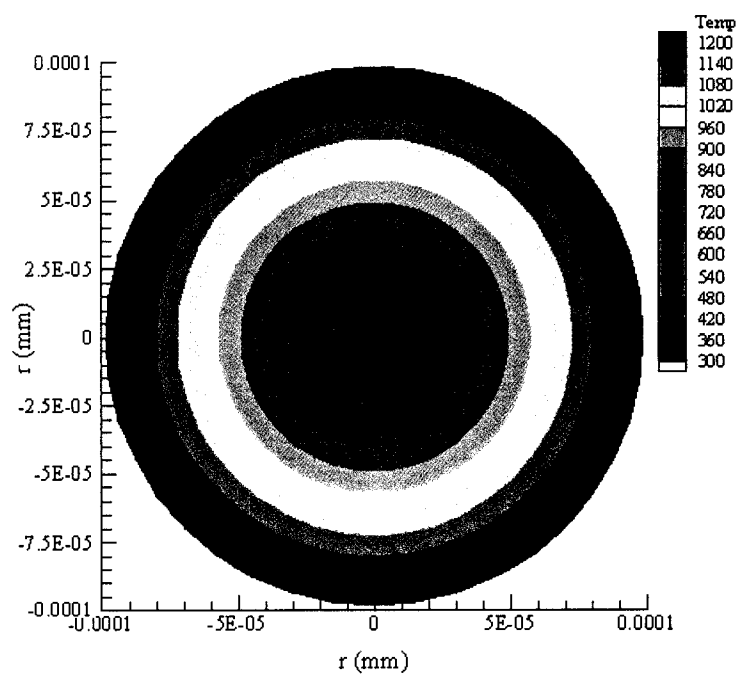

Figure 5.4 Contour plot of electron gas temperature along the $r\varphi$ cross-section at $t=0.25\,ps$. (Symmetric heat source)
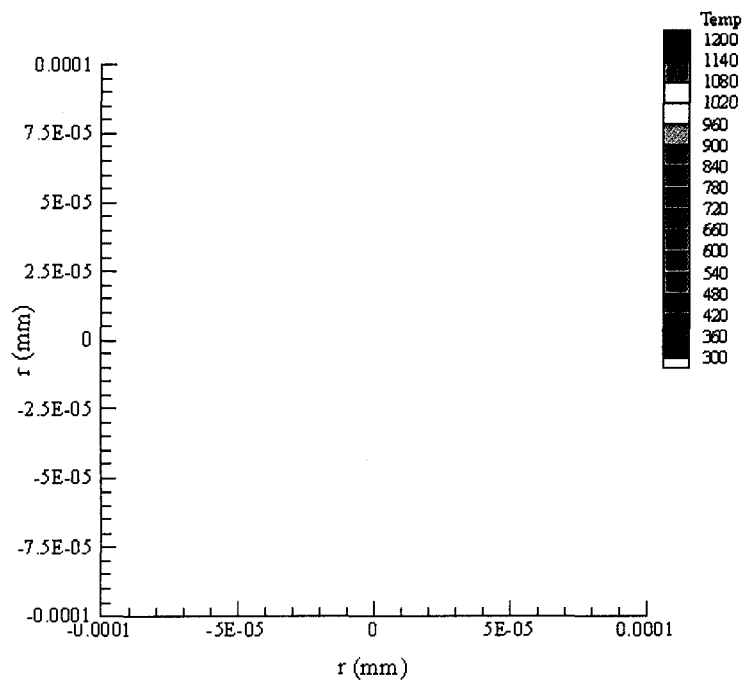
Figure 5.5 Contour plot of electron gas temperature along the $r\varphi$ cross-section at t=0.5 ps. (Symmetric heat source)
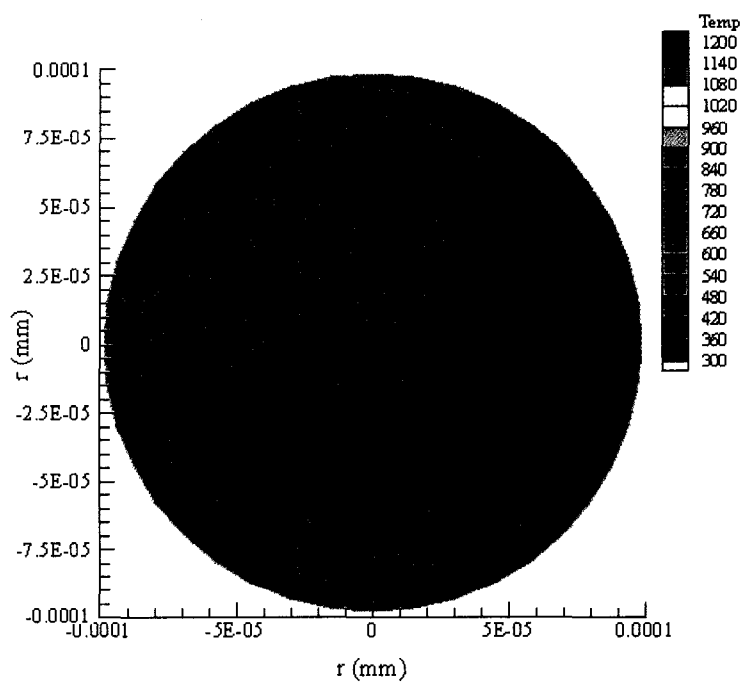

Figure 5.6 Contour plot of electron gas temperature along the $r\varphi$ cross-section at t=1.0 ps. (Symmetric heat source)
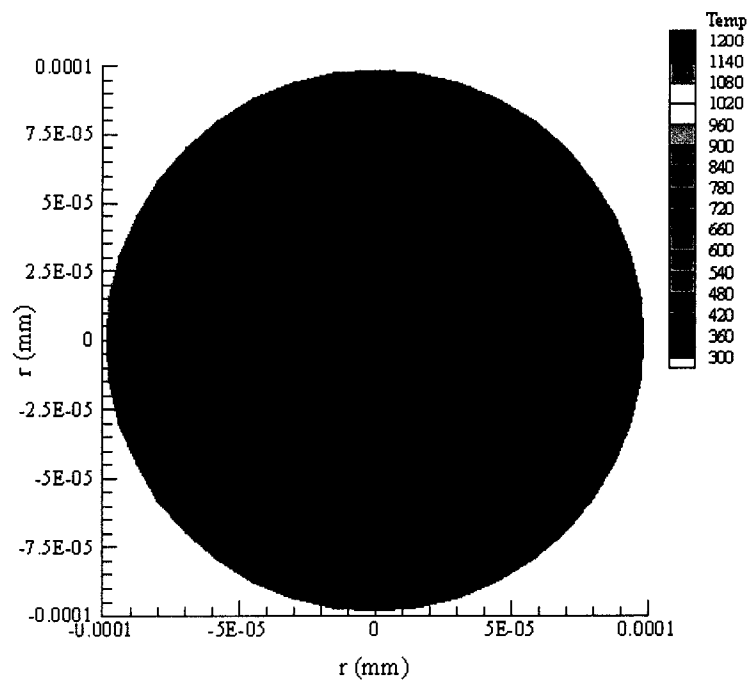
Figure 5.7 Contour plot of electron gas temperature along the $r\varphi$ cross-section at $t=2.0\,ps$. (Symmetric heat source)
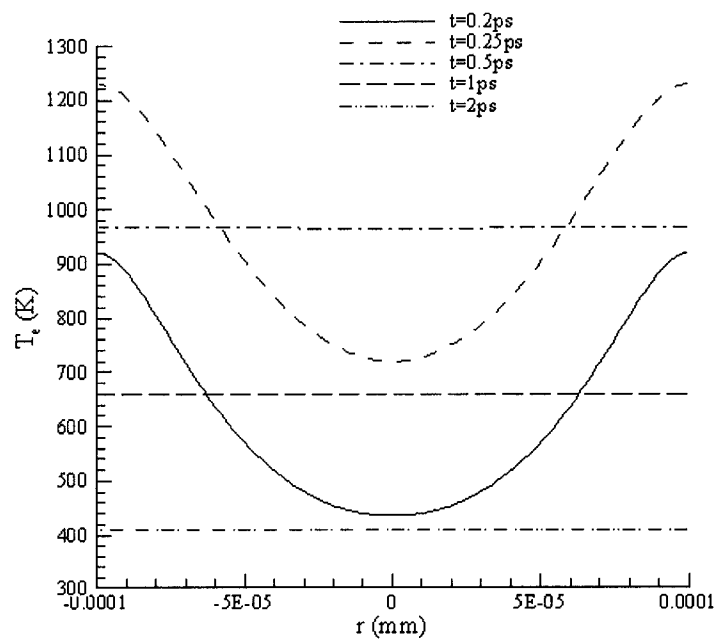

Figure 5.8 Electron gas temperature along the radial axis r. (Symmetric heat source)

Lattice Temperature. Figure 5.9 shows the normalized lattice temperature change $\left[\dfrac{\Delta T_l}{(\Delta T_l)_{\max}}\right]$ on the surface of the gold sphere. This temperature distribution is divided in three time intervals. In the first time interval, 0-0.25 *ps*, we have no activities at all. All the supplied energy is being transferred to the electron gas, no coupling is taking place at this time, and consequently the metal lattice temperature is almost unchanged. In the second time interval, which lasts from about 0.26 *ps* to 1.8 *ps*, the metal lattice temperature starts to rise quickly as the electron-lattice coupling kicks in thus raising the temperature of the lattice. In the final time domain, 1.8 *ps* and up, the lattice temperature is leveling off as thermal equilibrium with the electron gas is approaching. We see that this plot is completely different from the one obtained by [Tzou 1997] as seen in Figure 2.3. Also, the mesh size's impact on the temperature profile is insignificant which implies numerical stability.

Figures 5.10-5.14 show the contour plots of the lattice temperatures along the $r\varphi$ cross-section ($0 \le r \le L$, $0 \le \varphi \le \pi$) at times *t*=0.2 *ps*, 0.25 *ps*, 0.5 *ps*, 1.0 *ps*, and 2.0 *ps*, respectively. In Figure 5.10, *t*=0.2 *ps*, we are in the first phase of the electronic excitation. All the energy is being used by the electron gas and no coupling is occurring yet. The temperature difference is insignificant between the outer layer and the inner part of the sphere $(\Delta T_l) \approx 0$K. At *t*=0.25 *ps*, as shown in Figure 5.11. The temperature difference is still the same between the outer layer and the inner parts, $(\Delta T_l) \approx 0$K, but at this point the electron gas temperature has reached its maximum signifying the end of the first phase. Figure 5.12 shows that at *t*=0.5 *ps*, since thermal equilibrium has occurred within the electron gas, the coupling is about to start. The temperature is starting to rise

almost uniformly across the sphere. In Figure 5.13, which describes $t=1.0\,ps$, we see the effect of the lattice-electron coupling as the lattice temperature rises uniformly by 3K in 0.5 ps to around 306K. Finally, in Figure 5.14, we are in the third phase, $t=2.0\,ps$. The effect of the coupling is slowing down; the lattice temperature continues a slower rise toward thermal equilibrium *between* the electron gas temperature and the metal lattice temperature. Figure 5.15 describes the metal lattice temperature along the radial axis, r. We see that at $t=0.2\,ps$ and $t=0.25\,ps$ the lattice temperature is uniformly unchanged although it is showing a slight spike around the surface. It should also be noted that the exponential decay along the radial axis assumed in Equation (5.6) is being slightly transferred to the metal lattice as well. At $t=0.5\,ps$, the thermal equilibrium is reached within the electron gas and the metal lattice temperature has started its upward shift, which is continued at $t=1.0\,ps$ and $t=2.0\,ps$. As the lattice moves toward equilibrium with the electron gas, the exponential decay is being affirmed in a more pronounced way.
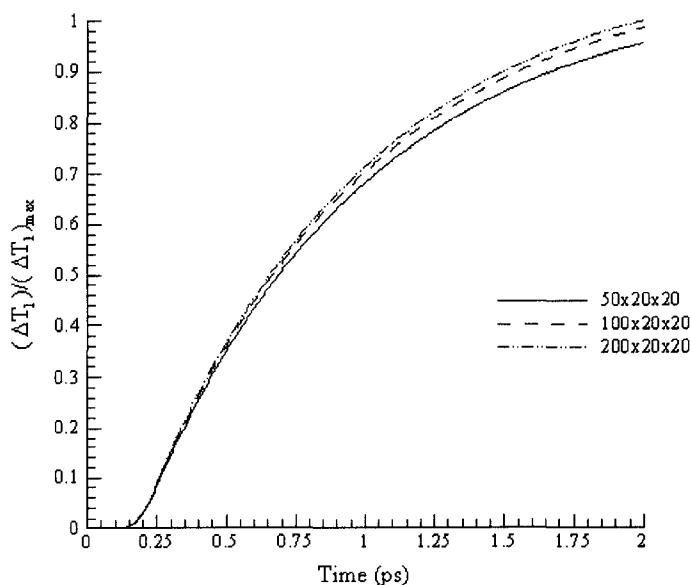

Figure 5.9 Normalized metal lattice temperature change plotted against time.
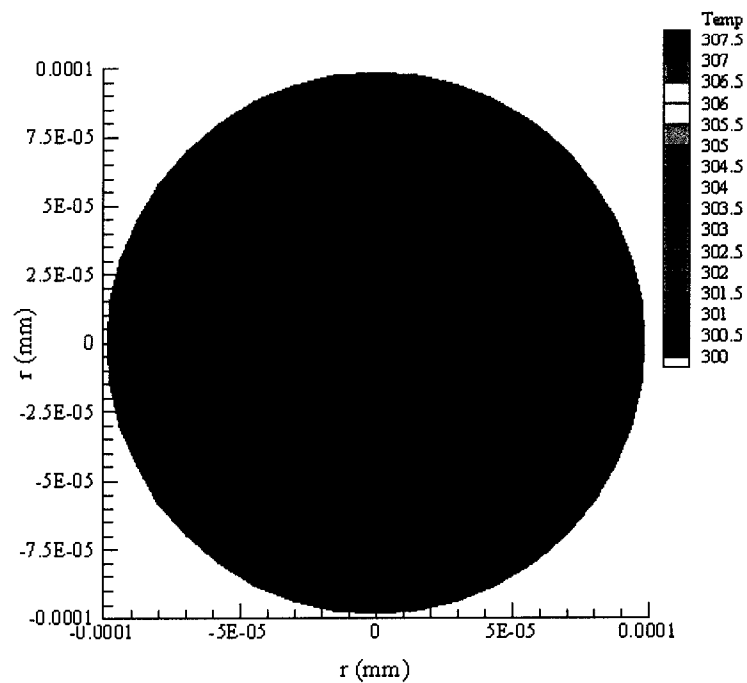(Symmetric heat source)

Figure 5.10 Contour plot of the metal lattice temperature along the $r\varphi$ cross-section at $t=0.2\,ps$. (Symmetric heat source)

Figure 5.11 Contour plot of the metal lattice temperature along the $r\varphi$ cross-section at $t=0.25\,ps$. (Symmetric heat source)

Figure 5.12 Contour plot of the metal lattice temperature along the $r\varphi$ cross-section at t=0.5 ps. (Symmetric heat source)

Figure 5.13 Contour plot of the metal lattice temperature along the $r\varphi$ cross-section at t=1.0 ps. (Symmetric heat source)

Figure 5.14 Contour plot of the metal lattice temperature along the $r\varphi$ cross-section at t=2.0 ps. (Symmetric heat source)
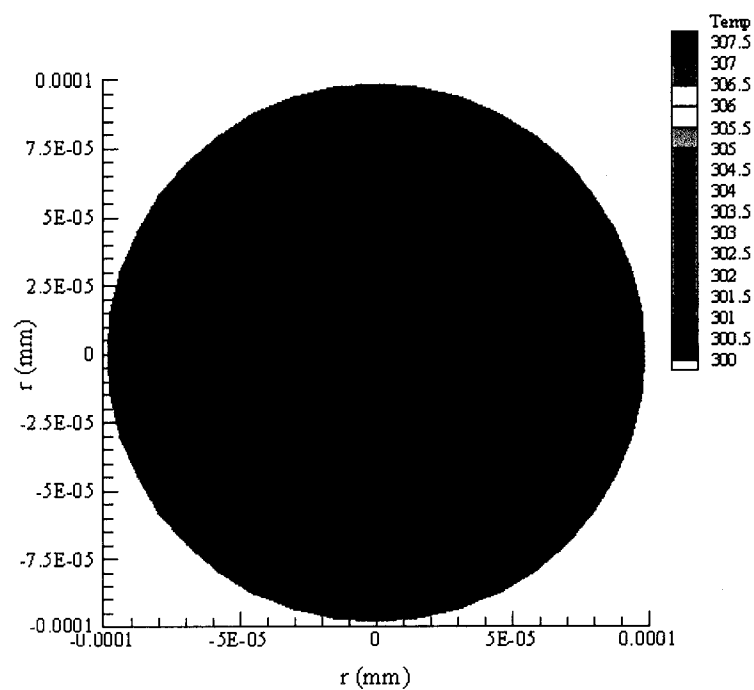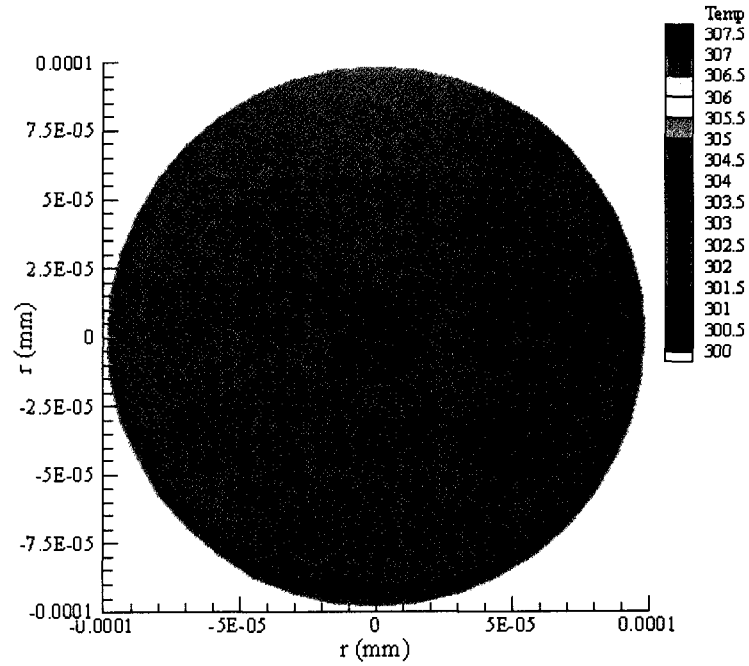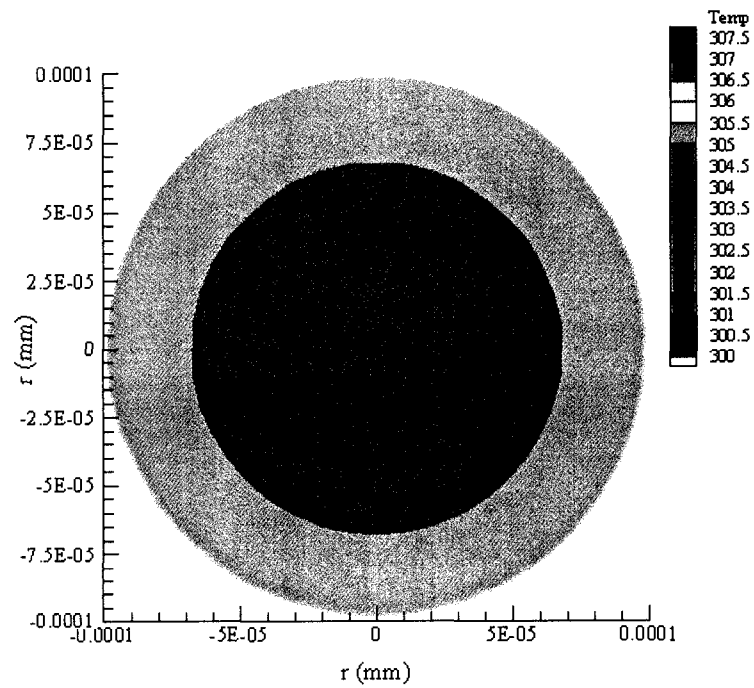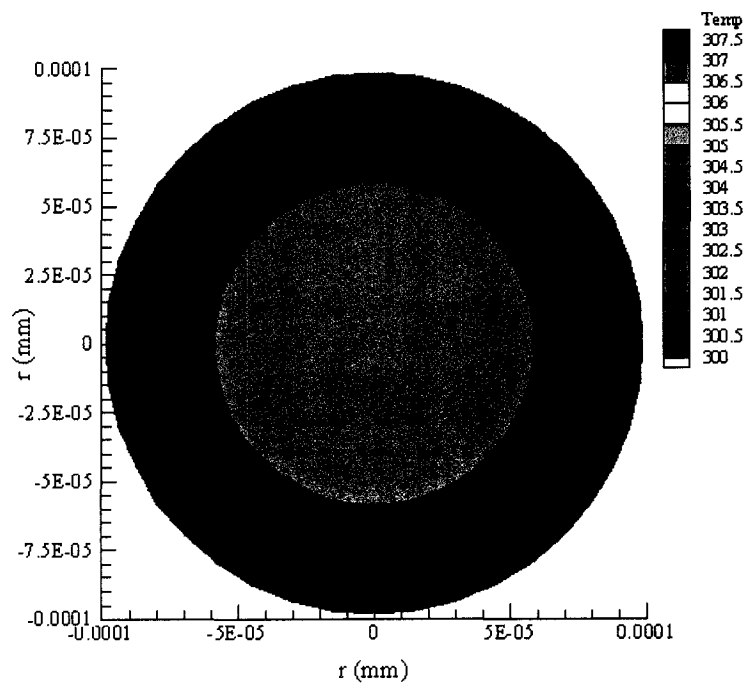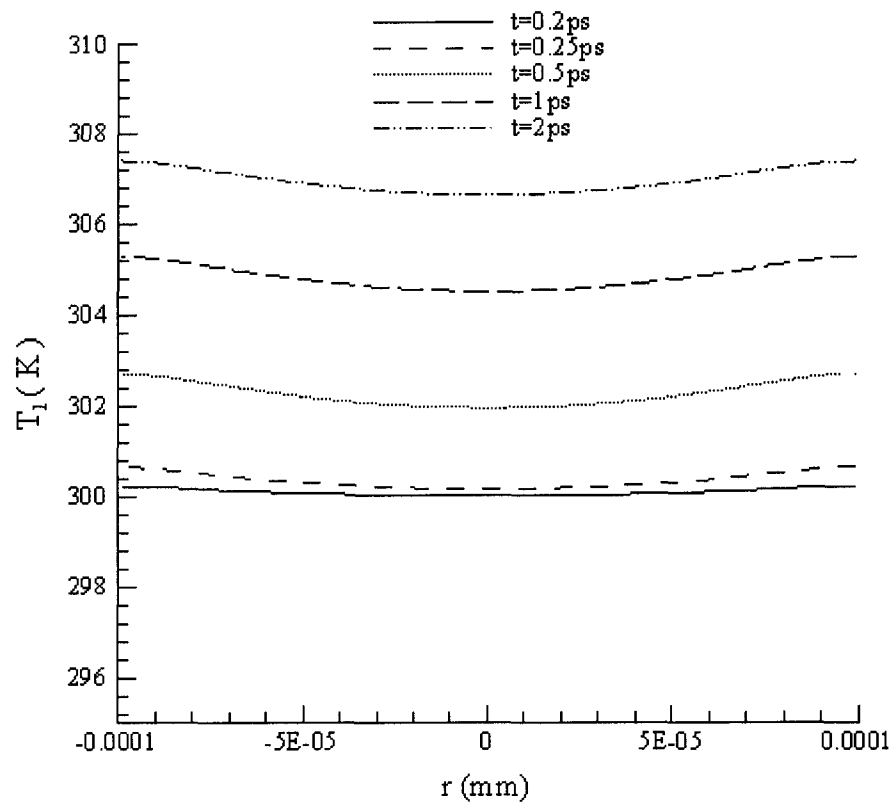
Figure 5.15 Metal lattice temperature along the radial axis r. (Symmetric heat source)

5.3 Heat Source Applied to a Hemisphere

5.3.1 Heat Source
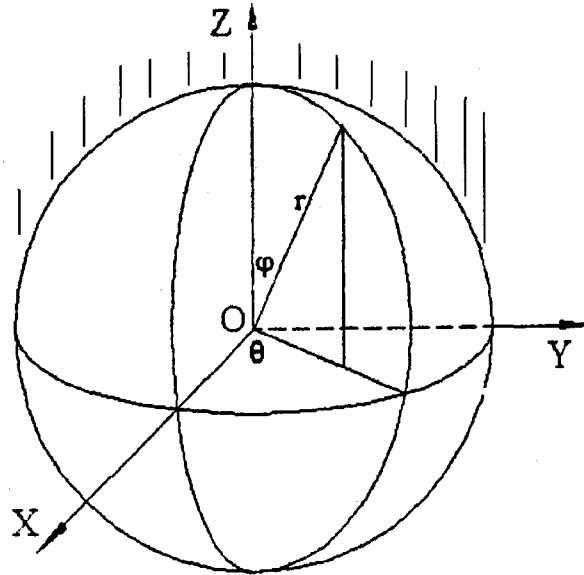
Figure 5.16 Gold hemisphere subjected to a unidirectional ultra-short pulse laser irradiation

The heat source is chosen to be

$$Q(r,\varphi,t) = 0.94J \left[\frac{1-R}{t_p \delta} \right] e^{-\frac{L-r}{\delta} - 2.77 \left(\frac{t-2t_p}{t_p} \right)^2} \cos\varphi, \qquad (5.7)$$

where J is the laser fluence, L is the radius of the sphere, δ is the penetration depth of laser irradiation, R is the radiative reflectivity of the sample to the laser beam, t_p the full-width-at-half-maximum pulse duration, φ is the angle between OP, and the positive z-axis, ranging from 0 to $\frac{\pi}{2}$.

5.3.2 Results

Electron gas temperature. Figure 5.17 shows the normalized electron gas temperature

change $\left[\dfrac{\Delta T_e}{(\Delta T_e)_{max}}\right]$ on the surface of the gold sphere. This temperature distribution is

divided in three time intervals. In the first time interval, 0-0.25 ps, we have a very fast

rise of the electron gas temperature on the surface, up to several hundred

degrees $(\Delta T_e)_{max} = 843\mathrm{K}$, due to the initial excitation of the laser pulse. In the second

time interval, which lasts from about 0.26 ps to 1.5 ps, the electron gas temperature drops

quickly as most of the supplied energy is being transferred to the inner part of the sphere

thus raising the temperature in those areas. In the final time domain, 1.5 ps and up, the

electron gas temperature is slowly moving towards thermal equilibrium. We see that the

plot is very similar to the one obtained in Figure 5.2, except that it is taking longer to

reach thermal equilibrium within the electron gas temperature. Additionally, the mesh

size's impact on the temperature profile is insignificant which implies numerical stability.

Figures 5.18-5.22 show the contour plots of the electron gas temperatures along the

$r\varphi$ cross-section ($0 \leq r \leq L$, $0 \leq \varphi \leq \pi$) at times $t=0.2\,ps$, $0.25\,ps$, $0.5\,ps$, $1.0\,ps$, and 2.0

ps, respectively. In Figure 5.18, $t=0.2$ ps, we are in the first phase of the electronic

excitation. The temperature difference is very large between the outer layer and the inner

part of the sphere, $(\Delta T_e) \approx 600\mathrm{K}$, and the outer temperature has still not reached its

maximum of about 1200K. At $t=0.25$ ps, as shown in Figure 5.19. The temperature

difference is the largest between the outer layer and the inner parts, $(\Delta T_e) \approx 870\mathrm{K}$, but at

this point the maximum temperature of 1200K is almost reached signifying the end of the

first phase. Figures 5.20 and 5.21 show that at $t=0.5\,ps$ and $t=1.0\,ps$, we are closing in on

thermal equilibrium within the electron gas as the difference in temperature falls from

$(\Delta T_e) \approx 870K$ in Figure 5.19 to around 400K in Figure 5.20 and to less than 100K in

Figure 5.21 thus signaling the end of the second phase. Finally, in Figure 5.22, we are in

the third phase, $t=2.0$ ps. The electron gas temperature has almost reached thermal

equilibrium, $(\Delta T_e) \approx 5K$. Figure 5.23 describes the electron gas temperature along the

radial axis, r. We see that at $t=0.2$ ps and $t=0.25$ ps, the electron gas temperature is rising

to its maximum value near the surface while the central regions lag a few hundred

degrees behind. At the other time indices, we see the transfer of energy from the top to

the bottom of the microsphere.
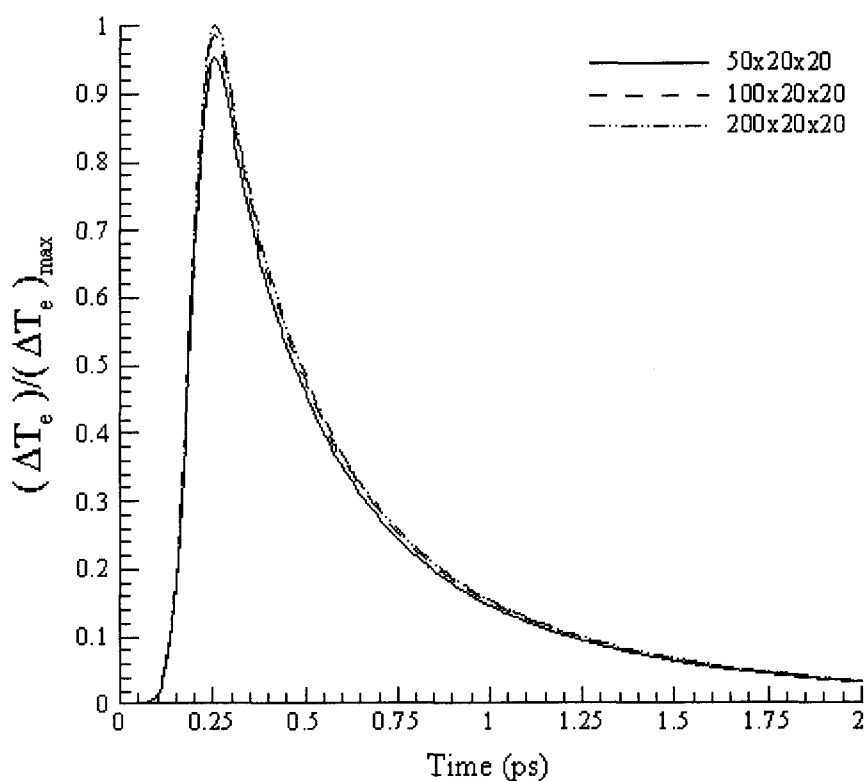
Figure 5.17 Normalized electron gas temperature change plotted against time.
(Heat source applied to a hemisphere)

Figure 5.18 Contour plot of the electron gas temperature along the $r\varphi$ cross-section at t=0.2 ps. (Heat source applied to a hemisphere)

Figure 5.19 Contour plot of the electron gas temperature along the $r\varphi$ cross-section at t=0.25 ps. (Heat source applied to a hemisphere)

Figure 5.20 Contour plot of the electron gas temperature along the $r\varphi$ cross-section at t=0.5 ps. (Heat source applied to a hemisphere)

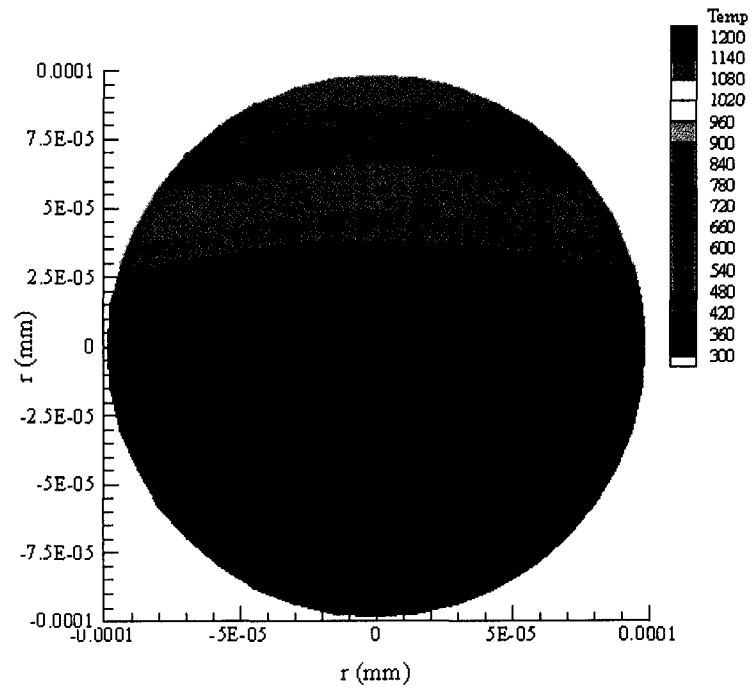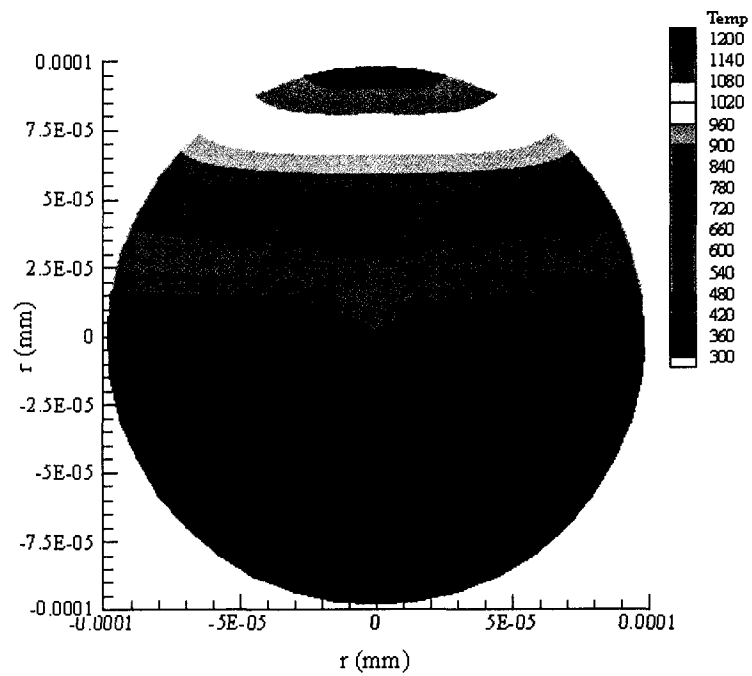Figure 5.21 Contour plot of the electron gas temperature along the $r\varphi$ cross-section at t=1.0 ps. (Heat source applied to a hemisphere)

Figure 5.22 Contour plot of the electron gas temperature along the $r\varphi$ cross-section at t=2.0 ps. (Heat source applied to a hemisphere)
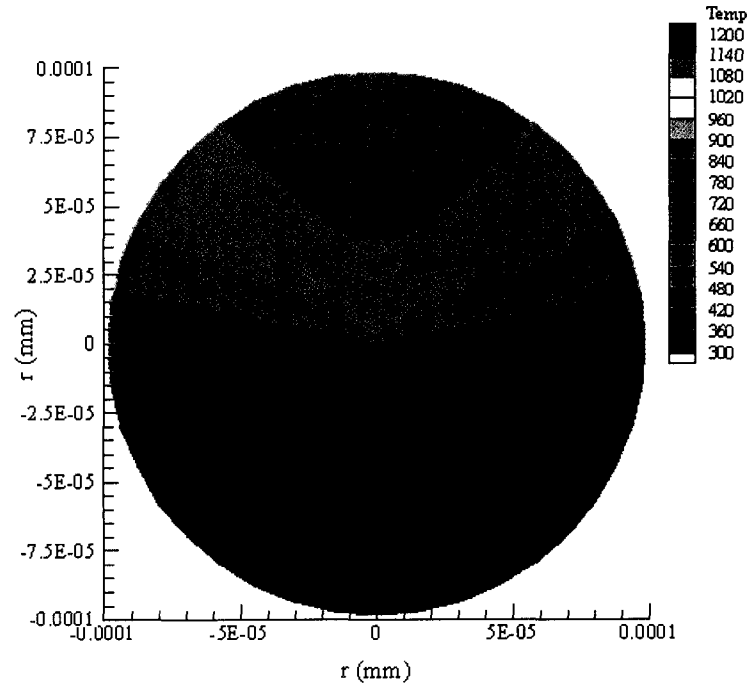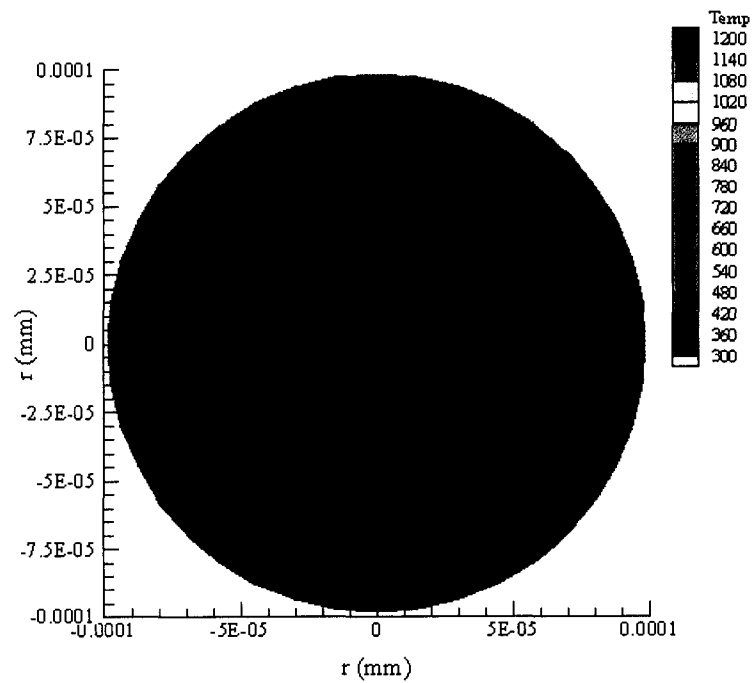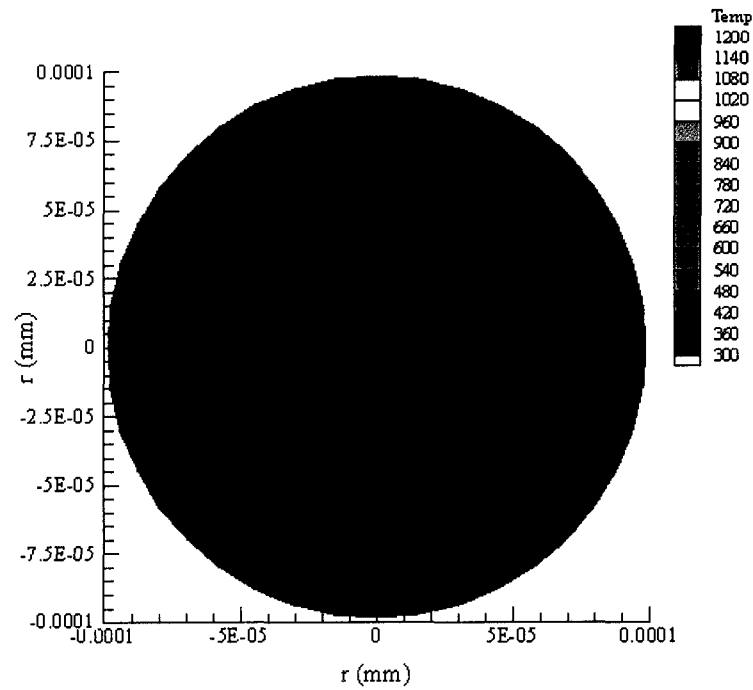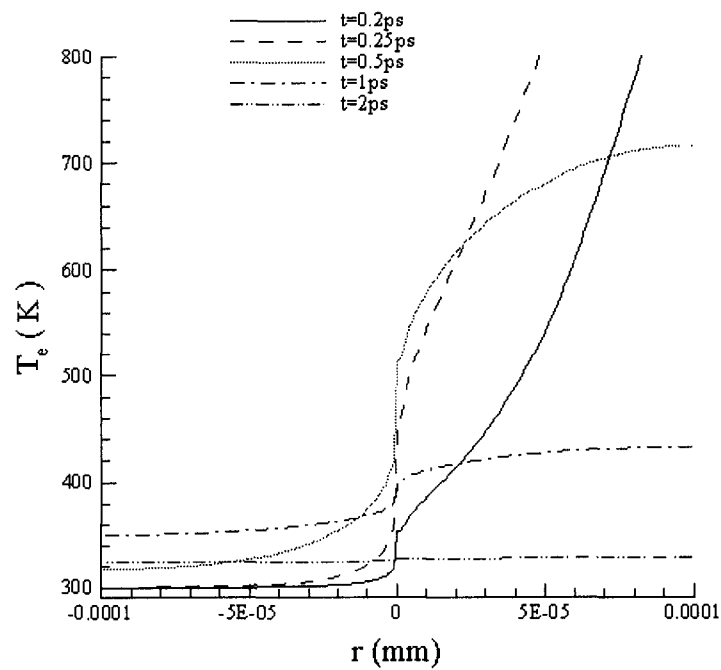

Figure 5.23 Electron gas temperature along the radial axis r.
(Heat source applied to a hemisphere)

Lattice Temperature. Figure 5.24 shows the normalized lattice temperature change $\left[\dfrac{\Delta T_l}{(\Delta T_l)_{\text{max}}} \right]$ on the surface of the gold sphere. This temperature distribution is divided in three time intervals. In the first time interval, $0\text{-}0.25\ ps$, we have no activities at all. All the supplied energy is being transferred to the electron gas, no coupling is taking place at this time, and consequently the metal lattice temperature is almost unchanged. In the second time interval, which lasts from about $0.26\ ps$ to $1.5\ ps$, the metal lattice temperature starts to rise slowly as the electron-lattice coupling kicks in, thus raising the temperature of the lattice. This plot is very similar to the one obtained in Figure 5.9 except that it is a lot steeper in the early stages due to the fact that at this point thermal equilibrium has not been reached within the electron gas yet. In the final time domain, $1.5\ ps$ and up, the lattice temperature is leveling off as thermal equilibrium within the electron gas is approaching. Also the mesh size's impact on the temperature profile is insignificant which implies numerical stability.

Figures 5.25-5.29 show the contour plots of the lattice temperatures along the $r\varphi$ cross-section ($0 \leq r \leq L$, $0 \leq \varphi \leq \pi$) at times $t=0.2\ ps$, $0.25\ ps$, $0.5\ ps$, $1.0\ ps$ and $2.0\ ps$, respectively. They show a progressive heating of the metal lattice as the temperature is being transferred from the inner surface towards the bottom of the sphere. Figure 5.30 describes the metal lattice temperature along the radial axis, r. We see the temperature slowly rising as there is a clear difference between the upper surface and the colder regions at the bottom of the sphere. This plot is very different from the obtained in Figure 5.15 as it is no longer a uniform temperature distribution.
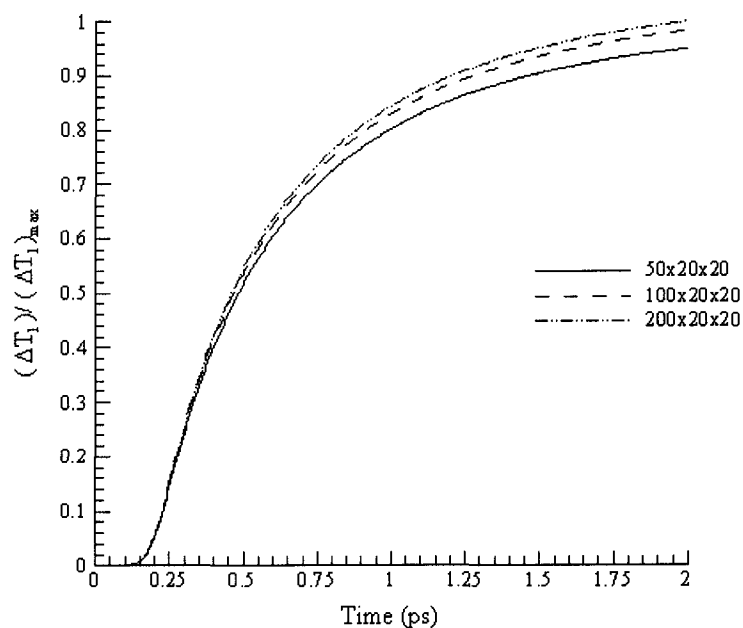
Figure 5.24 Normalized metal lattice temperature change plotted against time.
(Heat source applied to a hemisphere)
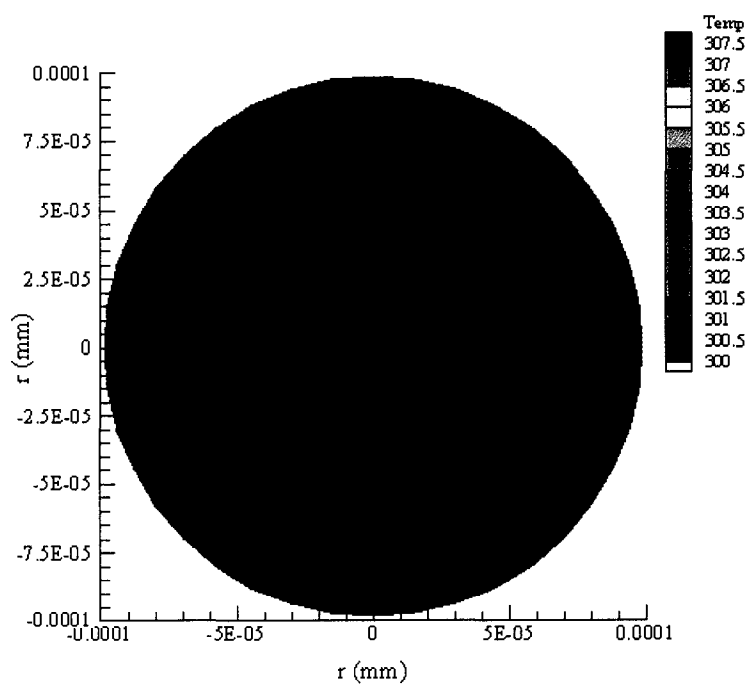
Figure 5.25 Contour plot of the metal lattice temperature along the $r\varphi$ cross-section at
$t=0.2\,ps$. (Heat source applied to a hemisphere)
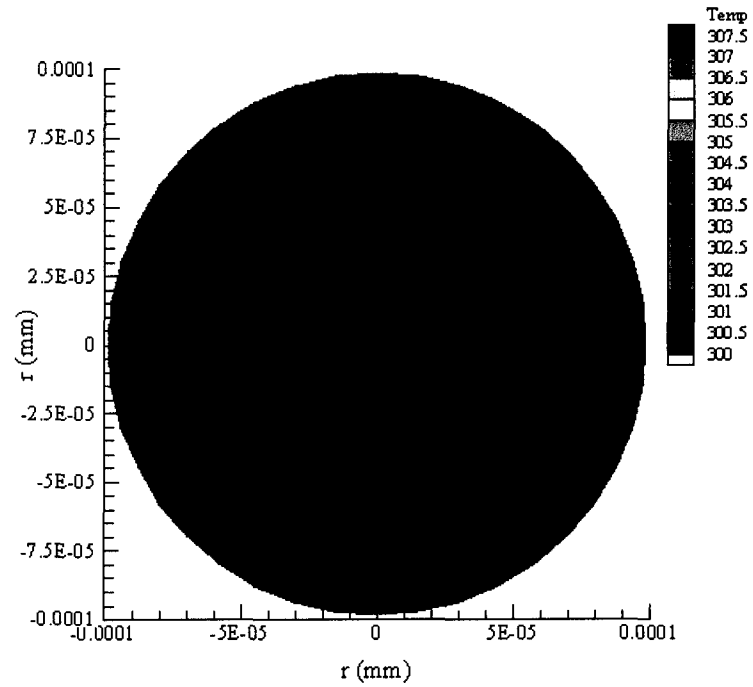
Figure 5.26 Contour plot of the metal lattice temperature along the $r\varphi$ cross-section at $t=0.25\,ps$. (Heat source applied to a hemisphere)
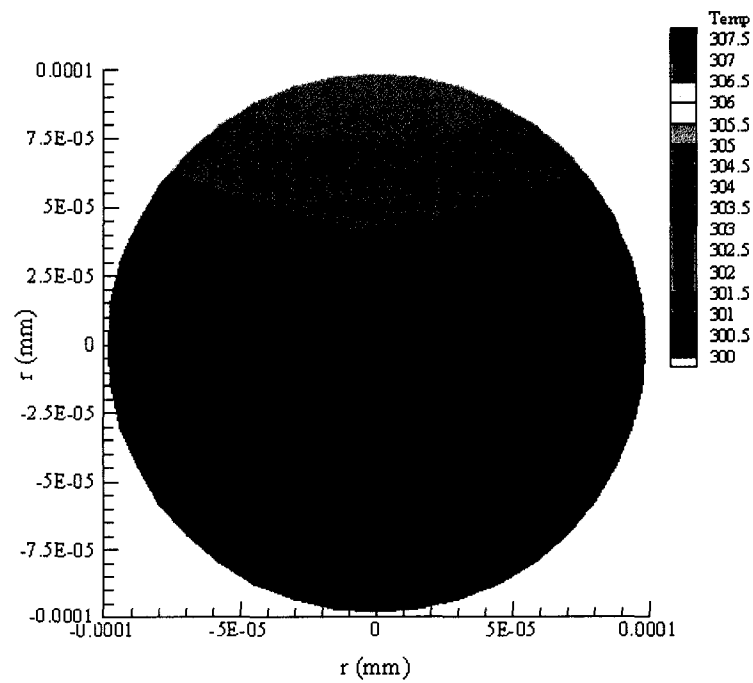
Figure 5.27 Contour plot of the metal lattice temperature along the $r\varphi$ cross-section at $t=0.5\,ps$. (Heat source applied to a hemisphere)
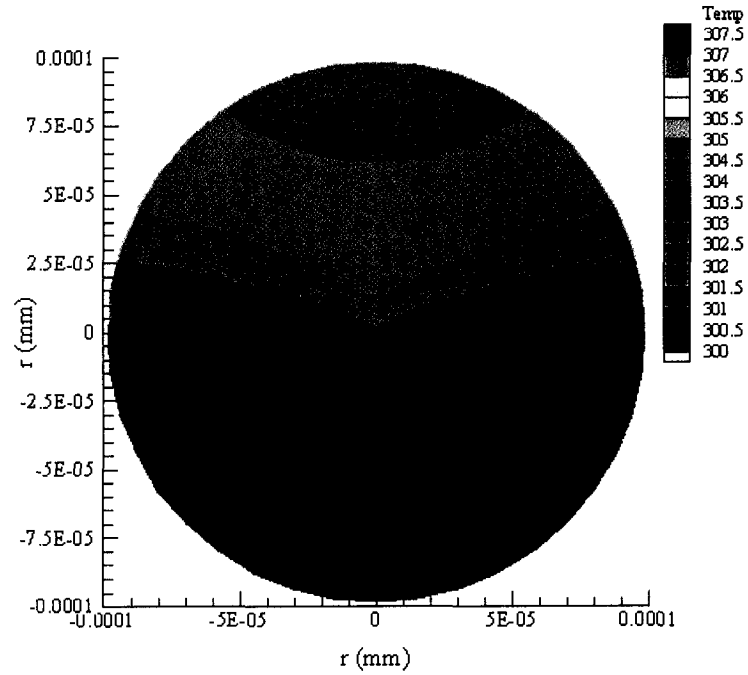
Figure 5.28 Contour plot of the metal lattice temperature along the $r\varphi$ cross-section at $t=1.0\,ps$. (Heat source applied to a hemisphere)
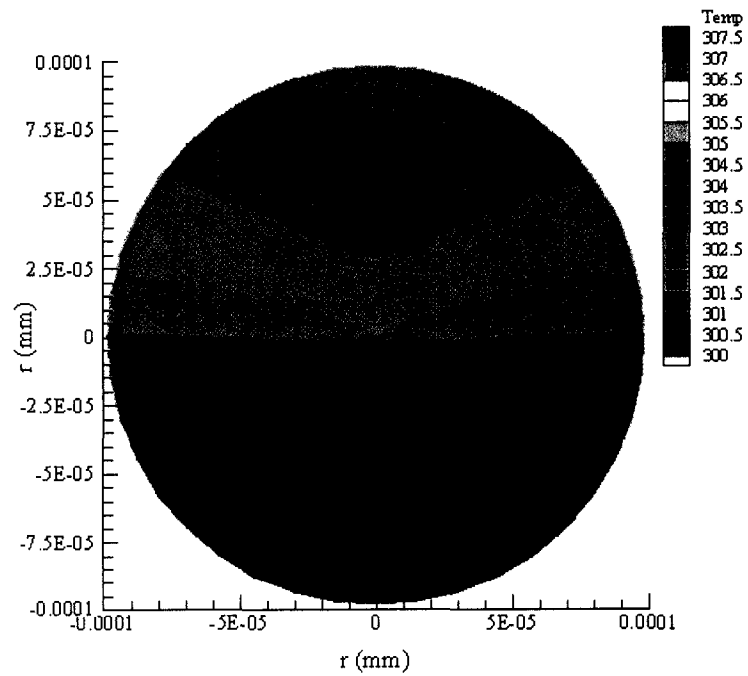
Figure 5.29 Contour plot of the metal lattice temperature along the $r\varphi$ cross-section at $t=2.0\,ps$. (Heat source applied to a hemisphere)
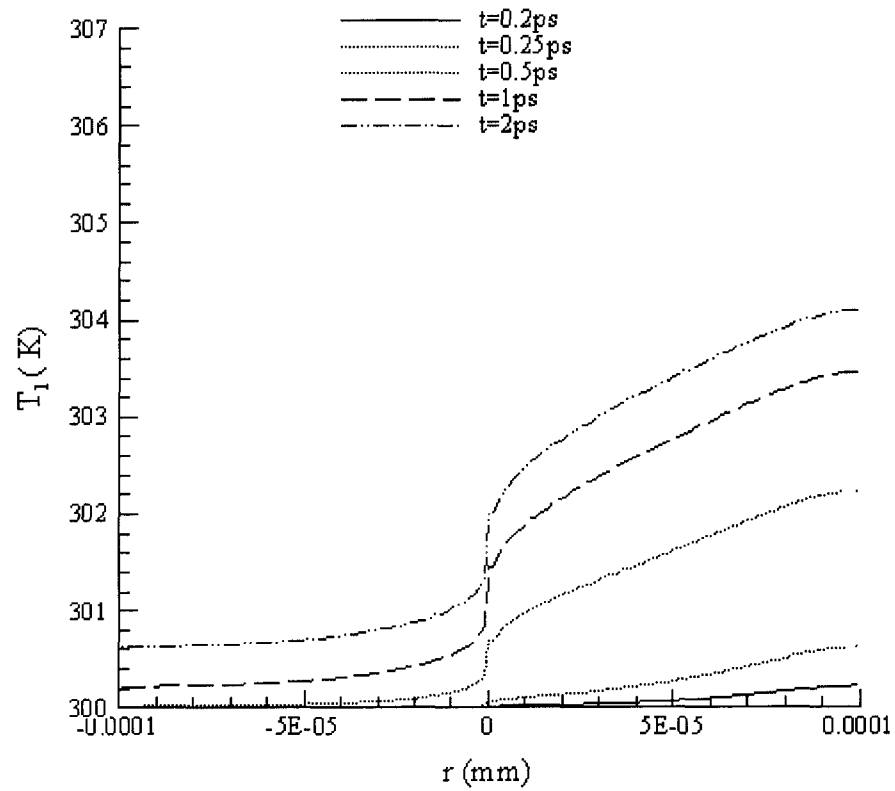
Figure 5.30 Metal lattice temperature along the radial axis *r*.
(Heat source applied to a hemisphere)

5.4 Heat Source Applied to a Spot

5.4.1 Heat Source
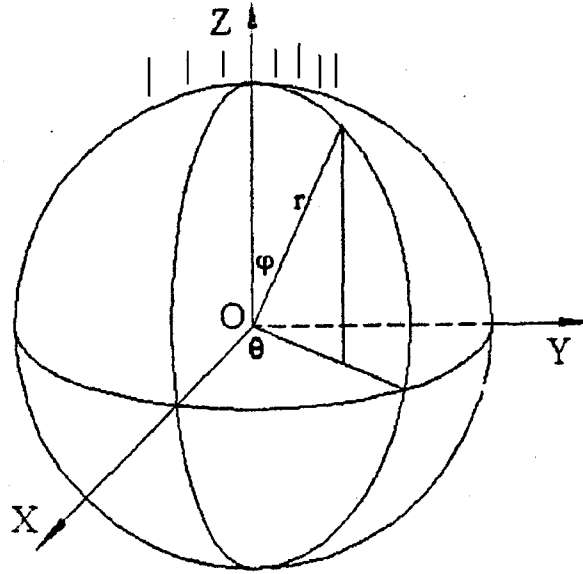
Figure 5.31 Gold sphere subjected to a unidirectional ultra-short pulse laser irradiation.

Angle of irradiation $(0 \leq \varphi \leq \dfrac{\pi}{4})$

The heat source is chosen to be equation (5.7):

$$Q(r,\varphi,t) = 0.94J \left[\frac{1-R}{t_p \delta}\right] e^{-\frac{L-r}{\delta} - 2.77\left(\frac{t-2t_p}{t_p}\right)^2} \cos\varphi, \qquad (5.7)$$

where J is the laser fluence, L is the radius of the sphere, δ is the penetration depth of laser irradiation, R is the radiative reflectivity of the sample to the laser beam, t_p the full-width-at-half-maximum pulse duration, φ is the angle between OP, and the positive z-axis, ranging from 0 to $\dfrac{\pi}{4}$.

5.4.2 Results

Electron gas temperature. Figure 5.32 shows the normalized electron gas temperature

change $\left[\dfrac{\Delta T_e}{(\Delta T_e)_{max}}\right]$ on the surface of the gold sphere. This temperature distribution is

divided in three time intervals. In the first time interval, 0-0.25 ps, we have a very fast

rise of the electron gas temperature on the surface, up to several hundred

degrees $(\Delta T_e)_{max} = 822K$, due to the initial excitation of the laser pulse. In the second

time interval, which lasts from about 0.26 ps to 1.3 ps, the electron gas temperature drops

quickly as most of the supplied energy is being transferred to the inner part of the sphere

thus raising the temperature in those areas. In the final time domain, 1.3 ps and up, the

electron gas temperature is slowly moving towards thermal equilibrium. We see that the

plot is very similar to the one obtained in Figure 5.17, except that the temperature drop is

more accelerated. Additionally, the mesh size's impact on the temperature profile is

insignificant which implies numerical stability.

Figures 5.33-5.37 show the contour plots of the electron gas temperatures along the

$r\varphi$ cross-section ($0 \le r \le L$, $0 \le \varphi \le \pi$) at times t=0.2 ps, 0.25 ps, 0.5 ps, 1.0 ps, and 2.0

ps, respectively. In Figure 5.33, t=0.2 ps, we are in the first phase of the electronic

excitation. The temperature difference is very large between the outer layer and the inner

part of the sphere, $(\Delta T_e) \approx 600K$, and the outer temperature has still not reached its

maximum of about 1200K. At t=0.25 ps, as shown in Figure 5.34, the temperature

difference is the largest between the outer layer and the inner parts, $(\Delta T_e) \approx 850K$, but at

this point the maximum temperature of 1200K is almost reached, signifying the end of

the first phase. Figures 5.35 and 5.36 show that at t=0.5 ps and t=1.0 ps, we are closing

in on thermal equilibrium within the electron gas as the difference in temperature falls

from $(\Delta T_e) \approx 850K$ in Figure 5.34 to around 320K in Figure 5.35 and to less than 80K in

Figure 5.36, thus signaling the end of the second phase. Finally, in Figure 5.37, we are in

the third phase, $t=2.0$ ps. The electron gas temperature has almost reached thermal

equilibrium, $(\Delta T_e) \approx 3K$. Figure 5.38 describes the electron gas temperature along the

radial axis, r. We see that at $t=0.2$ ps and $t=0.25$ ps the electron gas temperature is rising

to its maximum value near the surface while the central regions lag a few hundred

degrees behind. At the other time indices, we see the transfer of energy from the top to

the bottom of the microsphere.
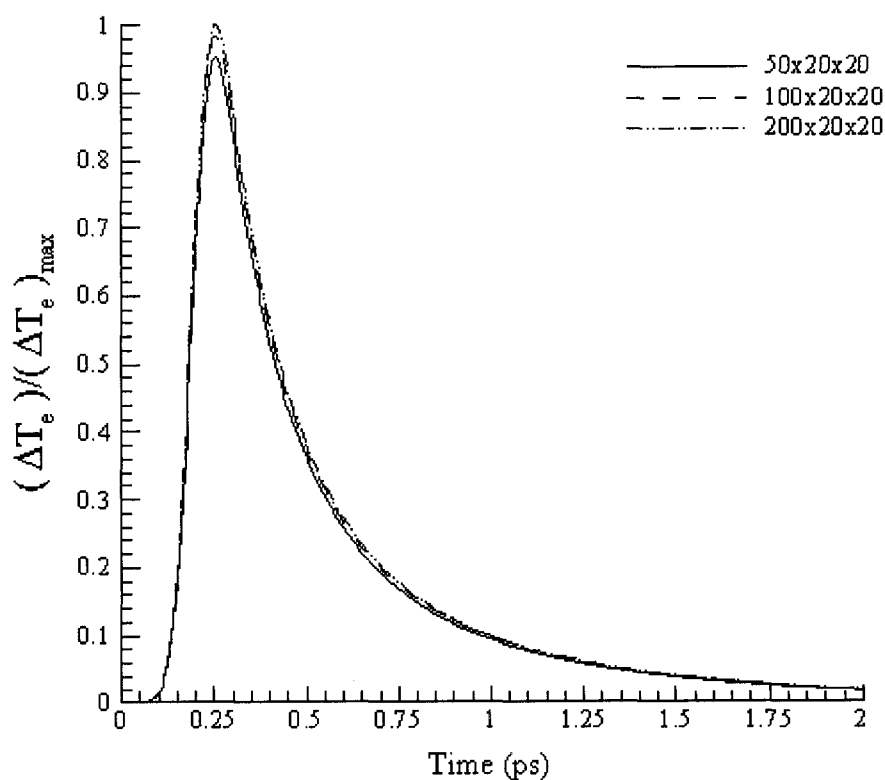
Figure 5.32 Normalized electron gas temperature change plotted against time.
(Heat source applied to a spot)

Figure 5.33 Contour plot of the electron gas temperature along the $r\varphi$ cross-section at t=0.2 ps. (Heat source applied to a spot)

Figure 5.34 Contour plot of the electron gas temperature along the $r\varphi$ cross-section at t=0.25 ps. (Heat source applied to a spot)

Figure 5.35 Contour plot of the electron gas temperature along the $r\varphi$ cross-section at t=0.5 ps. (Heat source applied to a spot)

Figure 5.36 Contour plot of the electron gas temperature along the $r\varphi$ cross-section at t=1.0 ps. (Heat source applied to a spot)

Figure 5.37 Contour plot of the electron gas temperature along the $r\varphi$ cross-section at $t=2.0\,ps$. (Heat source applied to a spot)

Figure 5.38 Electron gas temperature along the radial axis r. (Heat source applied to a spot)

Lattice Temperature. Figure 5.39 shows the normalized lattice temperature change

$$\left[\frac{\Delta T_l}{(\Delta T_l)_{max}} \right]$$ on the surface of the gold sphere. This temperature distribution is divided in

three time intervals. In the first time interval, 0-0.25 *ps*, we have no activities at all. All

the supplied energy is being transferred to the electron gas, no coupling is taking place at

this time, and consequently the metal lattice temperature is almost unchanged. In the

second time interval, which lasts from about 0.26 *ps* to 1.3 *ps*, the metal lattice

temperature starts to rise slowly as the electron-lattice coupling kicks in, thus raising the

temperature of the lattice. This plot is very similar to the one obtained in Figure 5.24

except that it is a steeper in the early stages due to the fact that at this point thermal

equilibrium has not been reached within the electron gas yet. In the final time domain,

1.3 *ps* and up, the lattice temperature is leveling off as thermal equilibrium within the

electron gas is approaching. Also, the mesh size's impact on the temperature profile is

insignificant which implies numerical stability.

Figures 5.40-5.44 show the contour plots of the lattice temperatures along the $r\varphi$

cross-section ($0 \le r \le L$, $0 \le \varphi \le \pi$) at times $t=0.2$ *ps*, 0.25 *ps*, 0.5 *ps*, 1.0 *ps* and 2.0 *ps*,

respectively. They show a progressive heating of the metal lattice as the temperature is

being transferred from the inner surface towards the bottom of the sphere. Figure 5.45

describes the metal lattice temperature along the radial axis, *r*. We see the temperature

slowly rising as there is a clear difference between the upper surface and the colder

regions at the bottom of the sphere. This plot is very similar to the one obtained in Figure

5.30 with the difference that the temperature rise is slower.
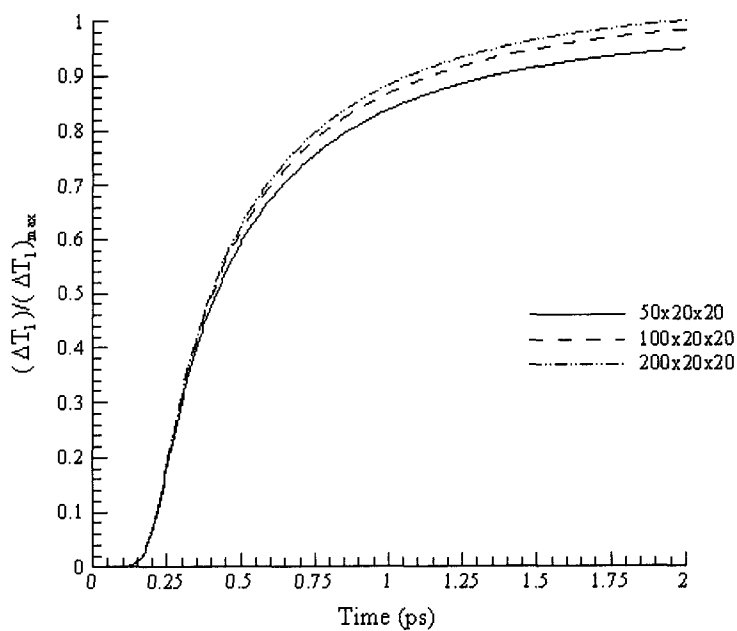
Figure 5.39 Normalized metal lattice temperature change plotted against time.
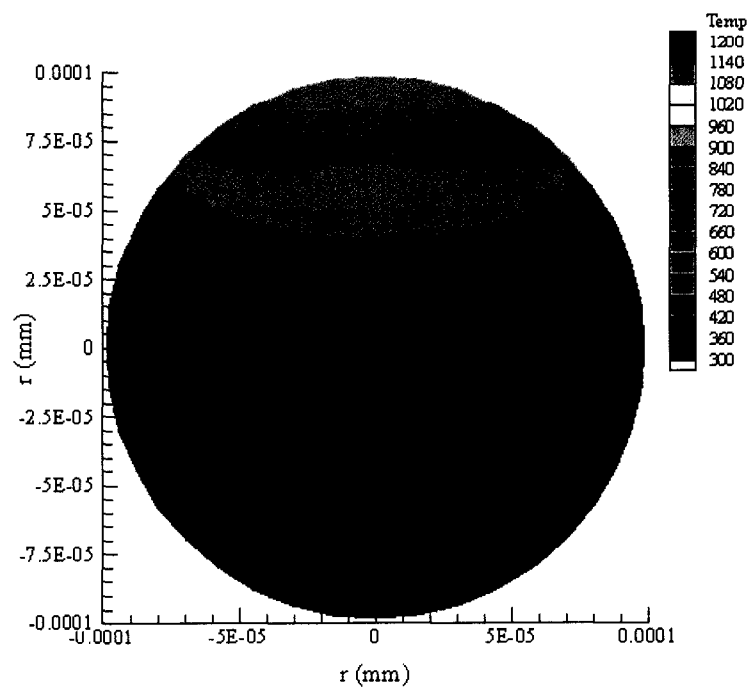(Heat source applied to a spot)
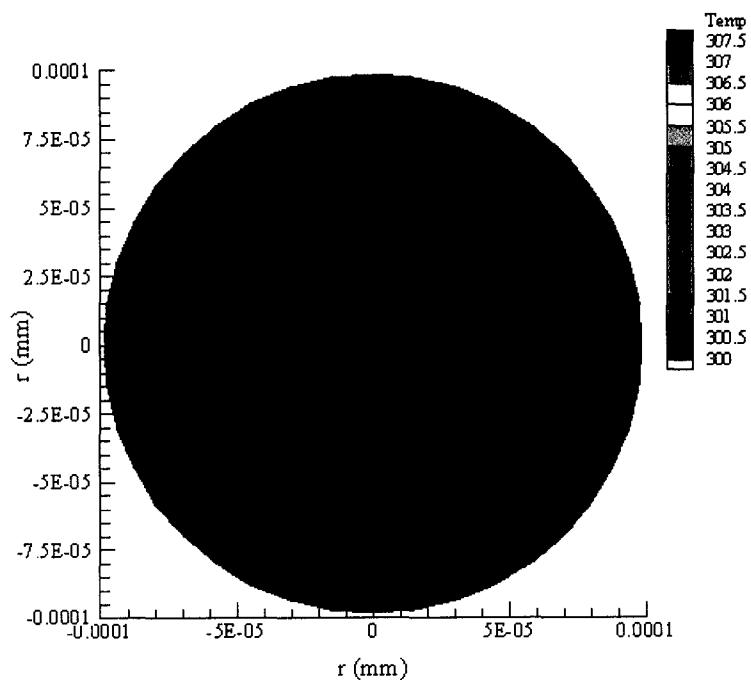
Figure 5.40 Contour plot of the metal lattice temperature along the $r\varphi$ cross-section at
$t=0.2\,ps$. (Heat source applied to a spot)
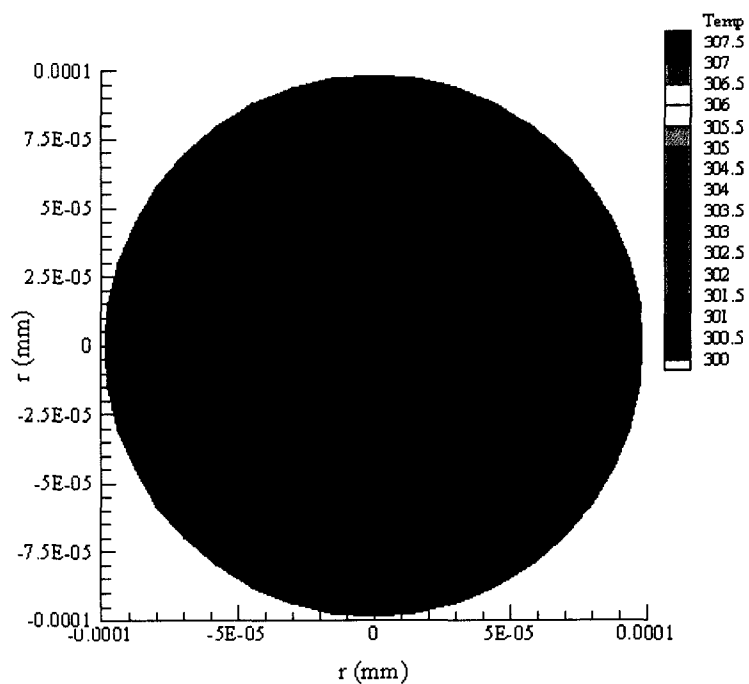
Figure 5.41 Contour plot of the metal lattice temperature along the $r\varphi$ cross-section at $t=0.25\ ps$. (Heat source applied to a spot)
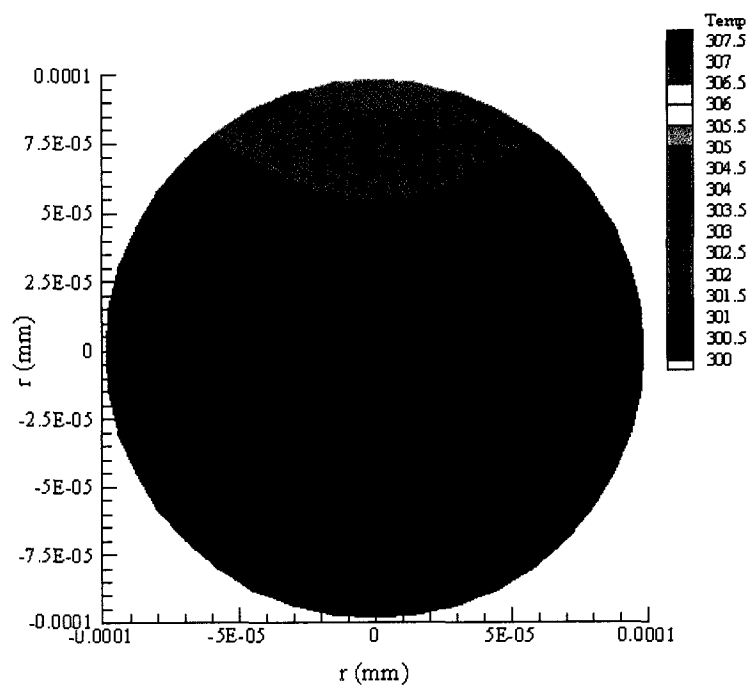
Figure 5.42 Contour plot of the metal lattice temperature along the $r\varphi$ cross-section at $t=0.5\ ps$. (Heat source applied to a spot)
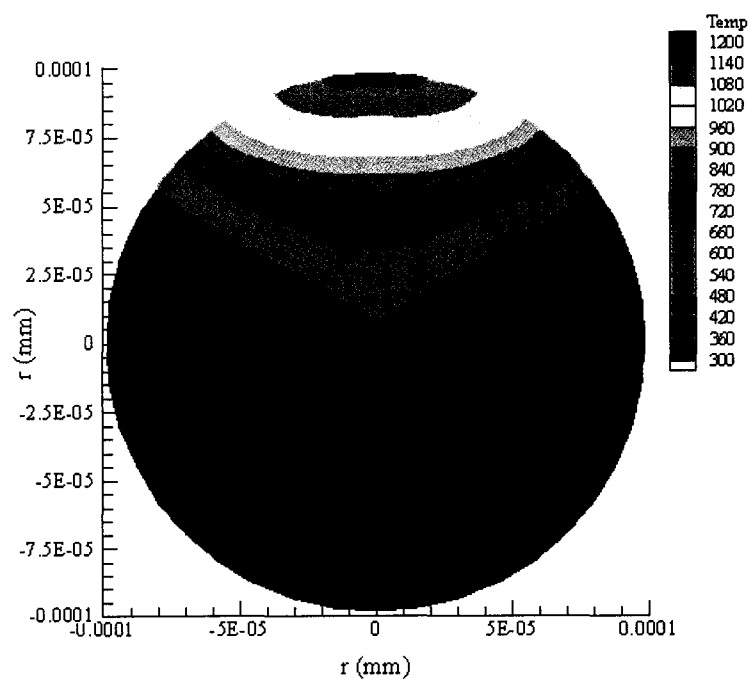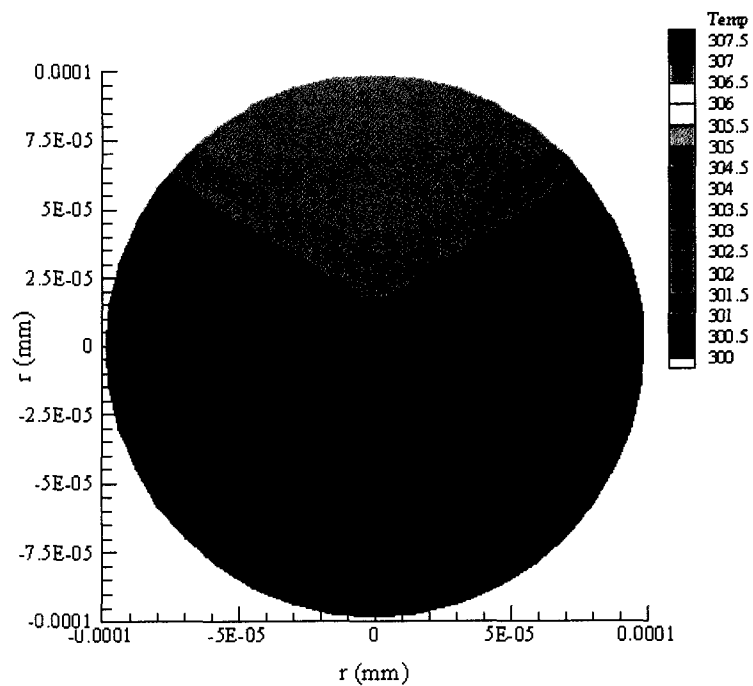
Figure 5.43 Contour plot of the metal lattice temperature along the $r\varphi$ cross-section at $t=1.0\,ps$. (Heat source applied to a spot)
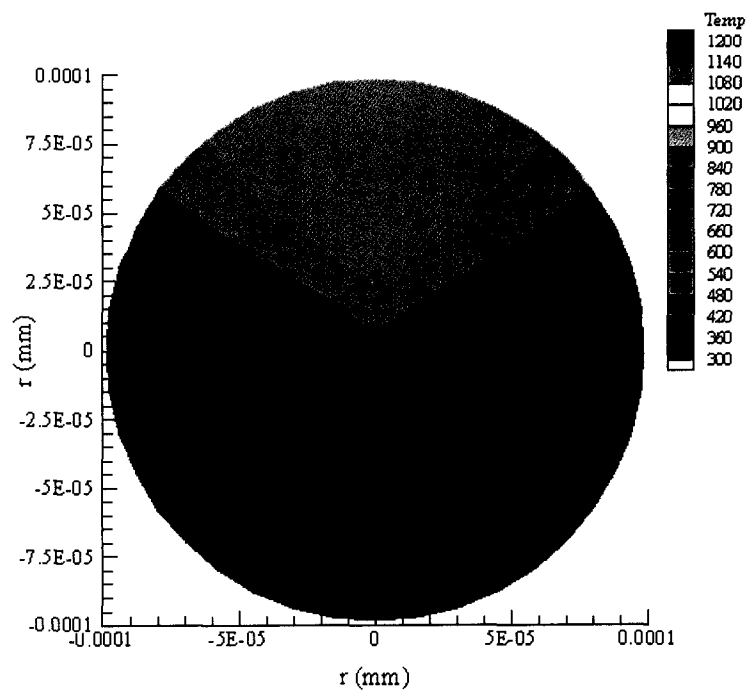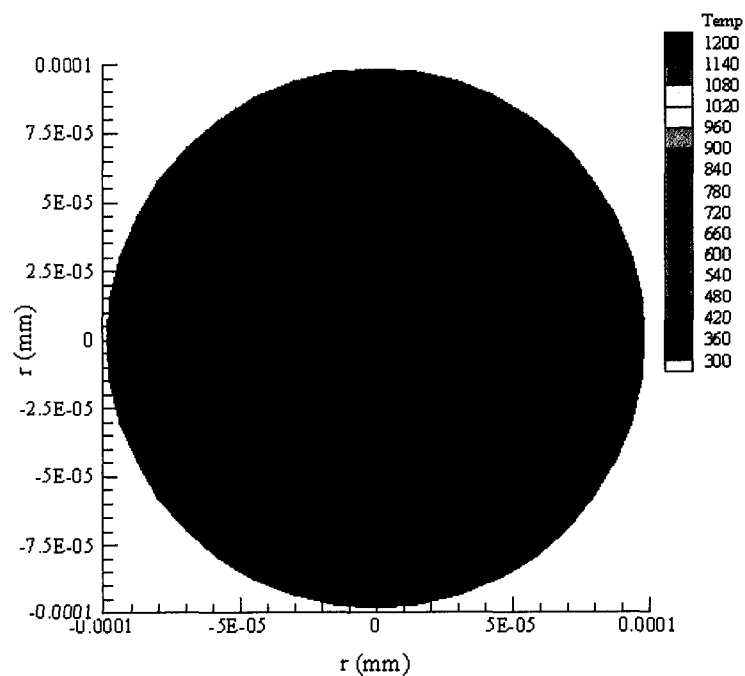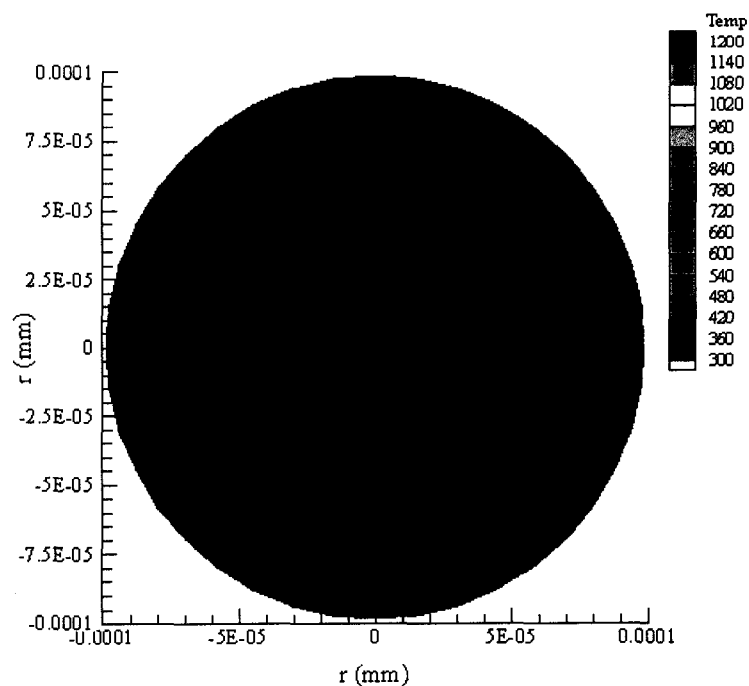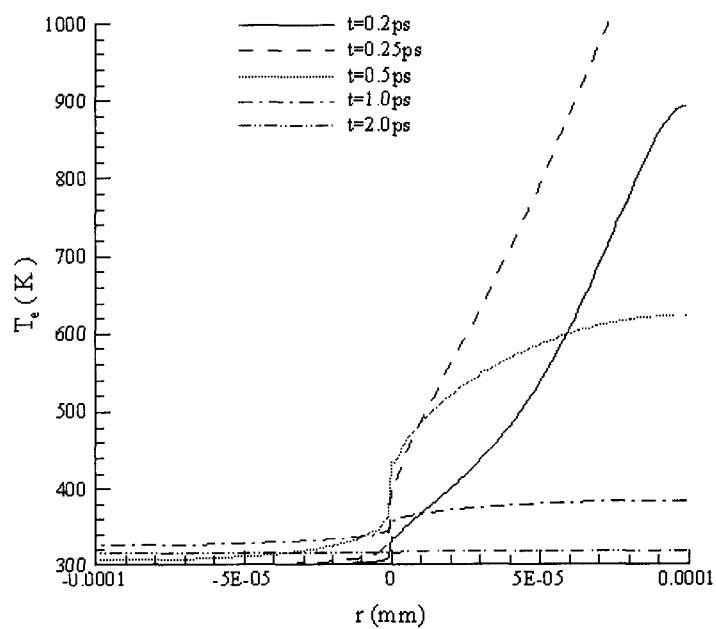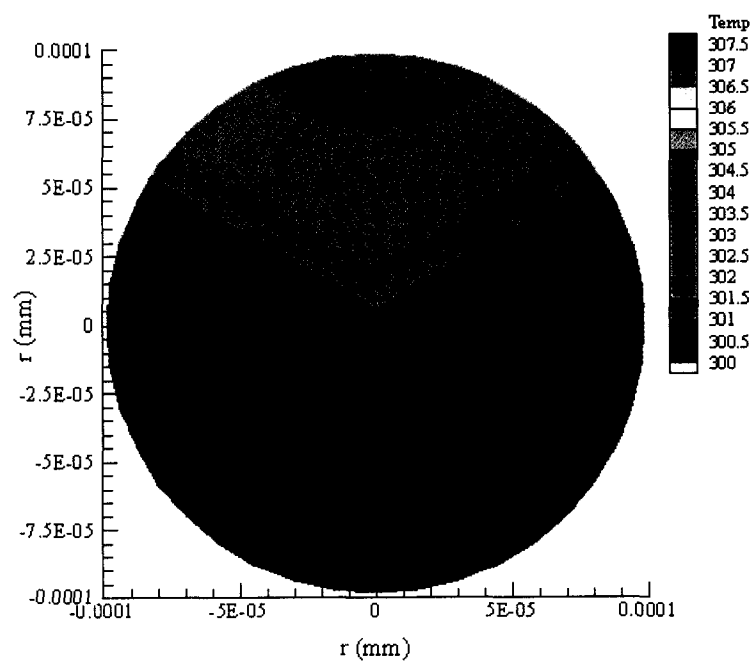

Figure 5.44 Contour plot of the metal lattice temperature along the $r\varphi$ cross-section at $t=2.0\,ps$. (Heat source applied to a spot)
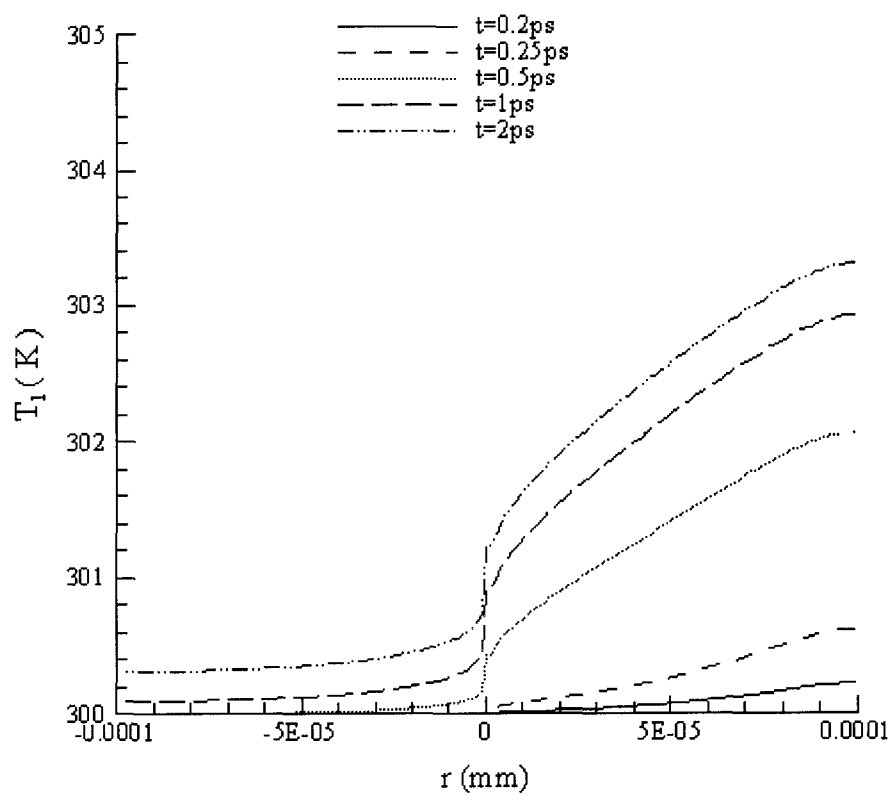
Figure 5.45 Metal lattice temperature along the radial axis r.
(Heat source applied to a spot)

CHAPTER 6

CONCLUSION

In this dissertation, we have investigated a micro sphere subjected to an ultrashort laser pulse. While continuous and long pulses create a risk of melting in the microstructure under fabrication, ultra-short pulse lasers offer an excellent alternative to optimize the thermal process and reduce the risk of thermal damage. The parabolic two-step model was used to model the transport phenomenon as it offered a set of equations that is more numerically efficient than the traditional single energy equation of microscale heat transfer. We established the well-posedness of the problem and proposed a numerical method to solve the governing equations. The scheme was shown to be unconditionally stable with respect to the source term. Numerical applications were used to validate the results.

Future studies will consist of extending our numerical method to solve the parabolic two-step equations in a multi-layered microsphere, and to develop a domain decomposition method to accelerate the convergence of the scheme. Additionally, higher order methods may be developed based on our method, and nonlinear thermal coefficients will be considered.

APPENDIX

SOURCE CODE OF THE NUMERICAL

METHOD

```
***********************************************************************
c     Title: Parabolic two-step modeling of heat transfer in a microsphere
c
c     Time units are in picosecond  and distance units are in millimeter
c     Temperatures are in Kelvin
c     L=0.1micrometer =100nm -----radius
c     dx=dr  in spherical  dy is the dtheta  dz is the dphi
c
c
***********************************************************************
c     Declaration of variables and data structures
c
c     t_variable refers to the electron gas and tl_variable to the lattice temperature
      dimension te0(0:201,0:51,0:51),te1(0:201,0:51,0:51)
      dimension tl0(0:201,0:51,0:51),tl1(0:201,0:51,0:51)
      dimension Q(0:201),tguess(0:201,0:51,0:51), tsurface(2:400)
      dimension tl2(0:201,0:51,0:51),te2(0:201,0:51,0:51)
      dimension tcenter(2:400),tlcenter(2:400),tlsurface(2:400)
      double precision Q,Ce,Cl,Ke,G,tp,d,R,Jn,dz,dx,dy,dt,temp7
      double precision te0,te1,te2,pi,temp6,temp3,temp4,temp5
      double precision tguess,tl0,tl1,tl2,denl,L,temp1,temp2,temp8
      double precision a1,a2,a3,a4,a5,a6,a7,a8,coef,temp9,tsurface
      double precision tcenter,tlcenter,tlsurface
c
***********************************************************************
c     Declaration and assignment of constants
c
      pi=3.1415926
      L=0.0001
      dz=0.05*pi
      dx=0.000001
      dy=0.1*pi
      dt=0.005
      Jn=0.0000134
      R=0.93
      G=0.000026
      d=0.0000153
      tp=0.1
      Ce=0.000021
      Cl=0.0025
      Ke=0.000000000000315
      a6=0.5*Ce/dt
      a7=G*Cl/(2*Cl+G*dt)
      a8=0.5*a7

      nx=100
```

```
      ny=20
      nz=20

c     A forced Gauss-seidel algorithm was used i.e no maximum number of iterations for
convergence

      ****************************************************************

c     Initial condition

      do i=1,nx-1
      do j=0,ny-1
      do k=1,nz-1
      tl0(i,j,k)=300.0
      tl1(i,j,k)=300.0
      te0(i,j,k)=300.0
      te1(i,j,k)=300.0
      enddo
      enddo
      enddo
c
c
c     Time iteration Counter
      nt=1
c
c---------------Begin iteration---------------------------------
c
 999  do i=1,nx-1
      do j=0,ny-1
      do k=1,nz-1
      tguess(i,j,k)=te1(i,j,k)
      enddo
      enddo
      enddo

      ****************************************************************

c   Case 1 ( Symmetric Heat Source)

 9    do i=1,nx-1
      Q(i)=0.94*(1.0-R)*Jn*exp(-(L-dx*i)/d-2.77*(nt*dt/tp-2.0)
     $  **2.0)/(tp*d)
      ****************************************************************
```

```
************************************************************************
c   Case 2  (Hemisphere)

9   if (k .lt. nz/2) then
    Q(i,k)=(0.94*(1.0-R)*Jn*exp(-(L-dx*i)/d-2.77*(nt*dt/tp-2.0)
$   **2.0)/(tp*d))*cos(k*dz)
    else
    Q(i,k)=0
    Endif
************************************************************************
c   Case 3  (Spot)

9   if (k .lt. nz/4) then
    Q(i,k)=(0.94*(1.0-R)*Jn*exp(-(L-dx*i)/d-2.77*(nt*dt/tp-2.0)
$   **2.0)/(tp*d))*cos(k*dz)
    else
    Q(i,k)=0
    Endif
************************************************************************


    denl=ke/(4.0*i*i*dx*dx)
    a2=denl*(i-0.5)**2.0
    a3=denl*(i+0.5)**2.0

    do j=0,ny-1
    do k=1,nz-1
    a1=denl/(dy*dy*sin(k*dz)*sin(k*dz))
    a4=(denl*sin((k-0.5)*dz))/(dy*dy*sin(k*dz))
    a5=(denl*sin((k+0.5)*dz))/(dy*dy*sin(k*dz))

    Coef=2*a1+a2+a3+a4+a5+a6+a8

    if (i .eq. 1) then
    temp1=a2*(2.0*te1(1,j,k)+te0(1,j,k))
    coef=coef-a2
    else
    temp1=a2*(te2(i-1,j,k)+2.0*te1(i-1,j,k)+te0(i-1,j,k))
    endif

    if (i .eq. nx-1) then
    temp2=a3*(2.0*te1(nx-1,j,k)+te0(nx-1,j,k))
    coef=coef-a3
    else
```

```
        temp2=a3*(tguess(i+1,j,k)+2.0*te1(i+1,j,k)+te0(i+1,j,k))
        endif

        if (j .eq. 0) then
        temp3=a1*(tguess(i,ny-1,k)+2.0*te1(i,ny-1,k)+te0(i,ny-1,k))
        else
        temp3=a1*(te2(i,j-1,k)+2.0*te1(i,j-1,k)+te0(i,j-1,k))
        endif

        if (j .eq. ny-1) then
        temp4=a1*(te2(i,0,k)+2.0*te1(i,0,k)+te0(i,0,k))
        else
        temp4=a1*(tguess(i,j+1,k)+2.0*te1(i,j+1,k)+te0(i,j+1,k))
        endif

        if (k .eq. 1) then
        temp5=a4*(2.0*te1(i,j,1)+te0(i,j,1))
        coef=coef-a4
        else
        temp5=a4*(te2(i,j,k-1)+2.0*te1(i,j,k-1)+te0(i,j,k-1))
        endif

        if (k .eq. nz-1) then
        temp6=a5*(2.0*te1(i,j,nz-1)+te0(i,j,nz-1))
        coef=coef-a5
        else
        temp6=a5*(tguess(i,j,k+1)+2.0*te1(i,j,k+1)+te0(i,j,k+1))
        endif

        temp7=te1(i,j,k)*(4.0*a1+2.0*a2+2.0*a3+2.0*a4+2.0*a5+a7)

        temp8=te0(i,j,k)*(a6-2.0*a1-a2-a3-a4-a5-0.5*a7)

        temp9=a7*(tl1(i,j,k)+tl0(i,j,k))

        te2(i,j,k)=(temp1+temp2+temp3+temp4+temp5+temp6-temp7+temp8
     $ +temp9+Q(i))/coef

        enddo
        enddo
        enddo
c------------------End Iteration-----------------------------------------------
c
c
c
```

```fortran
c---------Begin error analysis for iteration----------------------------------------
c
      er=0.0
      do 4 i=1,nx-1
      do 4 j=0,ny-1
      do 4 k=1,nz-1
      err=abs(te2(i,j,k)-tguess(i,j,k))
      if(err.le.er)goto 4
      er=err
  4   continue
      if (er.le.0.00000001)goto 99
      do i=1,nx-1
      do j=0,ny-1
      do k=1,nz-1
      tguess(i,j,k)=te2(i,j,k)
      enddo
      enddo
      enddo
      goto 9
c------------------End Error analysis
c
c
c
c
c----------------Begin replacement for Lattice Temperature-------------------------------
c
  99  do i=1,nx-1
      do j=0,ny-1
      do k=1,nz-1
      tl2(i,j,k)=(G*dt/(2.0*Cl+G*dt))*(te2(i,j,k)+2.0*tel(i,j,k)
     $ +te0(i,j,k)-2.0*tl1(i,j,k))+((2.0*Cl-G*dt)/(2.0*Cl+G*dt))
     $ *tl0(i,j,k)
      enddo
      enddo
      enddo
      nt=nt+1
c-----------------End Lattice temperature replacement----dt is incremented------------------
      ------
c
c---------------------begin print job-----------------------------------------------------
c
c------------------------surface temperature vs time-------------------------------------
      tsurface(nt)=te2(nx-1,10,10)
      tcenter(nt)=te2(1,10,10)
      tlsurface(nt)=tl2(nx-1,10,10)
      tlcenter(nt)=tl2(1,10,10)
```

```
c-------------------dte/dtemax vs depth & cross section plots at specified times-----------

if (nt .eq. 40) then
open(unit=6,file='100te_t=0.2ps.txt')
do i=nx-1,1,-1
 print 11,i, te2(i,10,10)
enddo
print 11,0, te2(1,10,10)
do i=1,nx-1
print 11,-1*i, te2(i,10,10)
enddo
close(6)
open(unit=6,file='100cross_t=0.2ps.txt')
write (6,14)
WRITE (6,12)
WRITE (6,13)
do k=0,nz
do i=1,nx-1
  if (k .eq. 0) then
  print 10, 0, i*dx, te2(i,0,k+1)

  elseif (k .lt. nz/2) then
    print 10, i*dx*sin(k*dz), i*dx*cos(k*dz), te2(i,0,k)

  elseif (k .eq. nz/2) then
  print 10, i*dx,0,te2(i,0,k)

  elseif (k .lt. nz) then
    print 10, i*dx*sin(k*dz) , i*dx*cos(k*dz), te2(i,0,k)

  else
  print 10, 0, -1*i*dx, te2(i,0,k-1)
  endif
enddo
enddo
do k=0,nz
do i=1,nx-1
  if (k .eq. 0) then
  print 10, 0, -1*i*dx, te2(i,0,k+1)

  elseif (k .lt. nz/2) then
    print 10, -1*i*dx*sin(k*dz), -1*i*dx*cos(k*dz), te2(i,0,k)

  elseif (k .eq. nz/2) then
  print 10, -1*i*dx,0,te2(i,0,k)
```

```
      elseif (k .lt. nz) then
       print 10, -1*i*dx*sin(k*dz) , -1*i*dx*cos(k*dz), te2(i,0,k)


      else
      print 10, 0, i*dx, te2(i,0,k-1)
       endif
    enddo
    enddo
    close(6)
    endif


    if (nt .eq. 50) then
    open(unit=6,file='100te_t=0.25ps.txt')
    do i=nx-1,1,-1
     print 11,i, te2(i,10,10)
    enddo
    print 11,0, te2(1,10,10)
    do i=1,nx-1
    print 11,-1*i, te2(i,10,10)
    enddo
    close(6)
    open(unit=6,file='100cross_t=0.25ps.txt')
    write (6,14)
    WRITE (6,12)
    WRITE (6,13)
    do k=0,nz
    do i=1,nx-1
      if (k .eq. 0) then
      print 10, 0, i*dx, te2(i,0,k+1)


      elseif (k .lt. nz/2) then
       print 10, i*dx*sin(k*dz), i*dx*cos(k*dz), te2(i,0,k)


      elseif (k .eq. nz/2) then
      print 10, i*dx,0,te2(i,0,k)


      elseif (k .lt. nz) then
       print 10, i*dx*sin(k*dz) , i*dx*cos(k*dz), te2(i,0,k)


      else
      print 10, 0, -1*i*dx, te2(i,0,k-1)
       endif
    enddo
    enddo
    do k=0,nz
```

```
do i=1,nx-1
   if (k .eq. 0) then
   print 10, 0, -1*i*dx, te2(i,0,k+1)

   elseif (k .lt. nz/2) then
     print 10, -1*i*dx*sin(k*dz), -1*i*dx*cos(k*dz), te2(i,0,k)

   elseif (k .eq. nz/2) then
   print 10, -1*i*dx,0,te2(i,0,k)

   elseif (k .lt. nz) then
     print 10, -1*i*dx*sin(k*dz) , -1*i*dx*cos(k*dz), te2(i,0,k)

   else
   print 10, 0, i*dx, te2(i,0,k-1)
   endif
enddo
enddo
close(6)
endif

if (nt .eq. 100) then
open(unit=6,file='100te_t=0.5ps.txt')
do i=nx-1,1,-1
 print 11,i, te2(i,10,10)
enddo
print 11,0, te2(1,10,10)
do i=1,nx-1
print 11,-1*i, te2(i,10,10)
enddo
close(6)
open(unit=6,file='100cross_t=0.5ps.txt')
write (6,14)
WRITE (6,12)
WRITE (6,13)
do k=0,nz
do i=1,nx-1
   if (k .eq. 0) then
   print 10, 0, i*dx, te2(i,0,k+1)

   elseif (k .lt. nz/2) then
     print 10, i*dx*sin(k*dz), i*dx*cos(k*dz), te2(i,0,k)

   elseif (k .eq. nz/2) then
   print 10, i*dx,0,te2(i,0,k)
```

```
      elseif (k .lt. nz) then
        print 10, i*dx*sin(k*dz) , i*dx*cos(k*dz), te2(i,0,k)

      else
      print 10, 0, -1*i*dx, te2(i,0,k-1)
      endif
enddo
enddo
do k=0,nz
do i=1,nx-1
  if (k .eq. 0) then
  print 10, 0, -1*i*dx, te2(i,0,k+1)

    elseif (k .lt. nz/2) then
      print 10, -1*i*dx*sin(k*dz), -1*i*dx*cos(k*dz), te2(i,0,k)

    elseif (k .eq. nz/2) then
    print 10, -1*i*dx,0,te2(i,0,k)

    elseif (k .lt. nz) then
      print 10, -1*i*dx*sin(k*dz) , -1*i*dx*cos(k*dz), te2(i,0,k)

    else
    print 10, 0, i*dx, te2(i,0,k-1)
    endif
enddo
enddo
close(6)
endif

if (nt .eq. 200) then
open(unit=6,file='100te_t=1ps.txt')
do i=nx-1,1,-1
 print 11,i, te2(i,10,10)
enddo
print 11,0, te2(1,10,10)
do i=1,nx-1
print 11,-1*i, te2(i,10,10)
enddo
close(6)
open(unit=6,file='100cross_t=1ps.txt')
write (6,14)
WRITE (6,12)
WRITE (6,13)
do k=0,nz
do i=1,nx-1
```

```
        if (k .eq. 0) then
        print 10, 0, i*dx, te2(i,0,k+1)

        elseif (k .lt. nz/2) then
          print 10, i*dx*sin(k*dz), i*dx*cos(k*dz), te2(i,0,k)

        elseif (k .eq. nz/2) then
        print 10, i*dx,0,te2(i,0,k)

        elseif (k .lt. nz) then
          print 10, i*dx*sin(k*dz) , i*dx*cos(k*dz), te2(i,0,k)

        else
        print 10, 0, -1*i*dx, te2(i,0,k-1)
        endif
enddo
enddo
do k=0,nz
do i=1,nx-1
        if (k .eq. 0) then
        print 10, 0, -1*i*dx, te2(i,0,k+1)

        elseif (k .lt. nz/2) then
          print 10, -1*i*dx*sin(k*dz), -1*i*dx*cos(k*dz), te2(i,0,k)

        elseif (k .eq. nz/2) then
        print 10, -1*i*dx,0,te2(i,0,k)

        elseif (k .lt. nz) then
          print 10, -1*i*dx*sin(k*dz) , -1*i*dx*cos(k*dz), te2(i,0,k)

        else
        print 10, 0, i*dx, te2(i,0,k-1)
        endif
enddo
enddo
close(6)
endif

if (nt .eq. 400) then
open(unit=6,file='100te_t=2ps.txt')
do i=nx-1,1,-1
 print 11,i, te2(i,10,10)
enddo
print 11,0, te2(1,10,10)
do i=1,nx-1
```

```
print 11,-1*i, te2(i,10,10)
enddo
close(6)
open(unit=6,file='100cross_t=2ps.txt')
write (6,14)
WRITE (6,12)
WRITE (6,13)
do k=0,nz
do i=1,nx-1
  if (k .eq. 0) then
  print 10, 0, i*dx, te2(i,0,k+1)

    elseif (k .lt. nz/2) then
      print 10, i*dx*sin(k*dz), i*dx*cos(k*dz), te2(i,0,k)

    elseif (k .eq. nz/2) then
    print 10, i*dx,0,te2(i,0,k)

    elseif (k .lt. nz) then
      print 10, i*dx*sin(k*dz) , i*dx*cos(k*dz), te2(i,0,k)

    else
    print 10, 0, -1*i*dx, te2(i,0,k-1)
    endif
enddo
enddo
do k=0,nz
do i=1,nx-1
  if (k .eq. 0) then
  print 10, 0, -1*i*dx, te2(i,0,k+1)

    elseif (k .lt. nz/2) then
      print 10, -1*i*dx*sin(k*dz), -1*i*dx*cos(k*dz), te2(i,0,k)

    elseif (k .eq. nz/2) then
    print 10, -1*i*dx,0,te2(i,0,k)

    elseif (k .lt. nz) then
      print 10, -1*i*dx*sin(k*dz) , -1*i*dx*cos(k*dz), te2(i,0,k)

    else
    print 10, 0, i*dx, te2(i,0,k-1)
    endif
enddo
enddo
close(6)
```

```
open(unit=6,file='te_surface.txt')
do i=2,400
 print 11,i,tsurface(i)
enddo
close(6)
open(unit=6,file='te_center.txt')
do i=2,400
 print 11,i,tcenter(i)
enddo
close(6)
endif
c --------------------------Now same thing for the TL's-------------------------------------

if (nt .eq. 40) then
open(unit=6,file='100tl_t=0.2ps.txt')
do i=nx-1,1,-1
 print 11,i, tl2(i,10,10)
enddo
print 11,0, tl2(1,10,10)
do i=1,nx-1
print 11,-1*i, tl2(i,10,10)
enddo
close(6)
open(unit=6,file='100crosstl_t=0.2ps.txt')
write (6,14)
WRITE (6,12)
WRITE (6,13)
do k=0,nz
do i=1,nx-1
  if (k .eq. 0) then
  print 10, 0, i*dx, tl2(i,0,k+1)

  elseif (k .lt. nz/2) then
   print 10, i*dx*sin(k*dz), i*dx*cos(k*dz), tl2(i,0,k)

  elseif (k .eq. nz/2) then
  print 10, i*dx,0,tl2(i,0,k)

  elseif (k .lt. nz) then
   print 10, i*dx*sin(k*dz) , i*dx*cos(k*dz), tl2(i,0,k)

  else
  print 10, 0, -1*i*dx, tl2(i,0,k-1)
  endif
enddo
enddo
```

```
do k=0,nz
do i=1,nx-1
  if (k .eq. 0) then
  print 10, 0, -1*i*dx, tl2(i,0,k+1)

  elseif (k .lt. nz/2) then
    print 10, -1*i*dx*sin(k*dz), -1*i*dx*cos(k*dz), tl2(i,0,k)

  elseif (k .eq. nz/2) then
  print 10, -1*i*dx,0,tl2(i,0,k)

  elseif (k .lt. nz) then
    print 10, -1*i*dx*sin(k*dz) , -1*i*dx*cos(k*dz), tl2(i,0,k)

  else
  print 10, 0, i*dx, tl2(i,0,k-1)
  endif
enddo
enddo
close(6)
endif

if (nt .eq. 50) then
open(unit=6,file='100tl_t=0.25ps.txt')
do i=nx-1,1,-1
 print 11,i, tl2(i,10,10)
enddo
print 11,0, tl2(1,10,10)
do i=1,nx-1
print 11,-1*i, tl2(i,10,10)
enddo
close(6)
open(unit=6,file='100crosstl_t=0.25ps.txt')
write (6,14)
WRITE (6,12)
WRITE (6,13)
do k=0,nz
do i=1,nx-1
  if (k .eq. 0) then
  print 10, 0, i*dx, tl2(i,0,k+1)

  elseif (k .lt. nz/2) then
    print 10, i*dx*sin(k*dz), i*dx*cos(k*dz), tl2(i,0,k)

  elseif (k .eq. nz/2) then
  print 10, i*dx,0,tl2(i,0,k)
```

```fortran
      elseif (k .lt. nz) then
        print 10, i*dx*sin(k*dz) , i*dx*cos(k*dz), tl2(i,0,k)

      else
        print 10, 0, -1*i*dx, tl2(i,0,k-1)
        endif
      enddo
      enddo
      do k=0,nz
      do i=1,nx-1
        if (k .eq. 0) then
        print 10, 0, -1*i*dx, tl2(i,0,k+1)

        elseif (k .lt. nz/2) then
          print 10, -1*i*dx*sin(k*dz), -1*i*dx*cos(k*dz), tl2(i,0,k)

        elseif (k .eq. nz/2) then
        print 10, -1*i*dx,0,tl2(i,0,k)

        elseif (k .lt. nz) then
          print 10, -1*i*dx*sin(k*dz) , -1*i*dx*cos(k*dz), tl2(i,0,k)

        else
        print 10, 0, i*dx, tl2(i,0,k-1)
        endif
      enddo
      enddo
      close(6)
      endif

      if (nt .eq. 100) then
      open(unit=6,file='100tl_t=0.5ps.txt')
      do i=nx-1,1,-1
       print 11,i, tl2(i,10,10)
      enddo
      print 11,0, tl2(1,10,10)
      do i=1,nx-1
      print 11,-1*i, tl2(i,10,10)
      enddo
      close(6)
      open(unit=6,file='100crosstl_t=0.5ps.txt')
      write (6,14)
      WRITE (6,12)
      WRITE (6,13)
      do k=0,nz
```

```
do i=1,nx-1
  if (k .eq. 0) then
  print 10, 0, i*dx, tl2(i,0,k+1)

  elseif (k .lt. nz/2) then
    print 10, i*dx*sin(k*dz), i*dx*cos(k*dz), tl2(i,0,k)

  elseif (k .eq. nz/2) then
  print 10, i*dx,0,tl2(i,0,k)

  elseif (k .lt. nz) then
    print 10, i*dx*sin(k*dz) , i*dx*cos(k*dz), tl2(i,0,k)

  else
  print 10, 0, -1*i*dx, tl2(i,0,k-1)
  endif
enddo
enddo
do k=0,nz
do i=1,nx-1
  if (k .eq. 0) then
  print 10, 0, -1*i*dx, tl2(i,0,k+1)

  elseif (k .lt. nz/2) then
    print 10, -1*i*dx*sin(k*dz), -1*i*dx*cos(k*dz), tl2(i,0,k)

  elseif (k .eq. nz/2) then
  print 10, -1*i*dx,0,tl2(i,0,k)

  elseif (k .lt. nz) then
    print 10, -1*i*dx*sin(k*dz) , -1*i*dx*cos(k*dz), tl2(i,0,k)

  else
  print 10, 0, i*dx, tl2(i,0,k-1)
  endif
enddo
enddo
close(6)
endif

if (nt .eq. 200) then
open(unit=6,file='100tl_t=1ps.txt')
do i=nx-1,1,-1
 print 11,i, tl2(i,10,10)
enddo
print 11,0, tl2(1,10,10)
```

```
do i=1,nx-1
print 11,-1*i, tl2(i,10,10)
enddo
close(6)
open(unit=6,file='100crosstl_t=1ps.txt')
write (6,14)
WRITE (6,12)
WRITE (6,13)
do k=0,nz
do i=1,nx-1
  if (k .eq. 0) then
  print 10, 0, i*dx, tl2(i,0,k+1)

  elseif (k .lt. nz/2) then
   print 10, i*dx*sin(k*dz), i*dx*cos(k*dz), tl2(i,0,k)

  elseif (k .eq. nz/2) then
  print 10, i*dx,0,tl2(i,0,k)

  elseif (k .lt. nz) then
   print 10, i*dx*sin(k*dz) , i*dx*cos(k*dz), tl2(i,0,k)

  else
  print 10, 0, -1*i*dx, tl2(i,0,k-1)
  endif
enddo
enddo
do k=0,nz
do i=1,nx-1
  if (k .eq. 0) then
  print 10, 0, -1*i*dx, tl2(i,0,k+1)

  elseif (k .lt. nz/2) then
   print 10, -1*i*dx*sin(k*dz), -1*i*dx*cos(k*dz), tl2(i,0,k)

  elseif (k .eq. nz/2) then
  print 10, -1*i*dx,0,tl2(i,0,k)

  elseif (k .lt. nz) then
   print 10, -1*i*dx*sin(k*dz) , -1*i*dx*cos(k*dz), tl2(i,0,k)

  else
  print 10, 0, i*dx, tl2(i,0,k-1)
  endif
enddo
enddo
```

```
close(6)
endif

if (nt .eq. 400) then
open(unit=6,file='100tl_t=2ps.txt')
do i=nx-1,1,-1
  print 11,i, tl2(i,10,10)
enddo
print 11,0, tl2(1,10,10)
do i=1,nx-1
print 11,-1*i, tl2(i,10,10)
enddo
close(6)
open(unit=6,file='100crosstl_t=2ps.txt')
write (6,14)
WRITE (6,12)
WRITE (6,13)
do k=0,nz
do i=1,nx-1
  if (k .eq. 0) then
  print 10, 0, i*dx, tl2(i,0,k+1)

  elseif (k .lt. nz/2) then
    print 10, i*dx*sin(k*dz), i*dx*cos(k*dz), tl2(i,0,k)

  elseif (k .eq. nz/2) then
  print 10, i*dx,0,tl2(i,0,k)

  elseif (k .lt. nz) then
    print 10, i*dx*sin(k*dz) , i*dx*cos(k*dz), tl2(i,0,k)

  else
  print 10, 0, -1*i*dx, tl2(i,0,k-1)
  endif
enddo
enddo
do k=0,nz
do i=1,nx-1
  if (k .eq. 0) then
  print 10, 0, -1*i*dx, tl2(i,0,k+1)

  elseif (k .lt. nz/2) then
    print 10, -1*i*dx*sin(k*dz), -1*i*dx*cos(k*dz), tl2(i,0,k)

  elseif (k .eq. nz/2) then
  print 10, -1*i*dx,0,tl2(i,0,k)
```

```
    elseif (k .lt. nz) then
      print 10, -1*i*dx*sin(k*dz) , -1*i*dx*cos(k*dz), tl2(i,0,k)

    else
    print 10, 0, i*dx, tl2(i,0,k-1)
    endif
  enddo
  enddo
  close(6)
  open(unit=6,file='tl_surface.txt')
  do i=2,400
   print 11,i,tlsurface(i)
  enddo
  close(6)
  open(unit=6,file='tl_center.txt')
  do i=2,400
   print 11,i,tlcenter(i)
  enddo
  close(6)
  endif


c -------------------------------------------------------------------
10    format(e12.6,4x,e12.6,4x,f12.7)
11    format(2x,I6,2X,f12.7)
14    FORMAT(' Contour plot of a Crossection ')
12    format(' Variables = "X","Y","Temp" ')
13    format(' ZONE I=99, J=42, K=1, F=POINT ')
c-----------------end dte/dtemax vs depth at specified times----------------------

c
c--------------------end print job---------------------------------------------------
c
c
c----------------Check if last time level has been reached and then replace value for next
iteration
c
    if(nt.eq.400)goto 1
    do i=1,nx-1
    do j=0,ny-1
    do k=1,nz-1
    te0(i,j,k)=te1(i,j,k)
    te1(i,j,k)=te2(i,j,k)
    tl0(i,j,k)=tl1(i,j,k)
    tl1(i,j,k)=tl2(i,j,k)
    enddo
```

```
        enddo
        enddo
        goto 999

c----------------end of preparation for next iteration---------------------------------------
------
c
c
c

 1    end
```

REFERENCES

[Al-Nimr 1997a] M.A. Al-Nimr and V.S. Arpaci, "Non-equilibrium laser heating of metal films", *ASME Journal of Heat Transfer*, Vol. 119, (1997), pp. 188-190.

[Al-Nimr 1997b] M.A. Al-Nimr, "Heat transfer mechanisms during laser heating of thin metal films", *International Journal of Thermophysics*, Vol. 18, (1997), pp. 1257-1268.

[Al-Nimr 1999] M.A. Al-Nimr and V.S. Arpaci, "Picosecond thermal pulses in thin metal films", *Journal of Applied Physics*, Vol. 85, (1999), pp. 2517-2521.

[Al-Nimr 2000a] M.A. Al-Nimr, M. Naji and V.S. Arpaci, "Non-equilibrium entropy production under the effect of the dual-phase-lag heat conduction model", *ASME Journal of Heat Transfer*, Vol. 122, (2000), pp. 217-222.

[Al-Nimr 2000b] M.A. Al-Nimr and M. Naji, "On the phase-lag effect on the non-equilibrium entropy production, *Journal of Microscale Thermophysics Engineering*, Vol. 4, (2000), pp. 231-243.

[Al-Nimr 2001] M.A. Al-Nimr and S. Kiwan, "Effect of thermal losses on the microscopic two-step heat conduction model", *International Journal of Heat and Mass Transfer*, Vol. 44, (2001), pp. 1013-1018.

[Al-Nimr 2003] M.A. Al-Nimr, M. Hader and M. Naji, "Use of the microscopic parabolic heat conduction model in place of the macroscopic model validation criterion under harmonic boundary heating", *International Journal of Heat and Mass Transfer*, Vol. 46, (2003), pp. 333-339.

[Anisimov 1974] S.I. Anisimov, B.L. Kapeliovich and T.L Perel'man, "Electron emission from metal surfaces exposed to ultrashort laser pulses", *Soviet Physics JETP*, Vol. 39, (1974), pp. 375-377.

[Antaki 1998a] P.J. Antaki, "Solution for non-fourier dual phase-lag heat conduction in a semi-finite slab with surface heat flux", *International Journal of Heat and Mass Transfer*, Vol. 41, (1998), pp. 2253-2258.

[Antaki 1998b] P.J. Antaki, "Effect of dual phase-lag heat conduction on ignition of a solid", *Journal of Thermophysics and Heat Transfer*, Vol. 14, (2000), pp. 276-278.

120

[Antaki 2002] P.J. Antaki, "Importance of non-equilibrium thermal conductivity during short-pulse laser-induced desorption from metals", *International Journal of Heat and Mass Transfer*, Vol. 45, (2002), pp. 4063-4067.

[Brorson 1987] S.D. Brorson, J.G. Fujimoto and E.P. Ippen, "Femtosecond electron heat transport dynamics in a thin gold film", *Physical Review Letters*, Vol. 59, (1987), pp. 1962-1965

[Brorson 1990] S.D. Brorson, A. Kazeroonian, J.S. Moodera, D.W. Face, T.K. Cheng, E.P. Ippen, M.S. Dresselhaus and G. Dresselhaus, "Femtosecond room-temperature measurement of the electron-phonon coupling constant λ in metallic superconductors", *Physical Review Letters*, Vol. 64, (1990), pp. 2172-2175.

[Brown 2001] J.W. Brown and R.V. Churchill, *"Fourier Series and Boundary Value Problems 6th Ed."*, McGraw-Hill, New York, NY, (2001).

[Cattaneo 1958] C. Cattaneo, "A form of heat conduction equation which eliminates the paradox of instantaneous propagation", *Compte Rendus*, Vol. 247, (1958), pp. 431-433.

[Chen 1999] J.K. Chen, J.E. Beraun and D.Y. Tzou, "A dual phase-lag diffusion model for interfacial layer growth in metal matrix composites", *Journal of Material Sciences*, Vol. 34, (1999), pp. 6183-6187.

[Chen 2000] J.K. Chen, J.E. Beraun and D.Y. Tzou, "A dual phase-lag diffusion model for predicting thin film growth", *Semiconductor Science and Technology*, Vol. 15, (2000), pp. 235-241

[Chen 2001a] J.K. Chen, J.E. Beraun and D.Y. Tzou, "A dual phase-lag diffusion model for predicting intermetallic compound layer growth in solder joints", *ASME Journal of Electronic Packaging*, Vol. 112, (2001), pp. 52-57.

[Chen 2001b] J.K. Chen and J.E. Beraun, "Numerical study of ultrashort laser pulse interactions with metal films", *Numerical Heat Transfer, Part A*, Vol. 40, (2001), pp. 1-20.

[Chester 1963] M. Chester, "Second Sound in Solids", *Physical Review*, Vol.131, (1963), pp. 2013-2015.

[Dai 1999] W. Dai and R. Nassar, "A finite difference method for solving the heat transport equation at the microscale", *Numerical Methods for Partial Differential Equations*, Vol. 15, (1999), pp. 697-708.

[Dai 2000a] W. Dai and R. Nassar, "A domain decomposition method for solving three dimensional heat transport equations in double layered thin films with microscale thickness", *Numerical Heat Transfer, Part A*, Vol. 38, (2000), pp. 243-256.

[Dai 2000b] W. Dai and R. Nassar, "A compact finite difference scheme for solving a three dimensional heat transport equation in a thin film", *Numerical Methods for Partial Differential Equations*, Vol. 16, (2000), pp. 441-458.

[Dai 2001a] W. Dai and R. Nassar, "A finite difference scheme for solving a three dimensional heat transport equation in a thin film with microscale thickness", *International Journal of Numerical Methods in Engineering*, Vol. 50, (2001), pp. 1865-1880.

[Dai 2001b] W. Dai and R. Nassar, "A domain decomposition method for solving 3-D heat transport equations in double layered thin films with microscale thickness and nonlinear interfacial conditions", *Numerical Heat Transfer, Part A*, Vol. 39, (2001), pp. 21-33.

[Dai 2002] W. Dai and R. Nassar, "An approximate analytic method for solving dual phase-lagging heat transfer equations", *International Journal of Heat and Mass Transfer*, Vol. 45, (2002), pp. 1585-1593.

[Dai 2004] W. Dai, L. Shen and R. Nassar, "A convergent three-level finite difference scheme for solving a dual phase-lagging heat transport equation in spherical coordinates", *Numerical Methods for Partial Differential Equations*, Vol. 20, (2004), pp. 60-71.

[Duncan 1994] A.B. Duncan and G.P. Peterson, "Review of microscale heat transfer", *ASME Journal of Applied Mechanics Review*, Vol. 47, (1994), pp. 397-428.

[Elliot 1989] D.J. Elliot and B.P. Piwczyk, "Single and multiple pulse ablation of polymeric and high density materials with excimer laser radiation at 193 nm and 248nm", *Materials Research Society Symposium Proceedings*, Vol. 129, (1989), pp. 627-636.

[Elsayed-Ali 1987] H.E. Elsayed-Ali, T.B. Norris, M.A. Pessot and G.A. Mourou, "Time-resolved observation of electron-phonon relaxation in copper", *Physical Review Letters*, Vol. 58, (1987), pp. 1212-1215.

[Elsayed-Ali 1991] H.E. Elsayed-Ali, "Femtosecond thermoreflectivity and thermotransmissivity of polycrystalline and single-crystalline gold films", *Physical Review B*, Vol. 43, (1991), pp. 4488-4491.

[Evans 1998] L.C. Evans, "*Partial Differential Equations*", American Mathematical Society, Providence, Rhode Island, (1998).

[Frankel 1985] J.I Frankel, B. Vick and M.N. Ozisik, "Flux formulation of hyperbolic heat conduction", *Journal of Applied Physics*, Vol. 58, (1985), pp. 3340-3345.

[Fujimoto 1984] J.G. Fujimoto, J.M. Liu and E.P. Ippen, "Femtosecond laser interaction with metallic tungsten and non-equilibrium electron and lattices temperature in thin gold films", *Physical Review Letters*, Vol. 53, (1984), pp. 1837-1840.

[Grigoropolus 1994] C.P. Grigoropolus, "Heat transfer in laser processing of thin films", *Annual Review of Heat Transfer, Part V*, Hemisphere, New York, *(1994)*.

[Groeneveld 1990] R.H.M. Groeneveld, R. Sprik, M. Wittebrood and A. Lagendijk, "Ultrafast relaxation of electrons probed by surface plasmons at a thin silver film", *Ultrafast Phenomena VII*, Springer, Berlin, (1990), pp. 368-370.

[Ho 1995] J.R. Ho, C.P. Grigoropolus and J.A.C. Humphrey, "Computational study of heat transfer and gas dynamics in the pulsed laser evaporation of metals", *Journal of Applied Physics*, Vol. 78, (1995), pp. 4696-4709.

[Ho 2003] J.R. Ho, C.P. Kuo and W.S. Jiamg, "Study of heat transfer in multilayered structure within the framework of dual phase-lag heat conduction model using lattice Boltzmann method", *International Journal of Heat and Mass Transfer*, Vol. 46, (2003), pp. 55-69.

[Hopkins 2000] J.M. Hopkins and J. Sibbett, "Ultrashort-pulse lasers: big payoffs in a flash", *Scientific American*, Vol. 283, (2000), pp. 72-79.

[Joseph 1989] D.D. Joseph and L. Preziosi, " Heat Waves", *Review of Modern Physics*, Vol. 61, (1989), pp. 41-73.

[Joseph 1990] D.D. Joseph and L. Preziosi, "Addendum to the paper on heat waves", *Review of Modern Physics*, Vol. 62, (1990), pp. 375-391.

[Joshi 1993] A.A. Joshi and A. Majumdar, "Transient Ballistic and diffusive phonon heat transport in thin films", *Journal of Applied Physics*, Vol. 74, (1993), pp. 31-39.

[Kaganov 1957] M.I. Kaganov, I.M. Lifshitz and M.V. Tanatarov, "Relaxation between electrons and crystalline lattices", *Soviet Physics JETP*, Vol. 4, (1957), pp. 173-178.

[Knapp 1990] J.A. Knapp, P. Borgesen and R.A. Zuhr, "Beam-solid interactions: physical phenomena", *Materials Research Society Symposium Proceedings*, Vol. 157, (1990).

[Lees 1961] M. Lees, "Alternating direction and semi-explicit difference methods for parabolic partial differential equations", *Numerical Mathematics*, Vol. 3, (1961), pp. 398-412.

[Lees 1966] M. Lees, "A linear three-level difference scheme for quasilinear parabolic equations", *Mathematics of Computation*, Vol.20, (1966), pp. 516-522.

[Lin 1997] C.K. Lin, C.C. Wang and Y.P. Chang, "The unsteady solution of a unified heat conduction equation", *International Journal of Heat and Mass Transfer*, Vol. 40, (1997), pp. 1716-1719.

[Liu 2000] J. Liu, "Preliminary survey on the mechanisms of wave-like behaviors of heat transfer in living tissues", *Forschung im Ingenieurwesen,* Vol. 66, (2000), pp. 1-10.

[Majumdar 1993] A. Majumdar, "Microscale Heat Conduction in Dielectric Thin Films", *ASME Journal of Heat Transfer,* Vol. 157, (1993), pp. 7-16.

[Momma 1997] C. Momma, S. Nolte, B.N. Chichkov, F.V. Alvensleben, A. Tunnermann, "Precise laser ablation with ultrashort pulses", *Applied Surface Science,* Vol. 109, (1997), pp. 15-19.

[Narayan 1991] J. Narayan, V.P. Gosbole, G.W.White, "Laser method for synthesis and processing of continuous diamond films on nondiamond substrates", *Science,* Vol. 52, (1991), pp. 416-418.

[Opsal 1991] J. Opsal, "The application of thermal wave technology to thickness and grain size of aluminum films", *SPIE,* Vol. 1596, (1991), pp. 120-131.

[Ozisik 1994] M.N. Ozisik and D.Y. Tzou, "On the wave theory in Heat Conduction", *ASME Journal of Heat Transfer,* Vol. 116, (1994), pp. 526-535.

[Qiu 1992] T.Q. Qiu and C.L. Tien, "Short pulse laser heating on metals", *International Journal of Heat and Mass Transfer,* Vol. 35, (1992), pp. 719-726.

[Qiu 1993] T.Q. Qiu and C.L. Tien, "Heat transfer mechanisms during short-pulse laser heating of metals", *ASME Journal of Heat Transfer,* Vol. 115, (1993), pp. 835-841.

[Qiu 1994a] T.Q. Qiu and C.L. Tien, "Femtosecond laser heating of multi-layer metals-I. Analysis", *International Journal of Heat and Mass Transfer,* Vol. 37, (1994), pp. 2789-2797.

[Qiu 1994b] T.Q. Qiu, T. Juhasz, C. Suarez, C.L. Tien, "Femtosecond laser heating of multi-layer metals-II. Experiments", *International Journal of Heat and Mass Transfer,* Vol. 37, (1994), pp. 2799-2808.

[Shirk 1998] M.D. Shirk and P.A. Molian, "A review of ultrashort pulsed ablation of metals", *Journal of Laser Applications,* Vol. 10, (1998), pp. 18-28.

[Strikwerda 1989] J.C. Strikwerda, *"Finite difference schemes and partial differential equations",* Chapman &Hall, New York, (1989).

[Tang 1999] D.W. Tang and N. Araki, "Wavy, wavelike, diffusive thermal responses of finite rigid slabs to high-speed heating of laser-pulses", *International Journal of Heat and Mass Transfer,* Vol. 42, (1999), pp. 855-860.

[Tien 1994] C.L. Tien and G. Chen, " Challenges in microscale conductive and radiative heat transfer", *ASME Journal of Heat Transfer,* Vol. 116, (1994), pp. 799-807.

[Tien 1998] C.L. Tien, A. Majumdar and F. Gerner, "*Microscale Energy Transport*", Taylor & Francis, Washington, DC, (1998).

[Tzou 1997] D.Y. Tzou, "*Macro to Microscale Heat Transfer*", Taylor & Francis, Washington, DC, (1997).

[Tzou 1999] D.Y. Tzou, "Ultrafast heat transport: the lagging behavior", 44th *SPIE's Annual Meeting*, (1999). July 18-22, Denver, CO.

[Tzou 2000a] D.Y. Tzou, "Ultrafast transient behavior in microscale heat/mass transport", *Advanced Photon Source Millennium Lecture Series*, Argonne National Laboratories, Chicago, (2000).

[Tzou 2000b] D.Y. Tzou, "Microscale heat transfer and fluid flow", 45th *SPIE's Annual Meeting*, (2000). July 30-August 4, San Diego, CA.

[Tzou 2002] D.Y. Tzou, J.K. Chen, and J.E. Beraun, "Hot electron blast induced by ultrashort-pulsed lasers in layered media", *International Journal of Heat and Mass Transfer*, Vol. 45, (2002), pp. 3369-3382.

[Vernotte 1958] P. Vernotte, "Les paradoxes de la théorie continue de l'équation de la chaleur ", *Compte Rendus*, Vol. 246, (1958), pp. 3154-3155.

[Vernotte 1961] P. Vernotte, "Some possible complication in the phenomena of thermal conduction", *Compte Rendus*, Vol. 252, (1961), pp. 2190-2191.

[Wang 2000] L. Wang and X. Zhou, "Dual-phase-lagging Heat Conduction", *Shandong University Press*, Jinan, (2000).

[Wang 2001a] L. Wang and X. Zhou, "Dual-phase-lagging Heat Conduction: Problems and Solutions", *Shandong University Press*, Jinan, (2001).

[Wang 2001b] L. Wang and M. Xu, "Well-posedness and solution structure of dual-phase-lagging heat conduction", *International Journal of Heat and Mass Transfer*, Vol. 44, (2001), pp. 1659-1669.

[Wang 2002] L. Wang and M. Xu, "Well-posedness and solution structure of dual-phase-lagging heat conduction: higher dimensions", *International Journal of Heat and Mass Transfer*, Vol. 45, (2001), pp. 1165-1171.